Differentiation and source processes at Mt Pelée and the Quill; active volcanoes in the Lesser Antilles Arc

Jon Davidson[1] and Marjorie Wilson[2]

1Department of Earth Sciences, University of Durham, Durham DH1 3LE, UK;

j.p.davidson@durham.ac.uk

2 School of Earth & Environment, The University of Leeds, Leeds LS2 9JT, UK;

B.M.Wilson@leeds.ac.uk

ABSTRACT

Volcanic rocks erupted at Mt. Pelée (Martinique; central Lesser Antilles) and the Quill volcano (Statia; northern Lesser Antilles) define distinct differentiation trends, each of which can be accounted for largely by fractional crystallisation of plagioclase, amphibole and Fe-Ti oxides. This assemblage is seen commonly in associated cumulate nodules, although the petrography of the lavas is pyroxene + plagioclase + Fe-Ti oxides. Thus differentiation is controlled, in part, by cryptic amphibole fractionation. At a given degree of differentiation incompatible trace element abundances tend to be higher at Mt. Pelée, and REE patterns are more fractionated than is the case at the Quill. Isotopic ratios of Sr and Pb correlate with indices of differentiation (e.g. wt % SiO_2) at both volcanoes (more convincingly at Mt. Pelée), indicating that differentiation is also an open-system process. When the differentiation trends for the two volcanoes are compared they do not

converge towards a single parental magma composition, suggesting that the primary magmas for the Quill and Mt. Pelée are different. This difference is most likely due to mantle source variations. The source of the Mt. Pelée magmas appears to be more enriched in incompatible elements, consistent with a greater proportion of admixed subducted sediment. This observation is in agreement with previous studies that have documented an increasing sediment contribution southwards along the arc. However comparison with available data for other volcanoes along the arc does not reveal a consistent along-arc trend, suggesting that a model of sediment-source mixing is overly simplistic and that additional factors such as variable fluid contributions from the subducted slab may be important.

INTRODUCTION

Much has been published regarding the differences in magma compositions along the Lesser Antilles island arc (Brown et al., 1977; Davidson, 1987; Macdonald et al., 2000; White and Dupré, 1986). Based on a regional geochemical study Brown et al. (1977) suggested that magma compositions vary from alkaline in the south, through calc-alkaline in the centre to island arc tholeiite in the northern islands of the arc. Other studies, however, pointed out that large compositional variations exist at individual volcanic centres (particularly in the central part of the arc; Gunn et al., 1974), rather than there being a simple, smooth along-arc trend. Nevertheless there are clearly major first-order differences along the arc. Truly mafic magmas (>8 wt % MgO) and associated ultramafic mantle-derived nodules are only found in the southern islands (Arculus, 1976;

Heath et al., 1998). Sr-Nd-Pb isotope diversity is significant in the southern islands but greatest in the central islands (Davidson 1986, 1987), while the northern islands show the most restricted range of isotopic compositions, with most resembling island arc magmas from elsewhere (e.g. Aleutians, South Sandwich, Marianas, Tonga). Both Hawkesworth et al. (1993) and White and Patchett (1984) have divided island arc rocks into those which have a restricted range of isotope compositions, displaced only slightly from those of MORB, and those which have a wider range of compositions, trending to more crust-like ratios. The Lesser Antilles straddles this subdivision, perhaps underscoring the arbitrary nature of such a discrimination.

The involvement of continental crustal components in island arc magma genesis has been recognised by most workers in the field (e.g. White and Patchett, 1984; Davidson et al, 2005). Variations in isotopic composition in island arcs are traditionally interpreted as due to variations in the type or amount of subducted crustal material incorporated into the mantle source region (Plank and Langmuir, 1993; Labanieh et al., 2010). Alternatively, it has been proposed that the crustal component could, at least in part, be added through crustal contamination during magma ascent and differentiation. Crustal contamination has been recognised as an important process in the Lesser Antilles, based principally on: (1) correlations between isotopic compositions and indices of differentiation (e.g. Thirlwall and Graham, 1984; Davidson, 1987) and (2) large variations in oxygen isotope ratios (Davidson and Harmon, 1989). Even though true continental basement is absent in oceanic island arcs, continental material may still be present as sediment layers in the arc crust – just as it is present as layers on the subducted

oceanic crust. Distinguishing the amount of crustal material added directly into the mantle source region from that incorporated as a result of shallow-level crustal contamination is more than simply of semantic interest. Constraining the elemental budgets recycled into the mantle via subduction depends on understanding melt/fluid trace element partitioning during the subduction process, while the role of arc magmatism in generating new continental crust is affected by whether elements are derived from the mantle, or simply recycled within the arc crust (Davidson and Arculus, 2006). The wide range of isotopic compositions reported for volcanic rocks from the Lesser Antilles arc has been interpreted as due to either an unusually large (and isotopically distinct) subducted sediment contribution or due to contamination by such materials within the arc crust. It is difficult to argue that either of these hypotheses provides an exclusive solution and both subducted and crustal contributions are likely. However, constraining the relative *importance* of each is critical, and this is addressed below, based upon data from two well-characterised volcanoes; one in the north (the Quill) and one in the centre (Mt. Pelée) of the arc.

APPROACH: CONSTRAINING SUBDUCTION ZONE SOURCES AND CONTRIBUTIONS

The objective of the approach described here (and summarised schematically in Fig. 1) is to constrain the differentiation mechanisms and their petrological/ geochemical effects at each volcano and thereby to establish the geochemical characteristics of the parental magmas involved in each case. If they share a common parent magma (Fig. 1a)

then we can reasonably conclude that the source processes and contributions are the same at both volcanoes, and perhaps, therefore, along the entire arc. If the parental magmas are different (and we will show that they are), then, accepting that the parental magmas are typically far from primary (in common with most arc rocks e.g. Nye and Reid, 1986; Bacon et al., 1997), two alternatives can be considered: (1) the parental magmas at both volcanoes evolve from a primary magma via different differentiation mechanisms deep in the arc crust (Fig. 1b), or (2) different parental magmas at the two volcanoes reflect different progenitor primary magmas and therefore different source compositions/melting processes (Fig. 1c). Different mantle-derived parent magmas could result from variations in the slab-derived component(s), mantle wedge composition or melting processes. The only way to distinguish between these two hypotheses is by detailed geochemical and isotopic studies of stratigraphically well-constrained volcanic suites, allowing a much more rigorous evaluation of the supra-subduction zone mantle wedge source contributions than can be obtained by simply analysing the most mafic rocks available from along the arc, or by comparing islands or arc segments which may include a number of individual volcanic centres, each with potentially different differentiation trends.

CONTEXT: THE LESSER ANTILLES ARC, MT PELÉE AND THE QUILL

The Lesser Antilles Arc has developed along the eastern margin of the Caribbean Plate as a result of westward subduction of Atlantic oceanic lithosphere (Fig. 2). The subduction system is bounded by transform systems to the north (Greater Antilles) and south (Venezuela) which accommodate relative eastward movement of the Caribbean

Plate. The Benioff zone dip varies from near-vertical in the south to ~45° in the north, with plate convergence at the slower end of the spectrum of subduction rates at around 1-2 cm yr^{-1} (Wadge and Shepherd, 1984; Macdonald et al., 2000). The bathymetric map shows a substantial accumulation of sediments in the trench, thickening southwards and even rising above sea level at the island of Barbados (Fig. 2).

Sevilla et al. (2010) have determined the crustal thickness in the northern part of the arc (Montserrat) at 30±4km based on receiver function analysis. This is consistent with previous estimates (Macdonald et al., 2000 and references therein). The lower crust is interpreted to be heavily intruded Caribbean Plate crust (Sevilla et al., 2010). South of Dominica the young arc volcanoes are superimposed upon an older arc basement (Eocene-Oligocene; Figure 2); north of Dominica the currently active arc is located to the west of the older arc and may, therefore, have a simpler crustal structure, although this is not well constrained. The westward shift in arc location which affects the northern islands is thought to have occurred ~9 Myr ago (Briden et al., 1979).

Mt. Pelée on Martinique and the Quill on St. Eustatius (Statia) were selected for detailed study as they are active volcanic edifices located within the central and northern Lesser Antilles respectively (Fig. 2). Extensive field studies at these two volcanoes (Smith and Roobol, 1990; Roobol and Smith, 2004) provide a stratigraphic framework that is unsurpassed along the arc.

Our samples were taken from stratigraphic sections which can be correlated reasonably confidently with published sections, for which extensive carbon-dating constraints are available (Figs. 3, 4). The samples are typically fresh blocks from block and ash flows, with occasional lapilli from fall units. Both suites are dominated by two-pyroxene andesites. At Mt. Pelée the samples range from basaltic andesite to dacite while at the Quill they are entirely within the andesite range. The samples are typically variably vesicular and porphyritic with 30-50% phenocrysts (antecrysts; Davidson et al., 2007) dominated by plagioclase followed by orthopyroxene (Fig. 3a). Rare olivine is found in the most mafic rocks, in which clinopyroxene forms up to 15% of the phenocryst assemblage. Opacitised amphibole is present (<5%) in the most evolved samples. Although amphibole is typically absent as a phenocryst phase in the lavas from both Mt. Pelée and the Quill, it is abundant in cumulate plutonic blocks from both volcanoes (Arculus and Wills, 1980; Macdonald et al, 2000; Fig. 3b).

Mt Pelée (Fig. 4) is the most recently active volcanic edifice on the island of Martinique. The island has been volcanically active since at least Eocene times (Westercamp and Tazieff, 1980; Briden et al., 1979) and comprises several compositionally distinct volcanic centres which appear to have migrated generally northwestward through time. Only the more recent edifices (Morne Jacob, Pitons du Carbet, Piton Mt. Conil and Mt. Pelée) can be confidently distinguished on the basis of combined morphology-stratigraphy-geochemistry-petrology. Mt. Pelée itself has been active for about 400 kyrs and is constructed on top of the remains of the 0.4-2.6 Ma Piton Mt Conil volcano. The 1902 eruption of Mt Pelée was infamous for its devastation, with

~29,000 people killed in what was then the capital, Fort de France. This eruption was also a milestone in modern volcanology as the eyewitness studies of Lacroix (1908) recognised and documented "*Nuee Ardentes*" and the block and ash flow deposits that were formed from them. The 1929 eruptions were further studied by Peret (1937), who made some of the first measurements of flow velocities. The 20th century eruptions were the result of dome collapse events, similar to those characterising the recent eruptions of Soufrière Hills on Montserrat to the north.

The stratigraphic record on Mt. Pelée is dominated by pyroclastic material – with the exception of the 1902 and 1929 summit domes lava flows are rare (or buried; Fig. 4b). Pyroclastic flows are channelled into ribbon-like deposits along valleys. Pyroclastic flows can be subdivided according to the juvenile component: vesiculated (scoria or pumice) or dense blocks. The pyroclastic flows are interbedded with air fall deposits (lapilli – to – ash grade) and finer grained ash flows (ash hurricanes or low density, high energy pyroclastic flows).

Statia is a smaller island than Martinique, with a far simpler geology and a less protracted history of volcanic activity. The westward jump in arc activity which affected the northern islands (Macdonald et al., 2000 and references therein) means that, unlike Martinique, Statia is not built on an ~Eocene basement of older arc material such as that which exists beneath the islands from Dominica southwards (Fig. 2). Essentially the island comprises an old, eroded andesite centre to the northwest, adjacent to the dominant structure of the near-symmetrical Quill volcano (Fig. 5a). Porphyritic andesite lavas make

up the northwest centre – the dominance of lavas compared with the younger deposits of the Quill is almost certainly an artefact of preferential erosion of loose volcaniclastic material, and a salutary observation for workers attempting to construct volcanic histories from potentially biased records.

The Quill shares many characteristics with Mt. Pelée and is a typical composite arc volcano. Lava flows at the Quill are rare, and the pyroclastic deposits resemble those of Mt. Pelée (Fig. 5b). However the cone is much younger and virtually undissected, such that its outer flanks are mantled by the most recent deposits and stratigraphic relationships are only exposed along coastal cliff sections. In contrast with the channelling observed at Mt Pelée, the pyroclastic flows at the Quill form fan-like deposits which are quite extensive and continuous along exposed sections. The White Wall limestone along the southern flank of the volcano comprises marine deposits which have clearly been recently uplifted, perhaps due to crypto-dome intrusion in the edifice. The oldest carbon date reported for the Quill is ~22,000 years, although volcanic activity likely extends back to 40-50,000 years (Roobol and Smith, 2004).

ANALYTICAL TECHNIQUES

Samples were split and weathered surfaces discarded prior to crushing. Major elements were determined by XRF (Phillips PW1400) at the University of Leeds on disks fused with lithium borate. Precision here was better than 2% on nearly all elements, <1% on most, and reproducibility determined on multiple completely re-made fused disks was

similarly better than 2%. Trace elements were measured by XRF on pressed pellets at Leeds (precision better than 5%) and again by ICP-MS (Perkin Elmer-Sciex Elan 6000) at the University of Durham using techniques described in Ottley et al., 2003. The latter data represent a more extensive data set, and for the most part these data are used and supersede those published previously, along with appropriate data quality indicators, by Davidson (1986, 1987) except where otherwise noted in Table 1. Errors on trace elements analysed by ICP-MS at Durham were all typically less than 2%.

Nd, Sr and Pb isotope ratios were originally measured at the University of Leeds (analytical details in Davidson, 1987). Many of the samples were subsequently re-analysed at the University of California, Los Angeles (UCLA) (analytical details in Davidson et al., 1993). The UCLA data supersede the older data of Davidson (1986, 1987). In Table 1 all of the Sr isotope analyses are from UCLA ($^{87}Sr/^{86}Sr$ of SRM 987 = 0·710253 ± 25). Nd isotope analyses are from Leeds and UCLA; $^{143}Nd/^{144}Nd$ analyses of the La Jolla standard are (just) within analytical error from the two labs (Leeds La Jolla $^{143}Nd/^{144}Nd$ = 0.511886±30; UCLA La Jolla $^{143}Nd/^{144}Nd$ = 0.511840±11). Pb isotopes were all re-analysed at the University of Durham using an ICP-MS multicollector mass spectrometer (SRM 981; $^{206}Pb/^{204}Pb$ =16.9405±10, $^{207}Pb/^{204}Pb$ = 15.4975±11; $^{208}Pb/^{204}Pb$ = 36.7160±32; analytical details in Font et al. 2008). There is encouragingly good agreement between the data obtained in three different laboratories across two continents and over 25 years, with the possible exception of $^{207}Pb/^{204}Pb$. Hf isotopes were analysed for a subset of samples at Durham (JMC475 $^{176}Hf/^{177}Hf$ = 0.2821535±6) using the analytical techniques outlined by Nowell et al. (2004).

Oxygen isotope ratios (Table 2) were determined on mineral separates by laser ablation at Royal Holloway, University of London. Analytical details are given in Mattey and Macpherson (1993) in which they report a value for the San Carlos olivine standard of 4.88‰ ± 0.06‰. Multiple analysis of the internal San Carlos olivine standard gave $\delta^{18}O$ = 4.88‰ (standard deviation = 0.131) for this study.

CONTROLS ON DIFFERENTIATION

Geochemical data for Mt. Pelée and the Quill are presented in Tables 1a and b respectively. The major and trace element variations are summarised in Figs. 6 and 7. A cursory glance at these plots shows that in some respects the differentiation trends at the two volcanoes are indistinguishable (e.g. MgO vs SiO_2), but for the most part there are clear differences. Overall, at a given degree of differentiation (wt. % SiO_2) samples from Mt. Pelée are more enriched in incompatible elements (K, Ba, Th, LREE); they also have more "crust-like" isotopic compositions (higher $^{87}Sr/^{86}Sr$ and $^{206}Pb/^{204}Pb$, lower $^{143}Nd/^{144}Nd$; Table 1).

Our objective in the context of the hypotheses illustrated in Fig. 1 is to constrain the differentiation mechanisms at the two volcanoes, and then to determine what controls the characteristics of their respective mantle sources.

Major elements

Major element oxide variation diagrams (Fig. 6), using SiO_2 as a differentiation index, show simple linear trends with progressive differentiation, from basalt/ basaltic andesite to dacite. The use of silica (rather than MgO or Mg-number) as an index of differentiation deserves justification. Like many subduction-related magma suites, those from Mt. Pelée and the Quill are highly differentiated compared with putative primary magmas. A classic differentiation trend of MgO versus SiO_2 should be strongly curved, reflecting the progressive crystallisation and changing solid solution compositions of mafic (olivine, pyroxene) and felsic (plagioclase) phases. For primitive magma compositions MgO typically falls sharply for a small increase in SiO_2, while for more differentiated compositions MgO varies relatively little as SiO_2 increases significantly. The linear arrays seen in Fig. 6 are most easily explained by mixing – either of two liquids or of a liquid and a fixed composition solid, as would be achieved during crystal fractionation (effectively a form of "unmixing"). For each volcano there are no significant differences among the stratigraphic sections sampled, despite the different ages represented. When the volcanoes are compared, for some elements there is no distinction (e.g. CaO, MgO); however, the Mt. Pelée samples have distinctly higher K_2O and have slight tholeiitic tendencies with respect to FeO*/MgO, although this is not reflected on an AFM diagram (Fig. 6f). This observation is inconsistent with the generalisations made in the original geochemical survey of the Lesser Antilles by Brown et al. (1977) who suggested that the central islands are calc-alkaline while those in the north are more tholeiitic.

The stratigraphic relationships (see wt. % SiO_2 versus stratigraphy in Figs. 4b and 5b) do not reveal any systematic progression with time to more evolved compositions and therefore do not represent a simple liquid line of descent. This lack of correlation between degree of differentiation and time, noted by several other authors for subduction-related volcanic suites (e.g. Hobden et al., 1999; Gamble et al., 1999; Dungan et al., 2001; Turner et al., 2003) is hardly surprising, and, coupled with the observed variations in isotope and incompatible trace element ratios, attests to the important role of open-system processes such as crustal contamination, magma mixing and recharge. Nevertheless, there are general trends in the major element data which most likely reflect persistent control by crystal-melt fractionation/ accumulation processes. Indeed the presence of phenocrysts and cumulate blocks shows that crystallisation has occurred and, until proven otherwise, it seems sensible to explore the degree to which the observed crystal phases might control compositional variations. Binary extract diagrams, on which the trends of the lavas are plotted relative to the compositions of potential fractionating minerals, show that plagioclase is a ubiquitous fractionating phase along with some combination of orthopyroxene, clinopyroxene, amphibole and olivine (opx±cpx±amph±ol; Fig. 8). The absence of inflections in the major element data trends indicates that there are no sudden modal abundance changes in the fractionated mineral assemblage (Fig. 6), i.e. we can treat the trends as simple two-component un-mixing trends. The appearance of plagioclase, for example, commonly generates humped Al_2O_3-SiO_2 trends in arc suites, whereas Al_2O_3 consistently decreases with SiO_2 here (Fig. 6a) within the range of compositions sampled. Using an Excel-based version of XTLFRAC (Stormer and Nicholls, 1978) and a crystal extract of plagioclase, amphibole and Fe-Ti

oxide (magnetite – ilmenite do not give good fits) we have applied least squares modelling (Table 3) between selected pairs of samples from both Mt Pelée and the Quill which give very good fits ($\Sigma R^2<0.2$). In general, amphibole is more abundant than plagioclase in the modelled extracts and changing the composition of the amphibole (using the range of published data for Mt. Pelée) does not significantly alter the results. Using more sodic plagioclase deteriorates the fit and increases the proportion of plagioclase to amphibole. Adding clinopyroxene, orthopyroxene or olivine as a fourth fractionating phase does not significantly change the ratios of plagioclase to amphibole to oxide, or the quality of the fit (any small improvements are most likely due to reducing the degrees of freedom by adding a 4th phase). Good least squares fits ($\Sigma R^2<0.2$) can also be achieved using the observed phenocryst assemblage of cpx+opx+plag+mt, although the fits (as expressed by the sums of the squares of the residuals) are not improved over the cumulate plutonic nodule mineral suite, even with the addition of an extra phase. Smith and Roobol (1990) reported excellent least squares fits ($\Sigma R^2\sim0.01$) for a 5 phase assemblage at Mt. Pelée comprising plagioclase and amphibole in roughly equal proportions, along with lesser amounts of clinopyroxene, magnetite and olivine.

Model vectors are plotted on Fig. 6 (solid lines) to show the effect of extracting the amph-plag-mt assemblage which gives a good least squares fit in Table 3. These vectors are compared with vectors which illustrate the effects of extracting the *petrographically observed* mineral assemblage (dashed lines) which is dominated by plagioclase with subordinate pyroxene, olivine and Fe-Ti oxide. This is not the same as the inferred phase assemblage for reasonable fit least squares models involving olivine and pyroxene (rather

than amphibole). It is notable that crystal fractionation involving the petrographically observed assemblage is unable to reduce MgO or TiO_2 abundances by the amounts observed with progressive differentiation, and it reduces Al_2O_3 and CaO contents more than is observed. Fractionation of up to 50% of a cumulate assemblage dominated by plagioclase and amphibole can therefore explain the major element data well (cf Fig. 8), even though the major element data alone cannot unambiguously distinguish between control by the cumulate mineral assemblage versus the observed phenocryst suite.

Trace elements

In a broad sense variations in trace element abundances are consistent with the fractionation models suggested from the major element data. Compared with the major element data, the incompatible trace element data suggest a comparable amount of fractionation, given that the concentrations of many incompatible trace elements increase by a factor of ~2 over the range from basaltic andesite to dacite, (Fig. 6) which corresponds to 50% fractionation with D_i (bulk liquid/solid partition coefficient) = 0. Elements which are compatible in Fe-Ti oxides (V) or mafic phases such as olivine, pyroxene and amphibole (Ni, Cr, Sc) all decrease with progressive differentiation. Indeed the uniformly low Ni and Cr contents suggest extensive fractionation has occurred from any likely primary magma composition that could have been in equilibrium with the mantle. Plagioclase fractionation is consistent with the slight decrease in Sr content with differentiation – except for a subset of the Quill data which shows a slight increase in Sr abundance between 56 and 60% SiO_2 (Fig. 7e). Interestingly this subset includes rocks

from both of the stratigraphic sections and is not obviously linked to any petrographic distinctions and is not apparent in any other chemical diagrams.

A role for amphibole as a major fractionating phase is supported by the REE patterns of samples from Mt. Pelée and the Quill (Fig. 9). Both volcanoes exhibit concave-up chondrite-normalised REE patterns (Mt. Pelée more strongly so than the Quill), consistent with removal of amphibole (Bottazzi et al., 1999), which typically has a complementary concave-down REE pattern. This conclusion is emphasised by the negative correlation between Dy/Yb and SiO_2 shown in Fig. 10d, which reflects the preferential partitioning of MREE over HREE by amphibole (Davidson et al., 2007). If amphibole is indeed important in controlling the major element trends, it is likely that magma compositions are controlled by amphibole fractionation in the mid/deep arc crust, with magmas bearing the imprint of such fractionation subsequently ascending to shallow-level magma storage reservoirs above the depth of amphibole stability. In the shallow storage systems orthopyroxene and clinopyroxene are stable and crystallise. Any amphibole entrained in the ascending magma would be quickly resorbed (Rutherford and Hill, 1994). Although the crustal thicknesses beneath Mt. Pelée and the Quill are not well known, crustal thicknesses along the arc have been typically estimated at 25-30 km (Sevilla et al., 2010), which are consistent with pressures well within the amphibole stability field (e.g. Alonso Perez et al., 2009).

Model trace element fractionation trends are included in Figs. 7 and 10. These are based on a likely parent magma from Mt. Pelée M8236, one of the most mafic

compositions with 5% MgO, and use the set of mineral/melt distribution coefficients (***Kd***$_i$) compiled from the literature in Table 4a. Two models are shown; 1) (solid line) using a cumulate phase assemblage based on the modal abundances of minerals in the cumulate blocks – which in turn reflects those used in the least squares modelling of Tables 3a and b, and 2) (dashed line) using the modal phenocryst assemblage as determined by point counting of M8236. Both models fail significantly in some cases (e.g. Sr, Dy/Yb) to reproduce the observed data. There may be several reasons for this; 1) the whole-rock compositions do not necessarily represent liquid compositions, 2) the crystal cargo is not in equilibrium with the host liquid, 3) the chosen ***Kd***s may not be appropriate. Unfortunately there exists no self-consistent set of distribution coefficients appropriate for intermediate magma compositions for all the trace elements and minerals of interest. We end up having to mix Kd data sets, which may not matter much when the elements are highly incompatible (***Kd***~0) but becomes critical when ***Kd*** values are significant, yet poorly constrained, and 4) we know from the available isotopic data that the samples are not related by closed-system fractionation. It is possible that some trace elements are especially sensitive to modification by crustal contamination.

An alternative approach to simply selecting distribution coefficients from the literature, albeit judiciously, is to calculate what they *need to be* to produce the incompatible element enrichments observed. This can be done using the Rayleigh fractionation equation;

$$\frac{c_l}{c_0} = F^{(D_i - 1)} \qquad \text{eqn. 1}$$

where c_l = concentration of element ***i*** in the differentiated liquid, c_0 = concentration of element ***i*** in the starting (parent) liquid, D_i = the bulk mineral melt distribution coefficient (i.e. mineral-melt ***Kd***s weighted by mineral abundances) and ***F*** = fraction of remaining liquid (so that [1-***F***]x100 = % fractionated). For Mt. Pelée if we take the parent-daughter pair M8236-M8237, Rb is the element that shows the greatest enrichment. From Table 1 we can see that the minimum concentration of Rb is 10 ppm (c_0) and the maximum is 31 ppm (c_l). The enrichment factor is c_l/c_0 = 3.1. If we assume that Rb is perfectly incompatible (D_{Nb} = 0) then equation (1) reduces to $c_l/c_0 = 1/F$. In this case ***F*** = 0.32, corresponding to 68% fractionation. We can then use the enrichment factors of the other incompatible trace elements to calculate their respective bulk D_is. These are listed in Table 4b for both Mt. Pelée and the Quill. Note we could perform a similar set of calculations using the ***F*** values (maximum ~ 0.5) determined by least squares calculations in Tables 3a and b. In this case the most incompatible elements give negative (invalid) D_is. Clearly the distribution coefficients are not precisely defined, in part because of the open-system processes alluded to above. Furthermore there are problems with elements such as Rb for the Quill for which the concentration is determined by XRF as an integer value, but changing it by just 1 ppm would change the distribution coefficient by ~ 30%. The *relative* magnitudes of the distribution coefficients are, however, consistent with the phases implicated from the least squares calculations (with D_{MREE} and D_Y ~ 1 consistent with amphibole involvement, and D_{Sr} >1 in both cases, consistent with plagioclase fractionation).

When the inferred $\mathbf{D_i}$ values (Table 4b) are compared with those calculated using data compiled from the literature for the observed phenocrysts and cumulate extracts (Table 4a) we can see that the inferred $\boldsymbol{D_i}$s are considerably higher than those from the literature compilation (Fig. 10). This may reflect an inappropriate choice of literature values (e.g. Claeson and Meurer (2004) choose much higher $\boldsymbol{Kd_i}$s for hydrous arc basalts for the same mineral phases considered here). Alternatively, the inferred $\boldsymbol{D_i}$s may be too high if some of the incompatible trace element enrichment is due to crustal contamination rather than simply fractional crystallisation. If, for instance, the "true" enrichment factor for the element showing the most enrichment was lower, then the value of $\boldsymbol{F}$ obtained assuming $\boldsymbol{D_i} = 0$ would be higher and the inferred $\boldsymbol{D_i}$s for the other elements would be lower than those indicated in Table 4b. In either case though, when we compare the *relative* values of D_is, the amphibole-bearing cumulate assemblage is a better fit to the inferred values than the amphibole-free phenocryst assemblage (Fig. 11).

Recent research (Handley et al., in press; Woodhead et al., in press) has called attention to the origin of hafnium anomalies (Hf/Hf*) in primitive mantle normalised trace element variation diagrams. The Hf anomaly is broadly analogous to the well-known Eu anomaly that may be present in REE patterns related to the addition or subtraction of plagioclase. It is calculated by comparing the measured Hf concentration with the value interpolated from the neighbouring elements Nd and Sm on a log-normalised trace element diagram such as Fig. 12. Hf anomalies have commonly been attributed to mantle source characteristics; however, Handley et al. (in press) and Woodhead et al. (in press) both point out that within arc suites from individual volcanoes

Hf/Hf* commonly correlates with SiO_2, suggesting that Hf anomalies can develop or be modified during magmatic differentiation, likely controlled by clinopyroxene fractionation. Figure 10e shows that Hf/Hf* correlates positively with SiO_2 for both Mt. Pelée and the Quill, although neither the cumulate nor phenocryst phase assemblages are capable of increasing Hf/Hf* sufficiently using the distribution coefficients reported in Table 4a. Nevertheless given our arguments that Dy/Yb is controlled mainly by amphibole, the correlation between Hf/Hf* and Dy/Yb (Fig. 10f) suggests that it could be amphibole rather than clinopyroxene that may be driving up Hf/Hf*.

Incompatible trace element data do not distinguish well between the different potential fractional crystallisation assemblages. While the involvement of amphibole is required to reduce Dy/Yb (Figs. 7f and 10d), the same cumulate assemblage is unable to reduce Sr with progressive differentiation as observed (Fig. 7e). For elements that are highly incompatible (e.g. Th, Hf, Ba, La; Fig. 7a-d) the fractionation vectors do not reproduce the observed enrichment with progressive differentiation. The generally poor fits of the models to the observed data may in part reflect the absence of well-constrained complete suites of mineral-melt distribution coefficients (Table 4a), although it must also partly reflect the open-system nature of the differentiation process as discussed below.

Based on the above we conclude that the differentiation trends are broadly similar at the two volcanoes and therefore that the P, T, H_2O crystallisation conditions at Mt Pelée and the Quill are comparable, and consistent with amphibole and plagioclase stability.

CONSTRAINTS ON CRYSTALLISATION CONDITIONS

Cumulate xenoliths – constraints on differentiation conditions in the deep crust

Cumulate plutonic blocks/nodules occur in most of the islands of the young volcanic arc (< 7.5 Ma; Powell, 1978; Arculus and Wills, 1980). Mineralogically they contain some or all of the phases ol±opx±cpx±plag±amph±mt. The larger blocks (> 50 cm) are typically banded, providing strong evidence that their protoliths were the product of crystal accumulation in crustal magma chambers. In many of the nodules olivine, plagioclase and clinopyroxene (±opx ± Fe-Ti oxide) are in apparent textural equilibrium, suggesting that they crystallised contemporaneously from the magma. Amphibole, in contrast, is not always a cumulus phase and in some cases overgrows and partially replaces the clinopyroxene, suggesting that it crystallised from trapped intercumulus liquid. Biotite, quartz, apatite and ilmenite also occur in the more evolved cumulates. Plagioclase (An_{100-36}) and amphibole dominate the mineral assemblage and plagioclase usually appears to have crystallised before amphibole. Olivine (Fo_{90-59}) is restricted to assemblages where plagioclase is more anorthitic than An_{89}. Orthopyroxene is more common when the associated plagioclase is more sodic than An_{83}.

Thermo-barometry calculations constrain the crystallisation conditions of the nodules to 3-10 kb pressure, 850 – 1050 ºC and oxygen fugacities from NNO+1 to NNO+2 (Powell, 1978; Arculus and Wills, 1980). These temperatures are probably underestimated as a result of subsolidus re-equilibration. A cumulate block from Statia

with the mineral assemblage ol-cpx-opx-plag-amph-mt was considered by Arculus and Wills (1980) to have equilibrated at 6 kb pressure and 1000 ºC.

Experimental studies – constraints on magmatic differentiation

As indicated by the data in Table 1 and Fig. 5, the most primitive mafic magmas sampled from Mt. Pelée and the Quill have less than 5 wt % MgO; consequently these magmas must themselves be derived from a more mafic precursor by higher pressure fractional crystallisation, probably in the deep crust.

Pichavant and Macdonald (2007) conducted crystallisation experiments on a high-MgO (12.5 wt. % MgO; 47 wt. % SiO_2) basalt from the island of St. Vincent which may provide a reasonable proxy for the composition of the near primary magma generated in the mantle wedge beneath the arc. Pichavant et al. (2002) suggested that a primary magma of this composition may have an H_2O content of ~ 5.5 wt %. Under pressures (~10 kb) appropriate to those in the deep crust and under H_2O-saturated conditions (~ 10 wt % H_2O), amphibole in equilibrium with clinopyroxene and magnetite is stabilised close to the liquidus of this basalt. At lower pressures (~ 4 kb) more appropriate for the mid-crust amphibole is, however, no longer stable; instead olivine is on the liquidus followed by clinopyroxene and plagioclase.

Müntener et al. (2001) demonstrated the important role for H_2O in the crystallisation of primitive arc magmas, concluding that increasing the H_2O concentration in the melt changes the crystallisation sequence. They conducted experiments on an arc

basalt with 10.8 % MgO and 52 % SiO_2 under water-undersaturated conditions (2.5 to 5 wt % H_2O) at 12kb pressure. Low H_2O contents stabilise plagioclase before amphibole and garnet, whereas higher H_2O (>3 wt %) contents suppress plagioclase crystallisation in favour of amphibole and garnet. Garnet is not found in any Lesser Antilles cumulates and garnet fractionation would increase Dy/Yb with differentiation (whereas the reverse is seen in Fig. 9d), so we conclude that depths of differentiation are shallower than those of garnet stability. At temperatures greater than 1050 °C hydrous phases (i.e. amphibole) are not stable on the liquidus of primitive arc magmas.

Müntener et al. (2001) emphasised that the timing of plagioclase saturation exerts a strong control on the Al_2O_3 content of the derivative liquids and that suppression of plagioclase in favour of ferromagnesian minerals provides an important control on the development of calc-alkaline differentiation trends. Pichavant et al. (2002) note that the water content of the melt influences how easily it can rise to the surface; more hydrous magmas will tend to pond and differentiate in the deep crust.

The role of amphibole fractionation in controlling magmatic differentiation trends in island arcs can be explained in terms of phase equilibria in the system CaO-MgO-Al_2O_3-SiO_2-Na_2O under water-saturated conditions (Fig. 13, after Cawthorn and O'Hara, 1976). This diagram can be used to provide a clear explanation for the range of modal mineralogies and textures observed in the Lesser Antilles cumulate xenoliths, emphasizing the important role of amphibole in controlling magmatic differentiation processes in the deep crust. In the context of Fig. 13 an arc basalt of composition **B**

would first crystallize olivine and clinopyroxene, driving the residual liquid towards point **C** where the olivine and clinopyroxene react with the liquid to produce amphibole. Under equilibrium crystallization conditions the liquid then migrates along the ol-cpx-amph-liquid-vapour curve (**CD**) precipitating amphibole. Olivine and clinopyroxene remain in reaction relation with the liquid until they are completely consumed at point **D** (the intersection of the line projected from the amphibole composition A through the basalt composition B). With further crystallization the liquid precipitates amphibole alone and migrates through the amphibole stability volume along the line **DE**, eventually reaching the orthopyroxene stability field. Point **E** corresponds to a typical andesite composition.

Under fractional crystallization conditions liquids of composition **C** will crystallize amphibole only and migrate through the amphibole volume away from **A** along the line **CF**. Once the liquid begins to crystallize plagioclase as well as amphibole the projection is technically no longer valid (Cawthorn & O'Hara, 1976). However it is clear that co-precipitation of amphibole plus plagioclase will produce liquids trending towards andesitic compositions (~**E**).

Cawthorn & O'Hara (1976) created the schematic phase diagram (Fig. 13) based upon experimental data at 5 kb pressure. However they suggested that the relative stabilities of olivine, pyroxene and amphibole should be fairly insensitive to pressure changes in the range 2 to 10 kb (i.e. down to the base of the Lesser Antilles crust). At pressures greater than 5 kb the amphibole stability field may expand slightly at the expense of olivine and clinopyroxene; conversely at lower pressures a smaller amphibole

field is likely. The stability of amphibole is sensitive to both total pressure and the partial pressure of water; however the relative stabilities of the phases are unlikely to change significantly under water-undersaturated conditions.

Water contents of the magmas

Pichavant and Macdonald (2007) empirically regressed the Al_2O_3 contents of experimental, plagioclase-saturated, hydrous mafic liquids (SiO_2 < 55 wt %) as a function of the melt H_2O content to produce a geohygrometer applicable to arc basalts. The regression does not include a pressure term as most of the calibrating experiments were at pressures < 4 kb. Application of the geohygrometer to the mafic rocks listed in Table 1 gives H_2O contents in the range 3.1 to 4.5 wt % for Mt. Pelée and 4.0 to 4.6 wt % for the Quill, assuming a temperature of crystallisation of 1050 ºC. Such H_2O contents are consistent with extensive amphibole crystallisation in deep crustal magma reservoirs.

TRACE ELEMENTS, ISOTOPES AND OPEN SYSTEM DIFFERENTIATION

The trace element trends shown in Fig. 7 highlight greater differences between the Quill and Mt. Pelée than do the major element plots in Fig. 6. The differences are further emphasised for some incompatible trace element ratios; for example Th/La and Th/U are higher for the Mt. Pelée samples, while Ba/La is lower and none of these ratios change significantly with progressive differentiation (Fig. 10). This is largely a reflection of the sensitivity of trace elements to open-system processes, and to variations in distribution

coefficients. Incompatible trace element distribution patterns (Fig. 12) show that: (1) the most mafic samples (parental lavas in Fig. 12a) have typical subduction-related characteristics, with relatively high LILE (K, Rb, Ba, Pb, Sr) and low HFSE (Nb, Ta); (2) the differentiates (derivative lavas in Fig. 12b) exhibit largely comparable patterns to their parents, albeit at higher absolute abundances. Specific distinctions in the trace element patterns between the two volcanoes, such as Th/U, are propagated through from mafic progenitors to differentiates (see also Fig. 10).

Figure 12c compares parent-daughter compositions directly (by normalising daughter to parent). From this it can be clearly seen that most elements, except for Sr and the MREE which are sequestered into plagioclase and amphibole respectively, behave incompatibly. Although some elements (Nb, Pb, K, Th, U) appear to change little between parent and daughter for the Quill sample pairs, the general trend for all the data for these elements is to increase with differentiation (i.e. incompatible behaviour). Similarly, what appears to be unusual behaviour for Zr in the Mt Pelée samples, with relatively low Zr in the two parent samples plotted, is not evident for the Mt Pelée data suite as a whole, which shows a simple positive trend for Zr against SiO_2, overlapping that defined by the Quill samples (not shown).

We know that the trace element abundances cannot be entirely controlled by crystal-melt fractionation because: (1) some highly incompatible elements increase by a factor of >2 with progressive differentiation, which would require >50% fractionation ($F<0.5$, as in Table 4b), far more than the major element models of Tables 3a and b which

indicate F>0.5, and (2) radiogenic isotope ratios vary with differentiation (Fig. 14), an effect which cannot be achieved by simple crystal fractionation (or melting) processes.

Mt. Pelée and the Quill are each distinctly different in terms of their Sr, Pb, Nd and Hf isotope ratios (Table 1, Fig. 15). Although there are significant variations within each suite, these are small relative to the extreme range of values seen in the Lesser Antilles arc as a whole. Both $^{87}Sr/^{86}Sr$ and $^{206}Pb/^{204}Pb$ vary with differentiation (more so at Mt. Pelée than at the Quill; Fig. 14) suggesting that the isotopic compositions of the primitive/parental magmas have been changed by open-system differentiation processes.

The young ages and freshness of the samples allows us to investigate oxygen isotope variations from mineral samples (Table 2). $\delta^{18}O$ values are within the range of magmatic differentiates and do not include the high values characteristic of some other rocks on Martinique (Davidson and Harmon, 1989). $\Delta^{18}O$ for mineral-mineral pairs generally correspond to magmatic fractionation temperatures ($\delta^{18}O_{plag} > \delta^{18}O_{cpx}$), and $\delta^{18}O$ for a given mineral correlates, albeit weakly, with the whole-rock Nd and Sr isotope ratios.

The differences in isotopic and incompatible trace element ratios can be used to constrain the origins of the magma suites at Mt. Pelée and the Quill. Firstly it is clear that the parent magmas at the two volcanoes are significantly different. Back-projection of the differentiation trends at each volcano does not converge on a common parent magma. Indeed some incompatible trace element ratios (such as Th/U and Ba/La; Fig. 10) are

relatively constant at each volcano and therefore the trends are sub-parallel and never converge.

It is possible that the earliest stages of differentiation (i.e. generating a basalt/basaltic andesite parental magma from a primitive basalt) are different between the two volcanoes, as illustrated schematically in Fig. 1b. This is a distinctly unsatisfying explanation as there are no samples representing this stage of differentiation. It is also very unlikely; among primitive low-SiO_2 magmas bulk distribution coefficients are likely to be low (~0) and provide very little leverage for fractionating incompatible element ratios from each other. It is difficult, for example, to envisage a basaltic mineral assemblage capable of fractionating Th/U by a factor of ~2, as would be required to generate the distinct compositions of Mt. Pelée and the Quill respectively (Fig. 10b). Even if open-system processes are implicated to explain the significant differences in the early stages of differentiation, we would have to appeal to special pleading. We have shown (e.g. Fig. 14) that open-system processes are likely to have influenced magma compositions at both Mt. Pelée and the Quill. A crustal contaminant is clearly needed; peraluminous magmas such as the garnet-bearing dacite on Martinique with extreme crust-like isotopic compositions could represent anatectic melts of such a contaminant (Davidson and Harmon, 1989). However, if crustal contamination is also responsible for the diverging cryptic fractionation trends from a hypothetical common parent (as in Fig. 1b) then one or more additional contaminants, with different isotopic compositions would be required. A more likely explanation is that the primary magmas introduced into the crustal magma systems at Mt. Pelée and the Quill are different (Fig. 1c), implying that

different mantle source compositions and even magma generation processes occur along the subduction zone. This concept is explored further below.

SOURCE CONTRIBUTIONS TO MAGMAS ALONG THE LESSER ANTILLES

Once the effects of magmatic differentiation within the arc crust have been accounted for, we can explore why the parental, and by inference the primary, magmas are different between Mt. Pelée in the central part of the arc and the Quill in the northern part. Along-arc studies have argued that the contribution of subducted sediments increases southwards along the arc (White and Dupre 1986; Turner et al., 1996). The Lesser Antilles is one of the few arcs for which there is a well-constrained record of the sediment inventory entering the trench, with a series of piston-core samples representing the more recent sediments over a wide geographic area, and two DSDP sediment cores representing the long-term (since the Cretaceous) sediment record outboard of the arc (White et al., 1985; Davidson, 1987; Carpentier et al., 2008). White and Dupre (1986) and, more recently, Labanieh et al. (2010) have shown how isotopic compositions of Lesser Antilles magmas can, in principle, be reproduced by mantle-sediment mixtures. There have been two arguments levied against the concept that Lesser Antilles magmas represent the melting products, or differentiates thereof, of simple mantle source + sediment mixing (see Thirlwall and Graham, 1984; Davidson, 1987). The first is that, in terms of Pb isotopes, the most radiogenic lavas analysed are actually more radiogenic than the most radiogenic sediments. The second is that that correlations between isotope ratios and indices of differentiation imply that at least some of the isotopic variation is

acquired during magmatic differentiation in the crust, as seems to be the case at the Quill and Mt Pelée (Fig. 14). Figure 16 shows the Quill and Mt. Pelée Pb-Sr isotope data along with model mixing lines between mantle and a range of potential subducted sediments. Given that we have shown that the isotopic variation with magmatic differentiation is an open-system intra-crustal feature, our task with these models is simply to reproduce the parental (most mafic) magma compositions rather than the entire data trends. This can be achieved by mixing between a fluid-modified mantle wedge source and a common sediment from site 543, with more sediment added to the source of the Mt. Pelée parent magmas than to that of the Quill parents, *or* by mixing different sediment compositions into the mantle source of Mt Pelée and the Quill respectively, in which case they could be different amounts (Fig. 16). In principle our models are consistent with those which argue for an along-arc variation in the sediment contribution to the mantle source. When tested in detail, however, such a model begins to show flaws. Figure 16b shows isotopic data from all of the Lesser Antilles arc. Although the most radiogenic Pb isotopic compositions from the arc can now be reproduced using the new sediment data from DSDP site 144 (Carpentier et al., 2008), we note that many of these samples are highly differentiated and have high (crust-like) $\delta^{18}O$ values (Davidson & Harmon, 1989). Simple mixing of sediment and mantle will also not reproduce some trace element ratios such as Ba/La. This ratio does not vary with differentiation (Fig. 10) yet the parental magmas at both the Quill and Mt. Pelée have higher Ba/La than any local sediment-mantle mixture. The most likely explanation here is that Ba has been added to the mantle wedge (along with Sr) in slab-derived fluids.

In the absence of a complete consideration of the data presented earlier, it would be tempting to ascribe all of the isotopic variation in the two suites in terms of variable mixing of subducted sediment into their respective mantle sources. After all, the mixing lines on Fig. 16 can be made to pass through the data arrays. However, we must remember that the isotopic ratios correlate with SiO_2 (Fig. 14). If the isotope data were simply due to sediment mixing in the source then a mechanism would need to be identified whereby the source with the least contamination produces magmas which go on to differentiate to a limited extent, whilst the source with the most contamination produces magmas which subsequently differentiate most extensively. It is difficult to conceive of a mechanism which effectively pre-ordains the extent of differentiation as a result of the amount of sediment added to the mantle source.

An important element of our study is to establish a systematic and integrated approach to geochemical/ petrological data sets for volcanic suites which can allow us to account for crustal-level differentiation processes and to filter these before trying to evaluate mantle source processes and components. The different parent magmas which appear to supply the crustal magma systems at Mt. Pelée and the Quill (e.g. Fig. 10, 12) can be explained by along-arc differences in the primitive/ primary magma compositions, which in turn reflect differences in the slab component added to the mantle wedge. Previous studies have suggested that this variation is systematic along the arc, with increasing sediment and decreasing fluid additions from north to south (e.g. Turner et al. 1996). This model can be tested using our approach by comparing primitive/ primary magma compositions from along the arc. We have extended the comparative exercise to

include more volcanoes from along the arc for which there are substantial published data sets. In each case, as for Mt. Pelée and the Quill, we have back-extrapolated differentiation trends to putative primitive magma compositions. We do not know what a truly primary magma composition would be, but it is likely to have in the region of 47-50 wt. % SiO_2 and choosing any value in this range will not alter the conclusions from Fig. 17. We suggest that 48% SiO_2 is a reasonable estimate of the SiO_2 content of a primary arc magma (e.g. Nye and Reid, 1986; Bacon et al., 1997). The extrapolation is then simply of the form;

$$\boldsymbol{C_i} = 48\boldsymbol{M} + \boldsymbol{C_0} \qquad \text{eqn 2}$$

where $\boldsymbol{C_i}$ is the concentration of element $\boldsymbol{i}$ (or indeed isotope ratio) at 48 wt % SiO_2 and $\boldsymbol{M}$ is the slope of the trend of $\boldsymbol{i}$ versus SiO_2. This approach assumes that the trend is approximately linear, which appears to be the case for most elements, at least in the range SiO_2>52 wt %, as shown in Figs. 6, 7 and 14. For compatible elements such as Ni and Cr the approach is unlikely to be valid, especially if significant olivine fractionation has occurred the from primary magmas.

Figure 17 shows primitive magma compositions from five volcanoes along the arc, extrapolated to 48 wt. % SiO_2, as explained above, based on published data. There is a tendency for $^{87}Sr/^{86}Sr$ and $^{206}Pb/^{204}Pb$ to increase southwards, consistent with claims that the sediment contribution increases southwards. However, this trend is not reproduced for La/Yb, Ba/La, Th/La or K_2O, and the three closely-spaced volcanoes in the north of the Lesser Antilles arc show significant variations over a distance of just a few tens of

kilometres. Our analysis therefore does not support a simple, systematic along-arc variation in the slab component(s) contributed to the mantle wedge.

A global analysis of sediment contributions to arcs was presented by Plank (2005), who suggested that the trace element compositions of basalts from the Lesser Antilles could be reproduced by mixing the observed sediment compositions from locations outboard of the arc with a MORB-source mantle component. Figure 18 shows the Th/La versus Sm/La variations among the Mt. Pelée and the Quill samples along with Plank's (2005) analysis. The principle of this analysis was to regress the compositions of Lesser Antilles basalts, which extrapolated to the known compositions of the sediments on the one hand, and to the composition of the unmodified mantle on the other (defined by the intersection between the basalt trend and the field of MORB). For Mt. Pelée and the Quill such an analysis fails. Mt. Pelée is characterised by higher Th/La than the Quill at a given Sm/La value. The trends defined by extrapolation through the parental magmas (stars in Fig. 18) actually cross-cut that of mantle-sediment mixtures (grey band) and do not extrapolate to realistic sediment or mantle compositions. If the parental magmas at the Quill and Mt. Pelée were formed by simple sediment-source mixing, then such mixtures should fall in the grey band shown in Fig. 18 and (1) the implied mantle source composition is more depleted than that of Plank (*op. cit*.) at Sm/La ~1.2, and (2) different sediment compositions are required to be mixed with the mantle to form the Mt. Pelée and the Quill parents respectively. Specifically Mt. Pelée requires a much higher Th/La sediment component to be mixed into its mantle source. This constraint, when applied to Fig. 16, suggests that the sources of the two volcanoes cannot then be produced by

mixing different amounts of the same sediment, but must rather be due to mixing of compositionally different sediment components. Alternatively, simple mixing should be rejected as unable to adequately satisfy the mixing relations, in which case we would need to consider the next degree of complication, specifically mixing with fluids or sediment melts or indeed partitioning into supercritical fluids.

Figure 19 shows the relative effects of sediment and fluid mixing with a depleted mantle source. It is not meant to be quantitative as nearly all the input parameters to the calculations – the starting compositions and their variability, the distribution coefficients, the melting mechanisms and whether the sediment is added in bulk or as a partial melt – are open to challenge. Nevertheless there are some general conclusions that can be drawn. Figure 19a shows the effects of mixing sediment into a depleted MORB-source mantle wedge (DMM). Given that the concentrations of incompatible trace elements are orders of magnitude higher in the sediment than in the mantle peridotite, even small additions (<1%) produce a source with a normalised trace element pattern resembling that of the sediment. Additions of more than ~5% sediment produce a source which has concentrations of some elements greater than those of the parental magmas. Since concentrations in the melt will be higher than those in the source (and higher for smaller degrees of melting) this indicates that any sediment addition to the mantle wedge must be <5%. Further constraints are provided by the isotopic data; the isotopic compositions of Pb, Nd and Sr in the parental Mt. Pelée magmas can be reproduced by simple mixtures of ~0.2%, 0.5% and 0.7% sediment respectively (the comparable amounts for the Quill are ~ 0.1%, 0.1% and 0.5%). For comparison, DuFrane et al. (2009) suggest, on the basis of U-

series data, a range of 0.2-2% bulk sediment addition for the Lesser Antilles in general. From the discussion above we suggest that simple bulk sediment mixing is not a satisfactory model, and that fluid may also be needed. This possibility is explored in Fig. 19b, for which a sediment-modified mantle is melted. We select DMM + 0.5% sediment since this reproduces the Nd isotope composition of the Mt. Pelée parent. Distribution coefficients for the source are taken from Workman and Hart (2005) and simple modal batch melting is used, with melt % increased until all elements fall at or below the concentrations in the parent magma. This value is ~20% melting (with lower percentages overshooting the parent concentrations). The deficit elements when the melt model and the parent are compared might then be assumed to be added via fluid. On this basis the HFSE Zr, Ta and Nb are all provided by the sediment, with all other elements added in variable amounts by the fluid. The greatest fluid additions are for the elements that we might expect to be the most fluid-mobile, especially the LILE. There are, however, additional caveats: (1) in order to satisfy the isotopic constraints, fluid additions of Sr and Pb cannot be from the sediment but rather must be from the less radiogenic oceanic crust and (2) elements such as Th and HREE, the fluid mobility of which are a subject of debate, appear to be fluid-mobile. A similar exercise can be repeated for the Quill parental magma, with similar results (similar overall pattern on Fig. 19a). Thus the general conclusion is that both fluid and sediment contributions are needed to reproduce the source of the Lesser Antilles primary magmas. In detail we recognise several potential flaws in this simplistic model – which preclude confidence and provide justification for more sophisticated treatments. The amount of sediment added to the source is, for instance, predicated on the basis of reproducing the Nd isotopic

compositions. However, the model melt of this source does not reproduce the Nd concentrations and requires some contribution from slab fluid – which presumably would have a different isotopic composition. We also recognise that bulk sediment mixing is simplistic and that a sediment melt or a supercritical fluid might be more realistic; however, in such a case the trace element distribution coefficients are not constrained and may have a profound influence over trace element behaviour, especially where accessory minerals are involved (e.g. Hermann and Rubatto, 2009). We can speculate that sediment melting might involve preferential sequestering of HFSE (in rutile or titanite for instance; Spandler et al., 2003). In such a case the model in Fig. 19b would be satisfied by lower degrees of melting (<20%), and the amount of fluid needed would be less because the pattern of DMM + sediment melt would be closer to that of the parental magma.

CONCLUSIONS

Comparison of magmatic suites from the northern (the Quill) and central (Mt. Pelée) Lesser Antilles arc allows us to conclude:

1. Both suites are controlled by crystal-liquid differentiation, driven largely by amphibole, plagioclase and magnetite fractionation. Although amphibole is rarely present in the lavas, it is common in associated cumulate blocks. This observation undescores the need to consider cryptic fractionation processes and not simply to use the observed petrography to constrain petrogenetic models.
2. Trace element data are consistent with major element fractionation models, although concomitant crustal contamination is indicated by a) overabundance of the most

incompatible elements compared with the models and b) variations in isotopic ratios of Sr and Pb with progressive differentiation.

3. Differentiation trends at the two volcanoes do not converge on a reasonable common parent. This suggests that the primary magmas are different at the two volcanic centres.
4. Differences in the primary magma compositions are related to variations in mantle source processes such as variable slab contributions along the arc. Some characteristics can be explained by varying the sediment contribution from north to south (increasing). However, when our approach of extrapolating to putative primitive magma compositions is used along the arc, the north-south variation is far from systematic.
5. Simple sediment-mantle mixing and subsequent melting of the modified source cannot reproduce the observed trace element and isotopic characteristics of the magmas, and additional considerations (addition of sediment melt rather than bulk sediment, and addition of fluid – probably supercritical) are needed.
6. Our approach and analysis argues that to constrain along-arc source variations it is first necessary to understand the petrogenesis of individual volcanoes, for which differentiation trends can be confidently extrapolated.

ACKNOWLEDGEMENTS

Chris Ottley and Geoff Nowell provided the trace element and Pb isotope data from NCIET, Durham. Hf data were produced by Matt Penfold as part of a 4th year undergraduate dissertation. Debbie Barr, Nevine Boghossian and Peter Holden were

instrumental in providing isotope data at UCLA, where funding was provided by NSF and UCLA. The original work was funded as a NERC studentship at the University of Leeds. Thorough reviews by Richard Price, John Foden and two anonymous reviewers are greatly appreciated and have substantially improved the manuscript.

REFERENCES

Aignertorres, M., Blundy, J., Ulmer, P. & Pettke, T. (2007). Laser Ablation ICPMS study of trace element partitioning between plagioclase and basaltic melts: an experimental approach. *Contributions to Mineralogy and Petrology* **153**, 647-667

Alonso-Perez, R., Müntener, O. & Ulmer, P. (2009). Igneous garnet and amphibole fractionation in the roots of island arcs: experimental constraints on andesitic liquids. *Contributions to Mineralogy and Petrology* **157**, 541–558.

Amante, C. & Eakins, B. W. (2009). ETOPO1 1 Arc-Minute Global Relief Model: Procedures, Data Sources and Analysis. NOAA Technical Memorandum NESDIS NGDC-24, 19 pp.

Arculus, R. J. (1976). Geology and geochemistry of the alkali basalt-andesite association of Grenada, Lesser Antilles. *Geological Society of America Bulletin* **87**, 612-624.

Arculus, R. J. & Wills, K. J. A. (1980). The petrology of plutonic blocks and inclusions from the Lesser Antilles island arc. *Journal of Petrology* **21**, 743-799.

Bacon, C. R., Bruggman, P. E., Christiansen, R. L., Clynne, M. A., Donnelly-Nolan, J. M. & Hildreth, W. (1997). Primitive magmas at five Cascades volcanic fields: melts from hot, heterogeneous sub-arc mantle. *Canadian Mineralogist* **35**, 397-424.

Bottazzi, P., Tiepolo, M., Vanucci, R., Zanetti, A., Brumm, R., Foley, S.F., & Oberti, R. (1999). Distinct site preferences for heavy and light REE in amphibole and the prediction of Amph/LDREE. *Contributions to Mineralogy and Petrology* **137**, 36–45.

Briden, J. C., Rex, D. C., Faller, A. M. & Tomblin, J. F. (1979). K-Ar geochronology and palaeomagnetism of volcanic rocks in the Lesser Antilles island arc. *Philosophical Transactions of the Royal Society of London* **A291**, 485-528.

Brown, G. M., Holland, J. G. ,Sigurdsson, H., Tomblin, J. F., & Arculus, R. J. (1977). Geochemistry of the Lesser Antilles volcanic arc. *Geochimica et Cosmochimica Acta* **41**, 785-801, 1977.

Carpentier, M., Chauvel, C. & Mattielli, N. (2008). Pb–Nd isotopic constraints on sedimentary input into the Lesser Antilles arc system. *Earth and Planetary Science Letters* **272**, 199–211.

Cawthorn, R. G. & O'Hara, M. J. (1976). Amphibole fractionation in cal-alkaline magma genesis. *American Journal of Science* **276**, 309-329.

Claeson, D. T. & Meurer, W. P. (2004). Fractional crystallization of hydrous basaltic ''arc-type'' magmas and the formation of amphibole- bearing gabbroic cumulates. *Contributions to Mineralogy and Petrology* **147**, 288–304.

Davidson, J. P. (1984). Petrogenesis of Lesser Antilles island arc magmas: Isotopic and geochemical constraints. Ph.D. thesis, University of Leeds, 308 p.

Davidson, J. P. (1986). Isotopic and trace element constraints on the petrogenesis of subduction-related lavas from Martinique, Lesser Antilles. *Journal of Geophysical Research* **91**, 5943-5962.

Davidson, J. P. (1987). Crustal contamination versus subduction zone enrichment: Examples from the Lesser Antilles and implications for mantle source compositions of island arc volcanics. *Geochimica et Cosmochimica Acta* **51**, 2185-2198.

Davidson, J. P. & Arculus, R. J. (2006). The significance of Phanerozoic arc magmatism in generating continental crust. In: Brown, M. & Rushmer, T. (eds*) Evolution and Differentiation of the Continental Crust.* Cambridge University Press, 135-172.

Davidson, J. P. & Harmon, R. S. (1989). Oxygen isotope constraints on the origin of volcanic arc magmas from Martinique, Lesser Antilles. *Earth and Planetary Science Letters* **95**, 255-270.

Davidson, J. P., Boghossian, N. D., & Wilson, B. M. (1993). The Geochemistry of the Igneous Rock Suite of St Martin, Northern Lesser Antilles. *Journal of Petrology* **34**, 839-866.

Davidson, J. P., Hora, J. M., Garrison, J. M. & Dungan, M. A. (2005). Crustal Forensics in Arc Magmas. *Journal of Volcanology and Geothermal Research* **140**, 157-170.

Davidson, J. P., Morgan, D. J., Charlier, B. L. A., Harlou, R. & Hora, J. M. (2007a) Microsampling and Isotopic Analysis of Igneous Rocks: Implications for the Study of Magmatic Systems. *Annual Reviews of Earth and Planetary Sciences* **35**, 273–311.

Davidson, J. P., Turner, S., Handley, H., Macpherson, C. & Dosseto, A. (2007b). An amphibole "sponge" in arc crust? *Geology* **35**, 787-790.

Defant, M. J., Sherman, S. Maury, R. C., Bellon, H., de Boer, J. Davidson, J. P. & Kepezhinskas, P. (2001). The geology, petrology, and petrogenesis of Saba Island, Lesser Antilles. *Journal of Volcanology and Geothermal Research*, **107**, 87-111.

Dufrane, S. A., Turner, S., Dossetto, A. & van Soest, M. (2009). Reappraisal of fluid and sediment contributions to Lesser Antilles magmas. *Chemical Geology* **265**, 272-278.

Dungan, M. A., Wulff, A. & Thompson, R. (2001). Eruptive stratigraphy of the Tatara-San Pedro Complex 36°S, Southern Volcanic Zone, Chilean Andes: Reconstruction method and implications for magma evolution at long-lived arc volcanic centers. *Journal of Petrology*, **42**, 555-626.

Font, L., Davidson, J. P., Pearson, D. G., Nowell, G. M., Jerram, D. & Ottley, C. J. (2008). Sr and Pb isotope micro-analysis in plagioclase crystals from Skye lavas: An insight into contamination processes in a flood basalt province. *Journal of Petrology* **49**, 1449-1472.

Fujimaki, H., Tatsumoto, M., & Aoki, K. (1984). Partition coefficients of Hf, Zr, and REE between phenocrysts and groundmasses. *Journal of Geophysical Research* **89**, 662–672.

Gamble, J. G. Wood, C. P., Price, R. C., Smith, I. E. M., Stewart, R. B. & Waight, T. (1999). A fifty year perspective of magmatic evolution on Ruapehu Volcano, New Zealand: verification of open system behaviour in an arc volcano. *Earth and Planetary Science Letters* **170**, 301–314.

Gill, J. B. (1981). Orogenic andesites and plate tectonics. New York: Springer-Verlag, 390 p.

Gunn, B., Roobol, M. J. & Smith, A.L. (1974). Petrochemistry of the Peléan-Type Volcanoes of Martinique. *Geological Society of America Bulletin* **85,** 1023-1030.

Handley, H. K., Turner, S. P., Macpherson, C. G., Davidson, J. P. & Gertisser, R. (*in press*) Hf-Nd isotope and trace element constraints on subduction inputs at island arcs: limitations of Hf anomalies as sediment input indicators. *Earth and Planetary Science Letters*

Hawkesworth, C. J., Gallagher, K., Hergt, J. M. & McDermott, F. (1993). Mantle and slab contributions in arc magmas. *Annual Review of Earth and Planetary Sciences* **21**, 175-204.

Heath, E., Macdonald, R., Belkin, H., Hawkesworth, C. & Sigurdsson, H. (1998). Magmagenesis at Soufriere Volcano, Lesser Antilles Arc. *Journal of Petrology* **39**, 1721-1764.

Herman, J. & Rubatto, D. (2009). Accessory phase control on the trace element signature of sediment melts in subduction zones. *Chemical Geology* **265**, 512-526.

Hobden, B. J., Houghton, B. F., Davidson, J. P. & Weaver, S. D. (1999). Small and short-lived magma batches at composite volcanoes: Time windows at Tongariro volcano, New Zealand. *Journal of the Geological Society of London* **156**, 865-867.

Irvine T. N, & Baragar W. R. (1971). A guide to the classification of the common igneous rocks. *Canadian Journal of Earth Sciences* **8**, 523-548.

Johnson, K. T. M. (1994). Experimental cpx/ and garnet/melt partitioning of REE and other trace elements at high pressures; petrogenetic implications. *Mineralogical Magazine* **58A**, 454–455.

Labanieh, S., Chauvel, C., Germa, A., Quedellar, X. & Lewin, E. (2010). Isotopic hyperbolas constrain sources and processes under the Lesser Antilles arc. *Earth and Planetary Science Letters, 298, 35-46*

Lacroix, A. (1908). La Montagne Pelée apres ses eruptions: Paris, Académie des Sciences, 136 p.

Macdonald, R., Hawkesworth, C. J. & Heath, E. (2000). The Lesser Antilles volcanic chain: a study in arc magmatism. *Earth Science Reviews* **49**, 1-76.

Mattey D. & Macpherson C. (1993). High precision oxygen isotope microanalysis of ferromagnesian minerals by laser-fluorination. *Chemical Geology* **105**, 305-318.

Miyashiro, A. (1974). Volcanic rock series in island arcs and active continental margins, *American Journal of Science*, **274**, 321-355.

Muntener, O., Kelemen, P. B. & Grove, T. L. (2001). The role of H_2O during crystallisation of primitive arc magmas under uppermost mantle conditions and genesis of igneous pyroxenites. *Contributions to Mineralogy and Petrology* **141**, 643-658.

Nowell, G. M., Pearson, D. G., Kempton, P. D., Noble, S. R., Carlson, R.W., Smith, C. B., Bell, D. R & Zartman, R. E. (2004). Hf isotope systematics of kimberlites and their megacrysts: New constraints on their source region. *Journal of Petrology* **45**, 1583-1612.

Nye, C. J. & Reid, M. R. (1986). Geochemistry of primary and least-fractionated lavas from Okmok Volcano, central Aleutians: Implications for arc magma genesis. *Journal of Geophysical Research* **91**, 10,271-10,287.

Ottley C. J., Pearson D. G. & Irvine G. J. (2003). A routine method for the dissolution of geological samples for the analysis of REE and trace elements via ICP-MS. In; Holland, J. G. & Tanner, S. D. (eds) *Plasma source mass spectrometry: Applications and emerging technologies (8th International Conference on Plasma Source Mass Spectrometry)* pp. 221-230.

Peret, F. A. (1937). The eruption of Mt Pelée 1929-32. Carnegie Inst. Wash. Publication **458**, 126 p.

Pichavant, M. & Macdonald, R. (2007). Crystallization of primitive basaltic magmas at crustal pressures and genesis of the calc-alkaline igneous suite: experimental evidence from St. Vincent, Lesser Antilles arc. *Contributions to Mineralogy and Petrology* **154**, 535-558.

Pichavant, M. Martel, C., Bourdier, J-L. & Scaillet, B. (2002). Physical conditions, structure, and dynamics of a zoned magma chamber: Mount Pelée (Martinique, Lesser Antilles Arc). *Journal of Geophysical Research,* **107,** No. B5 DOI 10.1029/2001JB000315

Plank, T. (2005). Constraints from Thorium/Lanthanum on sediment recycling at subduction zones and the evolution of the continents. *Journal of Petrology* **46**, 921-944.

Plank, T., Langmuir, C. H. (1993). Tracing trace elements from sediment input to volcanic output at subduction zones. *Nature* **362**, 739-743.

Powell, M. (1978). Crystallisation conditions of low-pressure cumulate nodules from the Lesser Antilles island arc. *Earth and Planetary Science Letters* **39**, 162-172.

Roobol, M. J. & Smith, A. L. (2004). *Volcanology of Saba and St. Eustatius, Northern Lesser Antilles.* Koninklijke Nederlandse Akademie Van Wetenschappen, 320 p.

Rutherford, M. J. & Hill, P. M. (1993). Magma ascent rates from amphibole breakdown: An experimental study applied to the 1980-1986 Mount St Helens eruptions: *Journal of Geophysical Research* **98**, 19,667-19,685.

Sevilla, W. I., Ammon, C. J. & Voight, B. (2010). Crustal structure beneath the Montserrat region of the Lesser Antilles island arc. *Geochemistry, Geophysics, Geosystems* **11**, Q06013, DOI:10.1029/2010GC003048

Sherman, S. B. (1992). Geochemistry and petrogenesis of Saba, Lesser Antilles. MSc thesis, University of South Florida, 114 p.

Smith, A. L. & Roobol, M. J. (1990). Mt Pelée Martinique; A study of an active island-arc volcano. *Geological Society of America, Memoir* **175**, 105 p.

Spandler, C., Hermann, J., Arculus, R. and Mavrogenes, J. (2003). Redistribution of trace elements during prograde metamorphism from lawsonite blueshist to eclogite facies; implications for deep subduction zone processes. *Contributions to Mineralogy and Petrology* **146**, 205-222.

Stormer, J. C. Jr. & Nicholls, J. (1978). XLFRAC; a program for the interactive testing of magmatic differentiation models. *Computers and Geosciences*, **4**, 143–159.

Sun, S. S. & McDonough, W. (1989). Chemical and isotopic systematics of oceanarc basalts: implications for mantle composition and processes. *Geological Society of London Special Publication* **42**, 313-345.

Thirwall, M. F. & Graham, A. M. (1984). Evolution of high-Ca, high-Sr C-series basalts from Grenada, Lesser Antilles: Contamination in the arc crust. *Journal of the Geological Society of London* **141**, 427-445.

Toothill, J., Williams, C. A., Macdonald, R., Turner, S. P., Rogers, N. W., Hawkesworth, C. J., Jerram, D. A., Ottley, C. J. & Tindle, A. G. (2007). A complex petrogenesis for an arc magmatic suite, St Kitts, Lesser Antilles. .*Journal of Petrology* **48,** 3-42.

Turner, S., Hawkesworth, C., van Calsteren, P., Heath, E., Macdonald R., & Black, S. (1996). U-series isotopes and destructive plate margin magma genesis in the Lesser Antilles. *Earth and Planetary Science Letters* **142**, 191-207.

Turner S., George R., Jerram D. A, Carpenter N, Hawkesworth C. J. (2003). Case studies of plagioclase growth and residence times in island arc lavas from Tonga and the Lesser Antilles, and a model to reconcile discordant age information. *Earth and Planetary Science Letters* **214,** 279-94.

Villemant, B., Jaffrezic, H., Joron, J. L. & Treuil, M. (1981). Distribution Coefficients of Major and Trace-Elements - Fractional Crystallization in the Alkali Basalt Series of Chaine-Des-Puys (Massif Central, France). *Geochimica et Cosmochimica Acta* **45***,* 1,997-2,016.

Wadge, G. & Shepherd, J. B. (1984). Segmentation of the Lesser Antilles subduction zone. *Earth and Planetary Science Letters* **71**, 297-304.

Westercamp, D. & Tazieff, H. (1980). Guides geologiques regionaux, Martinique-Guadeloupe, Masson, Paris, 135 p.

White, W. M., Dupre, B. & Vidal, P. (1985). Isotope and trace element geochemistry of sediments from the Barbados Ridge-Demerara Plain region, Atlantic Ocean, *Geochimica et Cosmochimica Acta* **49**, 1875-1886.

White, W. M. & Dupre, B. (1986). Sediment subduction and magma genesis in the Lesser Antilles: Isotopic and trace element constraints. *Journal of Geophysical Research* **91**, 5297-5941.

White, W. M. & Patchett, P. J. (1984). Hf-Nd-Sr Isotopes and incompatible element abundances in island arcs: Implications for magma origins and crust-mantle evolution. *Earth and Planetary Science Letters* **67**, 167-185.

Wills, K. J. A. (1974). The geological history of Southern Dominica and plutonic nodules from the Lesser Antilles. PhD Thesis, University of Durham, 414 p.

Woodhead, J., Hergt, J., Greig, A. & Edwards, L. (in press) Subduction zone Hf-anomalies: mantle messenger, melting artifact or crustal process? *Earth and Planetary Science Letters*

Workman, R. K. & Hart, S. R. (2005). Major and trace element composition of the depleted MORB mantle (DMM). *Earth and Planetary Science Letters* **231**, 53-72.

FIGURE CAPTIONS

Figure 1. Schematic illustration of generalised approach (after Davidson et al., 2005). Large shaded arrows labelled "volcano 1 and volcano 2" represent differentiation trends defined by data. These may all converge on a common parent (a) suggesting a common mantle source, or they may originate from distinctly different parents (b,c). If the parents are distinct then they may be generated either by different trends of evolution in the deep crust from a common primary composition (b) or may reflect the existence of different primary magmas (c). The primary magma composition is in equilibrium with the mantle and therefore can be used to evaluate slab contributions and degrees of melting.

Figure 2. Map of the Lesser Antilles island arc. Bathymetric map taken from NOAA ETOPO1 (Amante and Eakins, 2009). Sketch map shows the locations of the active volcanoes, Mt. Pelée and the Quill on the islands of Martinique and Statia respectively. The age division between "Old" and "Young" arcs is ~ 9 Ma, when the magmatic axis shifted abruptly westwards in the north.

Figure 3. Representative photomicrographs (plane polarised light) of (a) a typical andesite (SE8221b from the Quill); plag = plagioclase, opx = orthopyroxene, cpx = clinopyroxene, mt = magnetite, v = vesicle and (b) a cumulate xenolith (SE48A from the Quill); amph = amphibole.

Figure 4 a) Geologic map of Mt Pelée volcano, Martinique, after Smith and Roobol (1990), illustrating the main stratigraphic subdivisions and the locations of the stratigraphic sections sampled for this study. b) summary stratigraphic sections from the three locations in (a). Sections are correlated with those of Smith and

Roobol (1990) which are constrained by carbon dates. Carbon dates shown on the stratigraphic log of Section B are from charcoal collected during sampling and analysed at the Scottish Universities Research and Reactor Centre (SURRC; Davidson, unpublished data) Age values were calculated as conventional ^{14}C years (relative to AD 1950) and at the $\pm 1\sigma$ level.. In section C the correlation indicated is with pumice P_1 dated at 650 yrs by Westercamp (pers. com. 1982).

Figure 5. (a) Geologic sketch map of Statia showing the locations of the stratigraphic sections from the Quill sampled for this study. Unlike Mt. Pelée the geologic map reveals no detail for the Quill as the cone is very young and undissected. b) Summary stratigraphic sections from the Quill volcano, Statia. Key as in Fig. 4b. Sections are correlated as indicated with those of Roobol and Smith (2004.) which are constrained by their carbon dates: Both sections were probably entirely erupted within the last 8,000 years.

Figure 6. Major element variation diagrams for (a) $Al2O_3$ (b) TiO_2 (c) CaO (d) MgO (e) K2O and (f) FeO*/MgO versus SiO_2 (wt. %) comparing the Quill and Mt. Pelée. Medium K-low K classification in (e) is from Gill (1981). In (f) FeO* is total iron expressed as FeO and the tholeiitic - calc-alkaline divide is from Miyashiro (1974). The inset is an AFM diagram showing the tholeiitic - calc-alkaline divide defined by Irvine and Baragar (1971). Vectors plotted in (a) to (e) (solid lines) show the effects of the cumulate extract (amphibole-plagioclase-Fe-Ti oxide) as modelled in Table 3 for the Mt. Pelée parent/ daughter pair M8236-M8237. Also shown with a dashed line is the vector for the petrographically observed (via point counting) phenocryst assemblage in M8236, which comprises 71% plagioclase,

16% clinopyroxene, 10% magnetite and 3% olivine. Tick marks on the vectors are for 10% extract.

Figure 7. Trace element (ppm) variation versus SiO_2 (wt. %) for Mt. Pelée and the Quill. Extract vectors for calculated (least squares; Table 3a) cumulate phase assemblages and for petrographically observed phenocryst assemblages are shown as in Fig. 6. Distribution coefficients are given in Table 4a. Tick marks on the vectors are for 10% extract.

Figure 8. CaO vs SiO_2 diagrams for Mt. Pelée and the Quill (as in Fig. 6) with potential fractionation extracts plotted – phenocryst minerals from mafic samples, minerals from cumulate blocks and bulk cumulate blocks. Data from Davidson (1984), Wills (1974) and Smith and Roobol (1990). In both cases the magma differentiation trend back-extrapolates close to the composition of the bulk cumulate blocks comprising plagioclase, amphibole, Fe-Ti oxide ± pyroxene.

Figure 9. Chondrite-normalised REE patterns for Mt. Pelée and the Quill respectively, arranged by stratigraphic section (cf Figs. 4 and 5). Normalisation constants from Sun and McDonough (1989).

Figure 10. Trace element ratios versus wt. % SiO_2 for Mt. Pelée and the Quill. Extract vectors for calculated (least squares; Table 3) cumulate phase assemblages and for petrographically observed phenocryst assemblages are shown as in Fig. 6. Distribution coefficients are given in Table 4a. Tick marks on the vectors are for 10% extract.

Figure 11. Comparison between the inferred bulk distribution coefficients needed to reproduce the trace element trends at Mt. Pelée and the Quill (Table 4b) and the bulk distribution coefficients calculated from published data (Table 4a) for the modal phenocryst assemblage and the assemblage observed in the cumulate blocks that satisfies the least squares modelling (Table 3).

Figure 12. Normalised incompatible trace element diagrams showing (a) parental and (b) derivative (daughter) magmas from Mt. Pelée and the Quill used in the major element fractionation calculations (Fig. 7; Table 3). Normalisation constants from Sun and McDonough (1989). (c) parent/daughter trace element ratios showing the specific enrichments of incompatible elements in the derivative magmas relative to their respective parents. Inset to (a) shows the extrapolated primitive magmas for Mt. Pelée and the Quill. The trends for each element versus SiO_2 (e.g. Fig. 8) were extrapolated as linear regressions to an assumed parent magma composition with 48% SiO_2. Linear regression is based on the observed variations – it is possible that there is a significant period of olivine fractionation not preserved in the erupted compositions. This would change the absolute values of the calculated trace element concentrations (reducing them) but would not change the overall pattern (i.e. ratios among incompatible elements).

Figure 13. Schematic phase diagram (after Cawthorn and O'Hara, 1976) showing amphibole phase relations in the system CaO-MgO-Al_2O_3-SiO_2-Na_2O at 5 kbar pressure under water-saturated conditions. Composition **B** (basalt) crystallizes ol+cpx, driving the residual liquid towards **C** where the reaction ol+cpx+liquid = amph occurs. The liquid then migrates along the ol-cpx-amph-liquid-vapour curve

(**CD**) precipitating amphibole. Ol+cpx continue to react with the liquid until they are consumed at **D.** The liquid then precipitates amphibole alone along trajectory **DE**, eventually reaching the orthopyroxene stability field at point **E** which corresponds to a typical andesite composition. See text for further details.

Figure 14. Sr-Nd-Pb isotopic compositions versus wt. % SiO_2 as an index of differentiation; correlations in the case of Sr and Pb, most marked for Mt. Pelée are consistent with open-system differentiation – i.e. crustal contamination, whereby the isotopic composition of the magmas is modified during differentiation in the crust. a) $^{87}Sr/^{86}Sr$ vs SiO_2, b) $^{143}Nd/^{144}Nd$ vs SiO_2, c) $^{206}Pb/^{204}Pb$ vs SiO_2,

Figure 15. Sr-Nd-Pb-Hf isotopic data for Mt. Pelée and the Quill; a) $^{143}Nd/^{144}Nd$ vs $^{87}Sr/^{86}Sr$, b) $^{143}Nd/^{144}Nd$ vs $^{177}/Hf/^{176}Hf$, c) $^{208}Pb/^{204}Pb$ vs $^{206}Pb/^{204}Pb$, d) $^{207}Pb/^{204}Pb$ vs $^{206}Pb/^{204}Pb$, e) $^{206}Pb/^{204}Pb$ vs $^{87}Sr/^{86}Sr$.

Figure 16. Variations in $^{206}Pb/^{204}Pb$ vs $^{87}Sr/^{86}Sr$ showing mixing lines between mantle wedge sources and local sediments. Mantle wedge source = depleted MORB mantle (DMM) of Workman and Hart (2005) with isotopic compositions of DSDP site 543 MORB (White et al, 1985). (a) Data for Mt. Pelée and the Quill (cf Fig. 15e). Sediment composites are from DSDP site 543 (Davidson 1987; White et al., 1985); Site 144 Black shales represent sediments with highly radiogenic Pb from DSDP hole 144 SE of Grenada, from Carpentier et al. (2008). The grey mixing lines are shifted to higher $^{87}Sr/^{86}Sr$ reflecting the possible addition of a high $^{87}Sr/^{86}Sr$ fluid from the subducting slab. 9b) Same diagram as (a) with additional data from the other islands of the Lesser Antilles arc (Grenada from Thirlwall and

Graham, 1984; Soufriere, St Vincent from Heath et al., 1998; St Lucia, Dominica and Martinique from Davidson 1986 and 1987; Mt Misery, St Kitts from Toothill et al., 2007; Saba from Sherman 1992). Some of the most radiogenic samples (grey box) have high (crust-like) $\delta^{18}O$ values (Davidson and Harmon, 1989).

Figure 17. Along arc comparison of extrapolated (to 48 wt. % SiO_2) primitive magma compositions (SV = Soufriere, St Vincent, MP = Mt Pelée, SM = Soufriere Hills, Montserrat, MK = Mt Misery, St Kitts, Q = the Quill, Sb = Saba). Data sources as in Fig. 16, and Defant et al. (2001).

Figure 18. Th/La vs Sm/La for Mt. Pelée and the Quill. Stars represent primary magma compositions obtained by extrapolating differentiation trends back to 48% SiO_2 as in Fig. 17. Note that any mixing trend on this diagram will plot as a straight line. Lesser Antilles sediments (grey box) and mantle (grey circle) compositions are taken from Plank (2005), as is the MORB array (cross-hatched field). The sediment compositions are measured samples from outboard of the arc, the Lesser Antilles mantle composition is determined by extrapolating the trend of Lesser Antilles basalt compositions to its intersection with the MORB array. If the primary magmas of Mt. Pelée and the Quill are derived from partial melting of sources formed through mixing of mantle wedge peridotite and subducted sediment then the mixtures should fall in the diagonal grey band, which is produced by extrapolating the sediment field through the primary magma compositions (stars) towards the "MORB array". The data for Mt. Pelée and the Quill suggest that: (1) the mantle wedge composition(s) is more depleted (higher

Sm/La) than that estimated by Plank (2005) and (2) the volcanoes require different subducted sediment compositions to be added to their sources.

Figure 19 (a) Trace element characteristics (normalised) of mixtures of sediment with depleted mantle, compared with estimated primary magmas for Mt. Pelée and the Quill. Primary magmas are extrapolated compositions at 48% SiO_2. Depleted mantle (DMM) is from Workman and Hart (2005), sediment is average DSDP site 543. (b) Effects of sediment mixing with a depleted mantle source and melting of that modified source. Modified source is 0.5% average site 543 sediment + DMM, from (a). Batch melts of 5%, 10% and 20% of this modified source are shown, relative to the Mt. Pelée parental magma. The shaded area shows the relative amounts of elements that would need to be added via a fluid in order to produce the Mt. Pelée parent, starting from a 20% melt of sediment-modified depleted mantle. See text for further details.

Table 1a. *Major and trace element and isotopic compositions of Mt Pelée samples*

Section	B	B	B	B	B	B	B	B	B	B	B	B
Sample number	M8213	M8214	M8215	M8217	M8218	M8220	M8221	M8222	M8225	M8226	M8228	M8277
SiO_2	55.71	61.10	60.69	58.94	59.13	57.85	58.10	59.14	60.26	62.08	62.10	60.47
TiO_2	0.64	0.48	0.47	0.51	0.52	0.53	0.55	0.53	0.47	0.42	0.43	0.45
Al_2O_3	18.61	17.66	17.57	17.56	17.83	18.33	18.44	17.83	17.68	17.10	17.36	17.48
Fe_2O_3	8.85	7.18	7.08	7.33	7.13	7.71	7.91	7.33	7.03	6.19	6.42	6.81
MnO	0.21	0.21	0.21	0.20	0.19	0.21	0.21	0.20	0.20	0.19	0.19	0.20
MgO	3.64	2.59	2.52	2.77	2.81	2.93	2.98	2.86	2.46	2.19	2.15	2.39
CaO	7.95	6.40	6.35	6.70	6.90	7.31	7.40	6.88	6.34	5.87	5.92	6.24
Na_2O	3.61	3.87	3.76	3.55	3.59	3.50	3.58	3.87	4.27	3.77	3.85	4.11
K_2O	0.68	0.95	0.92	0.95	0.97	0.84	0.83	0.96	0.99	1.09	1.07	1.02
P_2O_5	0.18	0.17	0.18	0.17	0.14	0.16	0.16	0.16	0.17	0.15	0.16	0.18
Total	100.08	100.61	99.75	98.68	99.21	99.37	100.16	99.76	99.87	99.05	99.65	99.35
Cr												
Ni	*4*		*3*	*2*	*2*	*1*		*1*	*2*	*2*	*4*	
Cu	*37*	*21*	*27*	*19*	*24*	*28*	*40*	*25*	*21*	*17*	*25*	*27*
Zn	*87*	*80*	*78*	*71*	*72*	*79*	*80*	*75*	*76*	*73*	*72*	*71*
V	126	69	64	88	102	110	107	101	79	78	56	70
Sc	16.6	11.8	11.2	13.1	14.4	15.0	14.1	14.0	12.9	11.4	11.2	11.7
Rb	*15*	*23*	*25*	*25*	*25*	*21*	*21*	*25*	*26*	*28*	*28*	*27*
Sr	*293*	*284*	*286*	*284*	*265*	*279*	*281*	*274*	*284*	*275*	*276*	*285*
Y	20.58	21.22	20.06	20.93	21.23	20.93	20.94	21.75	20.75	20.62	20.44	19.78
Zr	*60*	*85*	*88*	*90*	*85*	*76*	*76*	*87*	*85*	*92*	*93*	*88*
Ba	*158*	*227*	*214*	*200*	*211*	*182*	*180*	*202*	*224*	*257*	*242*	*211*
Pb	4.04	4.28	5.18	5.30	5.19	4.38	3.76	5.21	5.77	4.43	5.81	5.89
U	0.42	0.67	0.69	0.70	0.74	0.59	0.56	0.71	0.69	0.80	0.83	0.75
Th	1.54	2.44	2.43	2.58	2.66	2.14	2.12	2.62	2.47	2.82	2.98	2.66
Nb	2.7	3.2	3.2	4.3	3.0	2.8	2.8	3.2	3.1	3.2	3.2	2.9
Ta	0.19	0.24	0.22	0.22	0.22	0.20	0.20	0.23	0.23	0.24	0.24	0.21
Hf	2.15	2.72	2.68	2.69	2.64	2.46	2.37	2.66	2.59	2.39	2.78	2.60
La	8.55	10.69	10.58	10.86	10.43	9.40	10.07	10.60	10.40	11.30	10.89	10.69
Ce	19.39	23.46	22.84	23.59	22.52	20.69	21.61	23.08	22.66	24.17	23.59	22.99
Pr	2.79	3.27	3.19	3.30	3.12	3.00	3.19	3.20	3.16	3.30	3.21	3.14
Nd	12.18	13.86	13.14	13.82	13.13	12.79	13.49	13.25	13.27	13.94	13.49	12.95
Sm	3.02	3.18	3.00	3.15	3.00	3.02	3.20	3.05	3.04	3.13	3.04	2.95
Eu	1.00	1.02	1.00	0.97	0.92	0.97	0.99	0.97	0.96	0.96	0.94	0.93
Gd	3.26	3.39	3.21	3.27	3.20	3.36	3.39	3.41	3.18	3.26	3.11	3.11
Tb	0.55	0.55	0.52	0.55	0.52	0.53	0.55	0.55	0.52	0.53	0.53	0.50
Dy	3.17	3.21	3.10	3.25	3.14	3.22	3.26	3.26	3.03	3.02	3.06	2.93
Ho	0.69	0.71	0.66	0.70	0.67	0.69	0.69	0.70	0.65	0.65	0.65	0.65
Er	1.99	2.09	1.95	2.04	1.98	1.98	2.01	2.04	1.91	1.91	1.93	1.83
Tm	0.32	0.34	0.33	0.33	0.33	0.32	0.33	0.34	0.32	0.31	0.31	0.31
Yb	2.13	2.28	2.14	2.24	2.19	2.20	2.20	2.21	2.14	2.08	2.13	2.05
Lu	0.36	0.40	0.37	0.39	0.39	0.37	0.37	0.39	0.37	0.37	0.38	0.37
$^{87}Sr/^{86}Sr$*	0.704140	0.704180	0.704163	0.704109	0.704100	0.704161	0.704228	0.704567	0.704223	0.704201	0.704233	
$^{143}Nd/^{144}Nd$**	0.512808		0.512790	0.512793		0.512815	0.512812	0.512740		0.512810		
$^{206}Pb/^{204}Pb$***	19.359	19.396		19.370	19.369	19.380		19.382	19.421	19.415		19.417
$^{207}Pb/^{204}Pb$	15.732	15.739		15.733	15.732	15.735		15.735	15.745	15.745		15.743
$^{208}Pb/^{204}Pb$	39.133	39.172		39.145	39.142	39.156		39.157	39.206	39.204		39.198
$^{176}Hf/^{177}Hf$****			0.283059	0.283052			0.283039			0.283055		

Section labels (B,C,D) refer to stratigraphic sections shown in Fig. 3

*Sr isotope ratios analysed at UCLA (SRM 987 = 0·710253 ± 25)

**Nd isotope ratios for samples M2815-M2826 analysed at Leeds (La Jolla $^{143}Nd/^{144}Nd$ = 0.511886±30), all others analysed at UCLA (($La Jolla $^{143}Nd/^{144}Nd$ = 0.511840±11).

***Pb isotope ratios analysed at Durham (SRM 981; $^{206}Pb/^{204}Pb$ =16.9405±10, $^{207}Pb/^{204}Pb$ = 15.4975±11; $^{208}Pb/^{204}Pb$ = 36.7160±32)

****Hf isotope ratios analysed at Durham (JMC475 $^{176}Hf/^{177}Hf$ = 0.2821535±6)

Trace elements; Italic values are XRF (Leeds) all others by ICP MS(Durham)

See text for analytical details

C	C	C	C	C	C	C	C	D	D	D	D	D	D	D	D
M8229	M8230	M8232	M8233	M8234	M8235	M8236	M8237	M8246	M8247	M8248	M8249	M8250	M8251	M8252	M8253
55.70	58.54	53.81	53.66	54.92	56.41	51.42	62.87	57.73	55.08	56.55	54.35	53.61	53.65	51.39	53.13
0.69	0.57	0.77	0.82	0.80	0.68	0.92	0.47	0.64	0.71	0.71	0.77	0.80	0.76	0.77	0.80
18.61	17.89	18.21	18.87	18.68	18.14	19.06	17.37	17.93	17.70	18.33	18.17	18.74	18.52	18.04	18.73
8.18	7.55	8.77	8.99	8.79	8.07	9.43	6.35	7.99	8.59	8.41	8.88	8.72	8.57	8.85	8.89
0.19	0.19	0.19	0.18	0.18	0.18	0.18	0.18	0.19	0.19	0.19	0.19	0.18	0.18	0.18	0.18
3.61	2.93	4.78	4.32	4.17	3.51	4.95	2.18	3.23	5.00	3.63	4.20	4.18	4.18	4.35	4.40
8.73	7.51	9.13	9.36	9.22	8.13	10.07	5.99	7.63	8.61	8.34	8.85	9.28	9.14	9.14	9.42
2.88	2.99	2.71	2.75	3.07	3.01	2.52	3.28	3.11	2.80	2.94	2.76	2.68	3.08	3.07	2.68
0.88	0.91	0.75	0.74	0.80	0.83	0.66	1.12	0.91	0.79	0.87	0.75	0.77	0.75	0.70	0.72
0.14	0.14	0.12	0.12	0.13	0.12	0.10	0.15	0.14	0.12	0.13	0.13	0.12	0.12	0.11	0.11
99.61	99.22	99.24	99.81	100.76	99.08	99.31	99.96	99.50	99.59	100.10	99.05	99.08	98.95	96.60	99.06
9	*5*	*31*	*16*	*16*	*11*	*25*		*4*	*57*	*12*	*20*	*18*	*18*	*19*	*25*
7	*5*	*13*	*8*	*6*	*7*	*10*	*4*	*9*	*19*	*8*	*8*	*11*	*10*	*11*	*11*
58	*37*	*64*	*56*	*107*	*41*	*105*	*46*	*25*	*53*	*53*	*77*	*39*	*69*	*55*	*70*
75	*70*	*72*	*73*	*71*	*68*	*72*	*65*	*76*	*74*	*77*	*77*	*65*	*70*	*66*	*72*
203	131	247	277	268	175	361	73	156	216		257	275	271	274	265
21.9	15.6	30.9	30.3	29.7	22.2	40.6	11.9	18.2	27.7		29.0	31.3	31.6	31.0	11.3
22	*30*	*19*	*18*	*22*	*22*	*10*	*31*	*25*	*18*	*23*	*21*	*19*	*17*	*14*	*17*
325	*296*	*298*	*320*	*312*	*302*	*378*	*276*	*284*	*279*	*302*	*302*	*314*	*308*	*310*	*311*
22.14	21.45	21.16	20.93	21.82	20.85	19.45	20.96	22.13	20.46		21.50	21.30	22.00	21.43	19.61
71	*89*	*59*	*55*	*62*	*76*	*40*	*104*	*82*	*64*	*77*	*61*	*59*	*60*	*55*	*58*
164	*181*	*149*	*141*	*146*	*172*	*125*	*221*	*172*	*150*	*180*	*150*	*138*	*156*	*139*	*135*
7.62	4.93	3.73	3.76	3.48	4.20	3.45	5.52	4.63	3.95		4.40	4.99	3.86	3.78	3.02
0.68	0.78	0.54	0.50	0.56	0.65	0.40	0.96	0.71	0.55		0.57	0.38	0.50	0.34	0.44
2.64	2.99	1.98	1.85	2.04	2.59	1.38	3.39	2.59	2.12		2.13	1.84	1.98	1.75	1.70
2.8	2.7	2.3	2.1	2.3	2.9	1.6	3.1	3.0	3.6		2.4	2.2	1.19	2.07	2.07
0.19	0.20	0.15	0.16	0.16	0.20	0.10	0.23	0.19	0.16		0.16	0.15	0.16	0.17	0.14
2.20	2.36	1.95	1.81	1.93	2.25	1.48	2.86	2.34	2.01		1.97	1.72	1.87	1.64	1.74
9.38	10.27	7.54	7.29	7.68	8.78	5.72	11.70	9.59	7.79		7.87	7.69	7.51	7.99	6.57
20.05	21.32	16.39	16.30	17.00	19.35	12.61	25.19	20.99	17.07		17.19	15.79	16.12	15.88	14.70
2.86	3.06	2.41	2.39	2.51	2.73	1.94	3.51	3.01	2.45		2.48	2.49	2.38	2.63	2.15
12.70	12.91	10.88	10.69	11.30	11.83	8.87	14.56	12.88	10.76		10.73	11.63	10.77	12.03	9.62
3.05	3.09	2.70	2.83	2.80	2.82	2.44	3.30	3.09	2.72		2.70	3.03	2.81	3.10	2.49
0.96	0.95	0.89	0.89	0.91	0.89	0.81	0.96	0.98	0.88		0.88	0.91	0.91	0.92	0.83
3.41	3.29	3.28	3.33	3.48	3.33	3.12	3.63	3.45	3.18		3.24	3.68	3.47	3.63	3.03
0.58	0.56	0.56	0.53	0.57	0.54	0.49	0.57	0.57	0.51		0.54	0.59	0.57	0.59	0.51
3.48	3.29	3.25	3.27	3.42	3.19	3.05	3.22	3.39	3.07		3.26	3.52	3.37	3.53	3.06
0.74	0.70	0.70	0.70	0.73	0.67	0.66	0.67	0.74	0.66		0.69	0.74	0.74	0.75	0.66
2.12	2.04	2.03	2.02	2.13	1.95	1.85	1.95	2.12	1.93		2.01	2.01	2.14	2.07	1.86
0.34	0.33	0.33	0.32	0.33	0.31	0.30	0.31	0.35	0.32		0.33	0.33	0.34	0.32	0.30
2.18	2.23	2.09	2.04	2.16	2.06	1.86	2.09	2.29	2.05		2.07	2.06	2.17	2.08	1.94
0.38	0.39	0.35	0.35	0.37	0.36	0.31	0.35	0.40	0.35		0.36	0.35	0.38	0.34	0.31
0.704011	0.704147	0.704036	0.703916	0.703817	0.704057	0.703900	0.704196			0.704059	0.703975	0.703975			0.703967
0.512784	0.512750	0.512801	0.512792	0.512838	0.512797	0.512782	0.512767			0.512790	0.512795	0.512805			0.512792
19.344	19.338		19.237	19.251	19.281		19.375	19.322	19.258		19.232		19.229	19.127	19.255
15.726	15.727		15.705	15.709	15.720		15.734	15.722	15.713		15.707		15.706	15.697	15.710
39.113	39.108		38.998	39.012	39.047		39.155	39.090	39.029		38.996		38.993	38.898	39.023
	0.283087	0.283046		0.283116						0.283070	0.283061				

Table 1b. *Major and trace element and isotopic compositions of the Quill samples*

SECTION	F	F	F	F	F	F	F	F	F	F	G	G	G	G
	SE8262	SE8237	SE8238	SE8239	SE8240	SE8241	SE8242	SE8243	SE8244	SE8245	SE8246	SE8247A	SE8247B	SE8248
SiO_2	58.98	60.37	57.12	57.71	57.59	57.76	57.72	58.80	55.23	57.12	56.02	55.24	57.18	53.44
TiO_2	0.60	0.58	0.66	0.67	0.64	0.64	0.64	0.61	0.72	0.74	0.78	0.82	0.71	0.85
Al_2O_3	17.42	17.25	17.58	17.74	17.49	17.49	17.59	17.50	18.29	17.82	17.95	18.07	18.10	18.89
Fe_2O_3	6.74	6.31	7.26	7.29	7.03	6.89	6.95	6.75	7.86	7.81	8.21	8.48	7.80	8.68
MnO	0.19	0.19	0.19	0.19	0.19	0.19	0.19	0.19	0.19	0.19	0.19	0.20	0.20	0.19
MgO	2.99	2.50	3.75	3.52	3.06	3.19	3.47	2.95	4.12	3.48	3.73	3.90	3.73	4.39
CaO	7.06	6.50	7.78	7.68	7.49	7.61	7.59	7.05	8.66	7.84	8.14	8.45	8.01	9.46
Na_2O	3.83	3.90	3.43	3.60	4.03	3.72	3.75	3.74	3.31	3.45	3.46	3.35	3.44	3.52
K_2O	0.68	0.66	0.56	0.58	0.64	0.66	0.61	0.62	0.50	0.63	0.58	0.56	0.57	0.57
P_2O_5	0.12	0.11	0.10	0.11	0.11	0.11	0.11	0.11	0.10	0.11	0.10	0.12	0.11	0.10
Total	98.61	98.37	98.43	99.09	98.27	98.26	98.62	98.32	98.98	99.19	99.16	99.19	99.85	100.09
Cr	*19*		*31*	*13*	*8*	*11*	*27*	*9*	*11*	*7*	*10*	*5*	*6*	*9*
Ni	*11*		*18*	*9*	*6*	*8*	*12*	*6*	*12*	*7*	*4*	*7*	*8*	*7*
Cu	*24*	*20*	*27*	*27*	*26*	*24*	*27*	*23*	*37*	*34*	*36*	*39*	*28*	*38*
Zn	*45*	*43*	*47*	*45*	*45*	*44*	*47*	*44*	*51*	*50*	*51*	*52*	*47*	*52*
V	103.15	84.01	143.48	126.05	131.35	124.15	123.53	108.47	193.88	171.50	191.41	193.85	157.23	233.64
Sc	13.72	10.85	19.50	16.51	17.00	16.64	16.51	13.79	23.13	18.93	20.37	19.77	17.66	25.07
Rb	*12*	*13*	*11*	*11*	*11*	*12*	*11*	*13*	*10*	*12*	*11*	*11*	*12*	*9*
Sr	*246*	*247*	*241*	*249*	*248*	*247*	*244*	*251*	*277*	*273*	*276*	*276*	*273*	*288*
Y	22.67	19.45	21.09	22.29	22.69	22.00	22.44	22.94	21.36	23.49	23.20	23.02	23.08	21.70
Zr	*85*	*92*	*77*	*79*	*80*	*82*	*79*	*86*	*68*	*79*	*74*	*69*	*74*	*60*
Ba	*157*	*161*	*139*	*146*	*153*	*145*	*145*	*157*	*127*	*144*	*131*	*122*	*146*	*110*
Pb	3.46	2.32	3.23	2.19	2.21	2.29	2.22	2.34	1.85	2.84	2.41	2.24	1.82	2.12
U	0.36	0.34	0.34	0.33	0.36	0.36	0.33	0.37	0.32	0.36	0.35	0.31	0.33	0.28
Th	0.75	0.64	0.71	0.69	0.73	0.74	0.69	0.75	0.64	0.75	0.73	0.64	0.67	0.57
Nb	2.06	2.57	2.23	1.99	1.96	2.30	1.93	2.15	2.72	1.92	1.75	1.78	1.94	2.39
Ta	0.16	0.16	0.15	0.14	0.15	0.15	0.15	0.17	0.14	0.15	0.15	0.15	0.15	0.12
Hf	2.37	2.43	2.05	2.13	2.17	2.17	2.22	2.37	1.91	2.17	2.10	1.99	2.18	1.71
La	5.60	4.69	4.66	5.05	4.82	4.93	5.17	5.57	4.43	5.01	4.85	4.76	5.15	4.01
Ce	13.63	12.68	11.26	12.23	11.97	12.00	12.69	13.43	10.81	12.29	11.99	11.88	12.93	10.03
Pr	2.13	1.88	1.77	1.95	1.89	1.89	2.05	2.13	1.75	1.95	1.89	1.93	2.07	1.62
Nd	10.18	8.94	8.63	9.18	8.85	9.13	9.75	10.19	8.64	9.50	9.32	9.50	9.95	8.15
Sm	2.73	2.35	2.43	2.58	2.44	2.47	2.70	2.71	2.36	2.72	2.63	2.65	2.72	2.40
Eu	0.98	0.83	0.88	0.94	0.88	0.89	0.95	0.96	0.89	0.94	0.94	0.94	0.98	0.86
Gd	3.44	2.87	3.12	3.25	3.19	3.03	3.38	3.40	3.12	3.39	3.49	3.41	3.56	3.11
Tb	0.59	0.49	0.54	0.56	0.55	0.55	0.56	0.58	0.54	0.60	0.60	0.58	0.60	0.54
Dy	3.55	3.02	3.13	3.34	3.28	3.22	3.42	3.46	3.22	3.50	3.54	3.59	3.60	3.29
Ho	0.79	0.69	0.72	0.74	0.74	0.74	0.78	0.81	0.72	0.80	0.80	0.81	0.83	0.75
Er	2.29	2.00	2.06	2.15	2.13	2.12	2.21	2.28	2.08	2.31	2.28	2.33	2.26	2.02
Tm	0.38	0.33	0.36	0.36	0.36	0.35	0.37	0.39	0.34	0.38	0.39	0.37	0.38	0.35
Yb	2.54	2.35	2.33	2.41	2.48	2.39	2.52	2.63	2.23	2.53	2.60	2.54	2.56	2.21
Lu	0.45	0.40	0.40	0.41	0.42	0.41	0.43	0.43	0.38	0.44	0.43	0.42	0.43	0.39
$^{87}Sr/^{86}Sr$*	0.703696	0.703736	0.703684	0.703682	0.703693	0.703656	0.703584	0.703658	0.703595	0.703602	0.703560	0.703729	0.703609	0.703577
$^{143}Nd/^{144}Nd$**	0.513051	0.513098	0.513051	0.513052	0.513009	0.513035	0.513039	0.513049	0.513038	0.513034	0.513036	0.513023	0.513051	0.513028
$^{206}Pb/^{204}Pb$***	18.996	18.995		18.994			18.998	19.003				18.901	18.908	
$^{207}Pb/^{204}Pb$	15.661	15.659		15.661			15.661	15.666				15.641	15.647	
$^{208}Pb/^{204}Pb$	38.737	38.729		38.737			38.736	38.758				38.631	38.647	
$^{176}Hf/^{177}Hf$****		0.283142			0.283162			0.283152		0.283136				

Section labels (F, G, D) refer to stratigraphic sections shown in Fig. 4

*Sr isotope ratios analysed at UCLA (SRM 987 = 0·710253 ± 25)

**Nd isotope ratios for samples SE8237-46 analysed at Leeds (La Jolla $^{143}Nd/^{144}Nd$ = 0.511886±30), all others analysed at UCLA (($La Jolla ^{143}Nd/^{144}Nd$ = 0.511840±11).

***Pb isotope ratios analysed at Durham (SRM 981; $^{206}Pb/^{204}Pb$ =16.9405±10, $^{207}Pb/^{204}Pb$ = 15.4975±11; $^{208}Pb/^{204}Pb$ = 36.7160±32)

****Hf isotope ratios analysed at Durham (JMC475 $^{176}Hf/^{177}Hf$ = 0.2821535±6)

Trace elements; Italic values are XRF (Leeds) all others by ICP MS (Durham)

See text for analytical details

D SE8216	D SE8216	D SE8217	D SE8218A	D SE8218B	D SE8218C	D SE8219	D SE8220	D SE8221A	D SE8221B	D SE8222	D SE8223	D SE8224	D SE8225	D SE8226	D SE8227	D SE8228
55.91	59.81	56.01	61.42	56.32	58.11	57.89	57.62	58.07	57.73	57.65	59.71	56.17	55.49	58.67	53.73	54.68
0.69	0.57	0.69	0.57	0.70	0.67	0.63	0.65	0.63	0.67	0.65	0.59	0.69	0.70	0.66	0.71	0.73
18.04	17.09	17.82	17.14	18.00	17.70	17.52	17.80	17.42	17.93	17.79	17.18	18.00	18.30	17.25	18.32	18.55
7.48	6.54	7.48	6.39	7.68	7.14	6.98	7.15	6.77	7.25	7.09	6.62	7.55	7.61	7.18	7.87	7.92
0.19	0.19	0.19	0.20	0.19	0.19	0.19	0.19	0.19	0.20	0.19	0.19	0.19	0.19	0.19	0.18	0.18
4.32	2.65	4.21	2.29	4.41	3.31	3.31	3.51	3.15	3.55	3.49	2.66	4.22	3.98	3.26	4.29	4.23
8.41	6.60	8.15	6.21	8.36	7.83	7.49	7.84	7.19	7.82	7.68	6.73	8.41	8.76	7.49	8.95	9.08
3.40	4.03	3.61	4.03	3.42	4.25	4.05	3.58	3.95	3.56	3.51	4.02	3.68	3.48	3.57	3.10	3.17
0.52	0.65	0.55	0.67	0.47	0.61	0.66	0.56	0.61	0.58	0.59	0.70	0.59	0.60	0.61	0.49	0.51
0.11	0.11	0.10	0.13	0.11	0.12	0.11	0.10	0.13	0.11	0.11	0.12	0.10	0.10	0.11	0.09	0.10
99.07	98.24	98.81	99.05	99.66	99.93	98.83	99.00	98.11	99.40	98.75	98.52	99.60	99.21	98.99	97.73	99.15
44	*3*		*38*	*61*	*15*	*7*	*22*	*7*	*22*	*21*	*3*	*44*	*11*	*11*	*13*	*7*
20	*5*	*19*	*3*	*24*	*8*	*10*	*13*	*8*	*10*	*10*	*5*	*19*	*10*	*8*	*9*	*7*
31	*22*	*28*	*20*	*25*	*20*	*23*	*24*	*23*	*24*	*26*	*19*	*26*	*33*	*34*	*37*	*34*
50	*42*	*49*	*41*	*46*	*38*	*47*	*48*	*44*	*47*	*50*	*43*	*50*	*48*	*42*	*52*	*55*
156.52	87.66	150.76		153.73	114.87	120.04	125.52	110.03	134.83	135.38	94.85	160.69	185.95	123.96	210.22	201.43
20.85	11.17	19.86		20.53	14.43	15.47	16.69	13.74	18.14	18.32	12.41	19.81	22.49	14.30	24.99	24.07
9	*13*	*10*	*15*	*9*	*8*	*12*	*12*	*12*	*11*	*12*	*13*	*10*	*10*	*11*	*10*	*10*
236	*251*	*236*	*257*	*235*	*264*	*244*	*241*	*247*	*242*	*241*	*249*	*238*	*275*	*251*	*285*	*284*
21.15	21.52	21.78		22.40	21.58	21.89	21.62	21.91	21.61	21.67	21.78	17.71	21.56	20.31	21.07	21.31
72	*89*	*71*	*92*	*70*	*79*	*80*	*78*	*81*	*78*	*78*	*88*	*72*	*60*	*67*	*53*	*55*
123	*158*	*133*	*167*	*125*	*147*	*141*	*136*	*153*	*133*	*133*	*158*	*132*	*122*	*131*	*121*	*128*
1.85	2.44	2.08		1.56	1.43	2.13	2.08	2.18	2.08	2.18	2.27	1.91	2.16	1.19	1.92	1.97
0.29	0.36	0.32		0.28	0.26	0.35	0.33	0.35	0.35	0.35	0.34	0.30	0.33	0.31	0.29	0.29
0.61	0.74	0.66		0.57	0.56	0.69	0.68	0.68	0.69	0.72	0.73	0.55	0.64	0.59	0.59	0.59
2.12	4.00	2.08		1.81	1.88	2.67	1.89	2.41	1.96	2.11	2.05	1.79	1.73	1.89	19.18	1.59
0.13	0.17	0.15		0.14	0.13	0.15	0.16	0.15	0.15	0.16	0.16	0.14	0.14	0.15	0.18	0.12
1.90	2.35	2.01		1.98	1.60	2.11	2.11	2.22	2.14	2.14	2.35	1.97	1.93	2.04	1.81	1.86
4.39	5.39	4.81		4.31	4.72	5.06	5.01	5.22	4.96	5.11	4.88	3.86	4.41	4.44	4.17	4.21
10.78	13.09	11.88		10.81	11.81	12.48	12.42	12.96	12.29	12.52	11.32	10.47	11.08	11.94	10.39	10.52
1.69	2.07	1.92		1.75	1.89	1.99	1.96	2.01	1.95	1.96	1.94	1.48	1.73	1.81	1.68	1.66
8.26	9.62	9.15		8.54	9.29	9.56	9.50	9.66	9.45	9.47	9.52	7.41	8.52	8.66	8.34	8.25
2.32	2.59	2.47		2.37	2.57	2.55	2.60	2.63	2.62	2.57	2.51	2.07	2.39	2.47	2.31	2.31
0.84	0.91	0.91		0.88	0.90	0.92	0.90	0.91	0.91	0.92	0.87	0.76	0.86	0.86	0.84	0.85
3.01	3.20	3.30		3.15	3.23	3.25	3.20	3.14	3.13	3.38	3.13	2.77	3.11	3.01	3.05	3.09
0.52	0.55	0.56		0.53	0.53	0.56	0.55	0.55	0.56	0.55	0.54	0.45	0.53	0.52	0.53	0.52
3.13	3.31	3.33		3.25	3.27	3.34	3.36	3.26	3.29	3.37	3.20	2.74	3.21	3.20	3.24	3.16
0.73	0.74	0.75		0.73	0.73	0.77	0.74	0.75	0.76	0.77	0.73	0.62	0.71	0.72	0.72	0.70
2.04	2.16	2.18		2.13	2.04	2.17	2.13	2.16	2.20	2.14	2.13	1.78	2.04	2.06	2.03	2.04
0.35	0.37	0.37		0.36	0.35	0.37	0.35	0.37	0.37	0.36	0.36	0.30	0.35	0.34	0.34	0.34
2.22	2.46	2.36		2.39	2.23	2.44	2.37	2.45	2.43	2.43	2.46	1.94	2.27	2.26	2.20	2.22
0.38	0.42	0.39		0.41	0.39	0.41	0.40	0.43	0.41	0.41	0.42	0.33	0.39	0.39	0.38	0.38
			0.703794	0.703793							0.703688	0.703752			0.703545	
				0.513017							0.512980	0.513015		0.513024	0.513021	
							18.989	18.998						18.982		
							15.660	15.665						15.667		
							38.728	38.748						38.729		
											0.283173					

Table 2. *Oxygen isotopic compositions of Mt Pelée and the Quill volcanic samp*

Mt Pelée	plagioclase	clinopyroxene	orthopyroxene	olivine	*whole rock
M8220	6.06				6.85
M8221	6.05				6.65
M8226	5.76	5.54	6.00		6.78
M8229	6.14				
M8230	6.64	5.68			
M8232	6.12	5.79			
M8233	6.02	5.52			
M8234	5.95	5.27			
M8235	6.54	5.54			
M8236		5.53	5.17		
M8237	6.38	5.76	5.76		
M8248	6.08				
M8249	5.88	5.56			
M8250	6.33	5.51	5.51		
The Quill					
SE8240			5.5	5.1	6.84
SE8241		5.3	5.5	5.0	7.00
SE8243		5.7	5.8	5.3	7.36
SE8245		5.3	4.4	5.0	6.59
SE8247A		5.2	5.4		6.32

Table 3. Fractional Crystallisation Models.

a) Least squares (XLFRAC; Stormer and Nicholls, 1978) for Mt Pelée. Parent-daughter pairs selected to represent various SiO_2 ranges and to show that there is little difference in phase *proportions* if fractionation is modelled in one (e.g. M8236-37) versus two (e.g. M8236-35 followed by M8235-37) stages. Shown are models using observed cumulate (rather than phenocryst) phase assemblages, which are the most successful and consistent with trace element considerations. Major element compositions of parent and daughter indicated for each model, are in Table 1.

MODEL		Plagioclase MP-350	Magnetite M-1	Amphibole MP 350	ΣR^2
M8236-37	(SiO_2=51.4-62.9%)	-17.8	-4.2	-24.7	0.156
M8236-35	(SiO_2=51.4-56.4%)	-11.0	-2.5	-15.8	0.039
M8235-37	(SiO_2=56.4-62.9%)	-9.6	-2.5	-12.5	0.136
M8247-46	(SiO_2=55.1-57.7%)	-1.2	-4.1	-14.5	0.086
M8213-28	(SiO_2=55.7-62.1%)	-10.6	-3.4	-12.5	0.306

Mineral compositions from Smith and Roobol (1990) and Wills (1974)

b) The Quill, least square models as in Table 3a. Major element compositions of parent and daughter indicated for each model, as in Table 1.

MODEL		Plagioclase 34E2	Magnetite 475E2	Amphibole 28E2	ΣR^2
SE8227-18A	(SiO_2=53.7-61.4%)	-14.3	-2.7	-17.7	0.183
SE8227-19	(SiO_2=53.7-57.9%)	-9.6	-1.4	-10.2	0.33
SE8219-18A	(SiO_2=57.9-61.4%)	-6.0	-0.8	-9.7	0.20
SE8248-47B	(SiO_2=53.4-57.2%)	-10.0	-1.8	-10.1	0.29
SE8244-39	(SiO_2=55.2-57.7%)	-6.3	-1.0	-7.0	0.028
SE8244-37	(SiO_2=55.2-60.4%)	-10.8	-1.9	-14.4	0.11
SE8239-37	(SiO_2=57.7-60.4%)	-5.3	-1.1	-8.7	0.033

Mineral compositions from Wills (1974)

Table 4. Distribution Coefficients.

a) Mineral-melt distribution coefficients used for modelling trace element vectors in Figures 7 and 9, compiled from Fujimaki et al., 1984, Johnson 1994, Aignertorres et al., 2007, Villermant et al., 1981, Bottazzi et al., 1999, and set at 0.01 where not available and known to be insignificant. ol = olivine, cpx = clinopyroxene. plag = plagioclase, mt = magnetite, amph = amphibole. Bulk D_is are for modal phenocryst assemblage (3% ol, 16% cpx, 71% plag, 10% mt) and for cumulate assemblage 38% plag, 53% amph, 9% mt.

	ol	cpx	plag	mt	amph	D_i phenocrysts	D_i cumulate
Sr	0.010	0.124	1.640	0.010	0.298	1.186	0.782
Ba	0.010	0.001	0.290	0.010	0.160	0.207	0.196
Th	0.010	0.012	0.250	0.100	0.004	0.190	0.106
U	0.010	0.010	0.250	0.110	0.004	0.190	0.107
La	0.008	0.105	0.035	0.010	0.116	0.043	0.076
Dy	0.005	0.622	0.011	0.010	0.967	0.060	0.218
Yb	0.031	0.601	0.016	0.020	0.816	0.087	0.351
Hf	0.040	0.121	0.01	0.010	0.330	0.109	0.518

b) Calculated bulk distribution coefficients using maximum enrichment factor (c_l/c_0) to identify the element with lowest distribution coefficient (Rb for Mt Pelée, Zr for The Quill). If this distribution coefficient is assumed to be $D_i = 0$ then other trace element D_is can be determined (see text for details).

	Mt Pelée M8236-37 (F = 0.32)	The Quill SE8227-37 (F = 0.57)
	D_i	D_i
Rb	**0**	0.52
Sr	1.28	1.26
Y	0.93	1.14
Zr	0.16	**0**
Ba	0.50	0.48
Pb	0.59	0.66
U	0.23	0.71
Th	0.21	0.86
Nb	0.40	-
Hf	0.42	0.46
La	0.37	0.79
Ce	0.39	0.64
Nd	0.56	0.24
Sm	0.73	0.52
Eu	0.85	0.53
Gd	0.87	0.49
Tb	0.88	0.56
Dy	0.95	0.66
Er	0.95	0.57
Tm	0.96	0.68
Yb	0.89	0.44
Lu	0.88	0.54

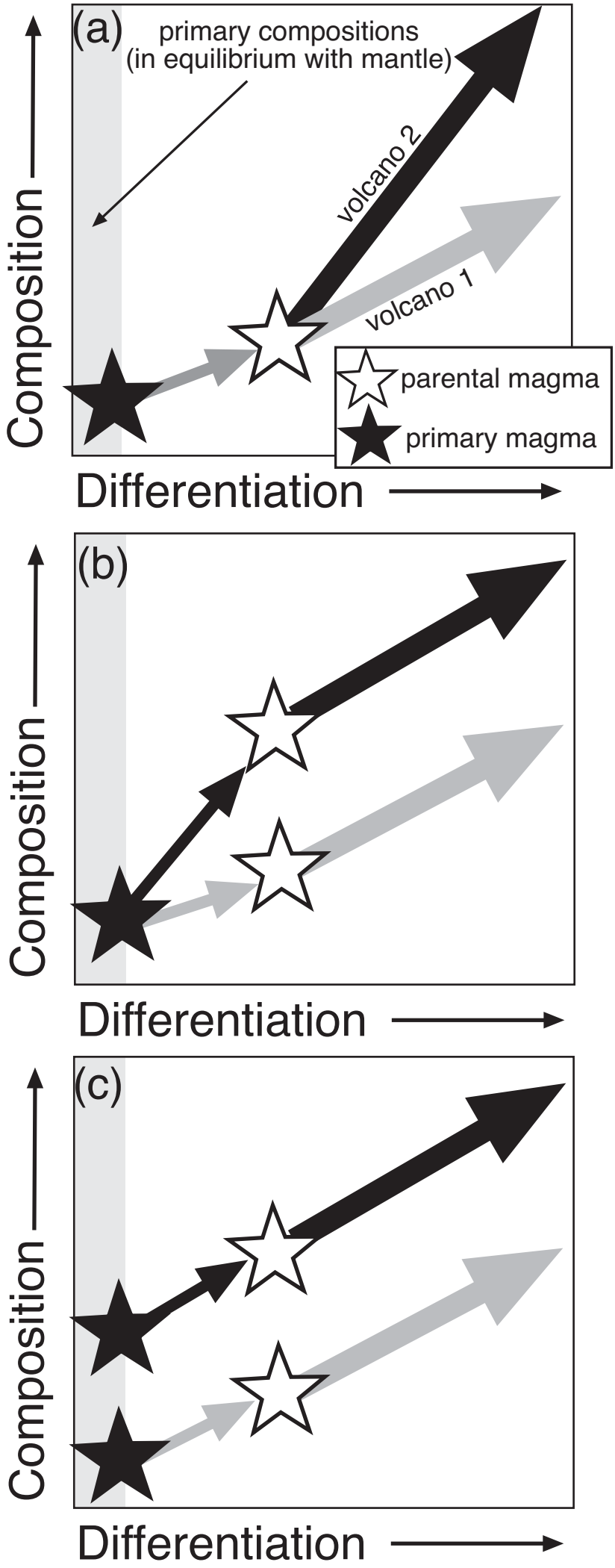
(a)
primary compositions
(in equilibrium with mantle)
volcano 2
volcano 1
parental magma
primary magma
Composition
Differentiation
(b)
Composition
Differentiation
(c)
Composition
Differentiation

Figure 1

Figure 2

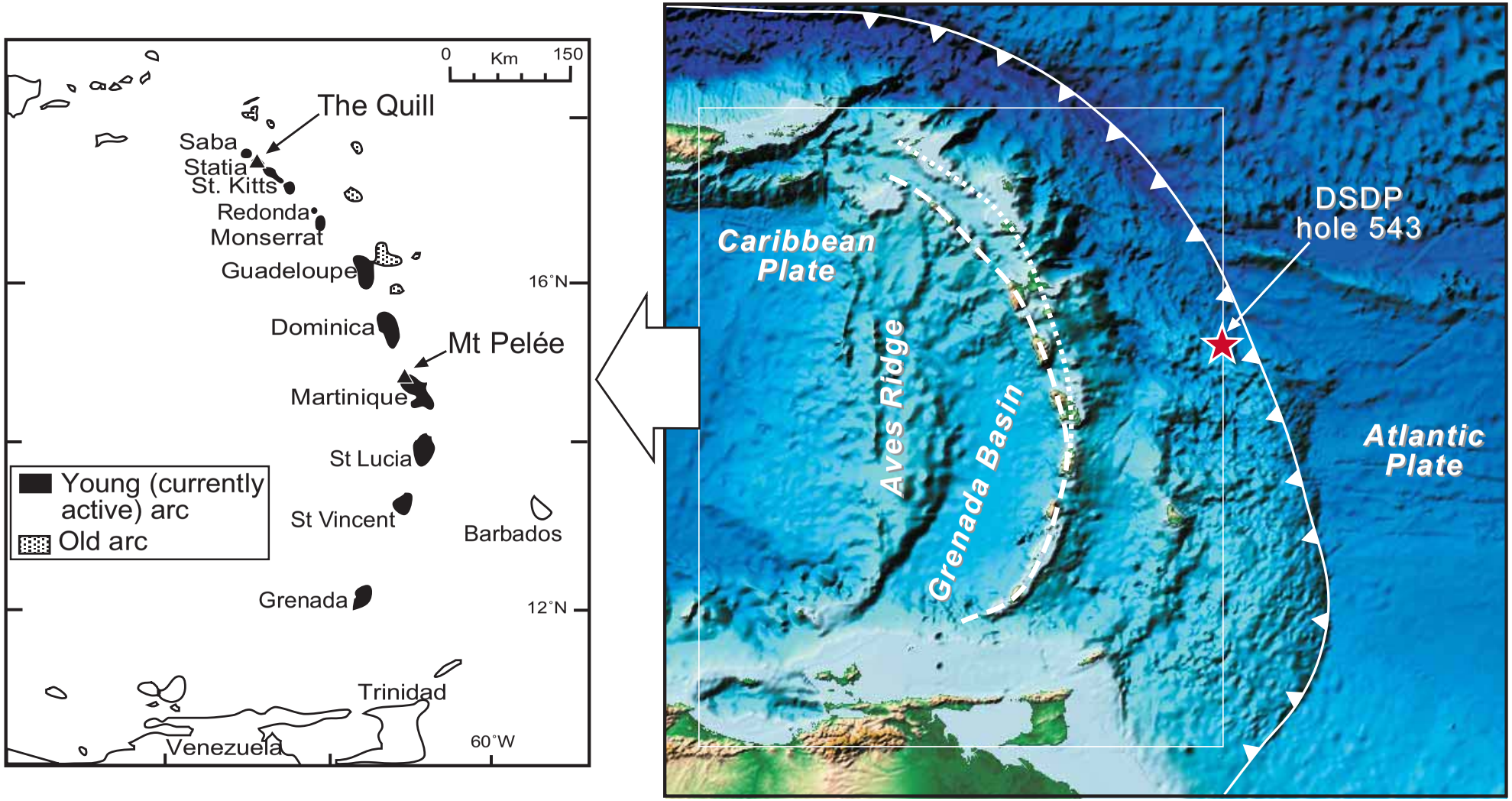
0 Km 150
The Quill
Saba
Statia
St. Kitts
Redonda
Monserrat
Guadeloupe
16°N
Dominica
Mt Pelée
Martinique
St Lucia
St Vincent
Barbados
Grenada
12°N
Trinidad
Venezuela
60°W
Young (currently active) arc
Old arc
Caribbean Plate
Aves Ridge
Grenada Basin
DSDP hole 543
Atlantic Plate

Figure 3

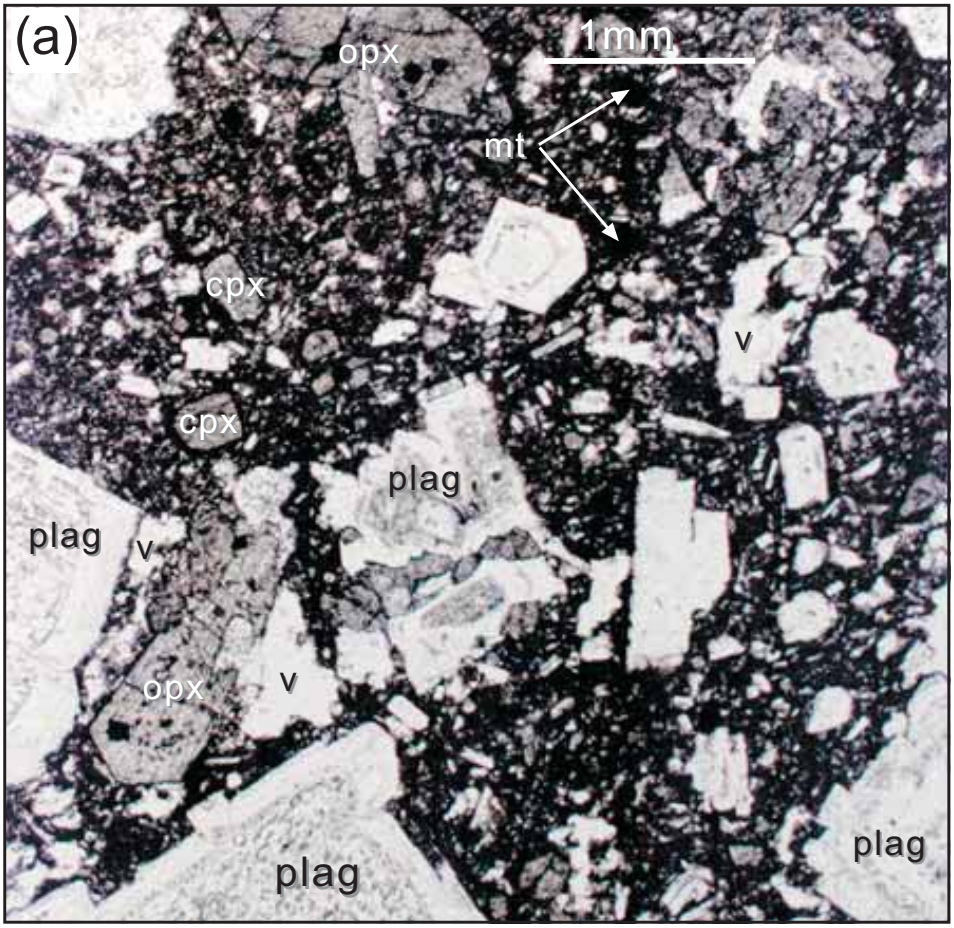
(a)
1mm
opx
mt
cpx
v
cpx
plag
plag
v
opx
v
plag
plag

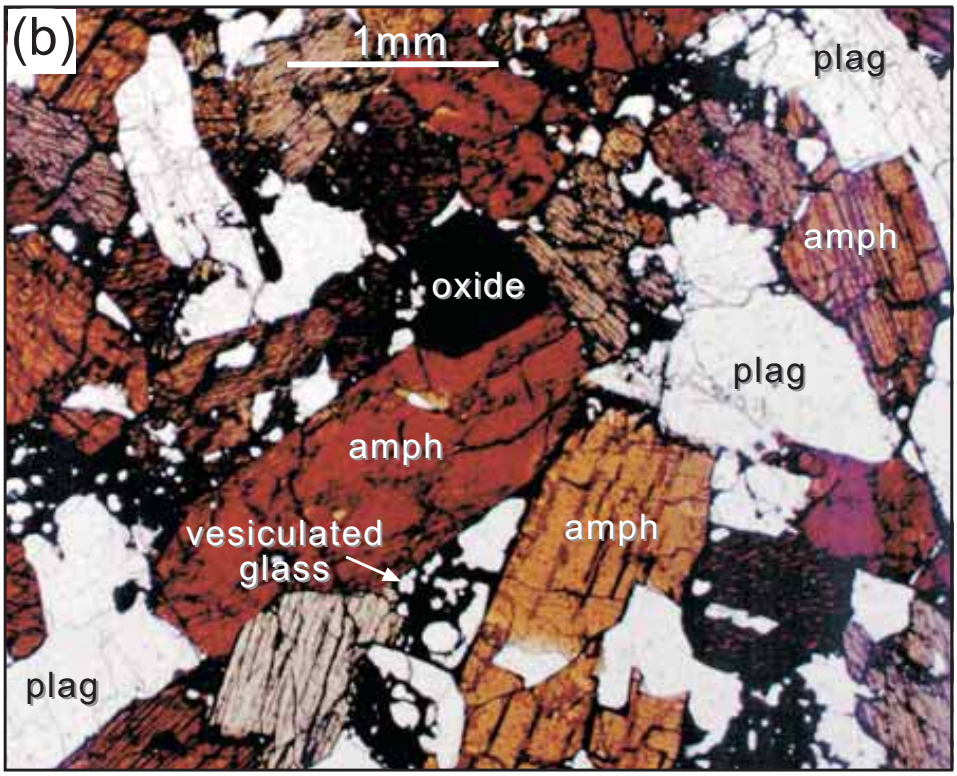
(b)
1mm
plag
amph
oxide
plag
amph
vesiculated
glass
amph
plag

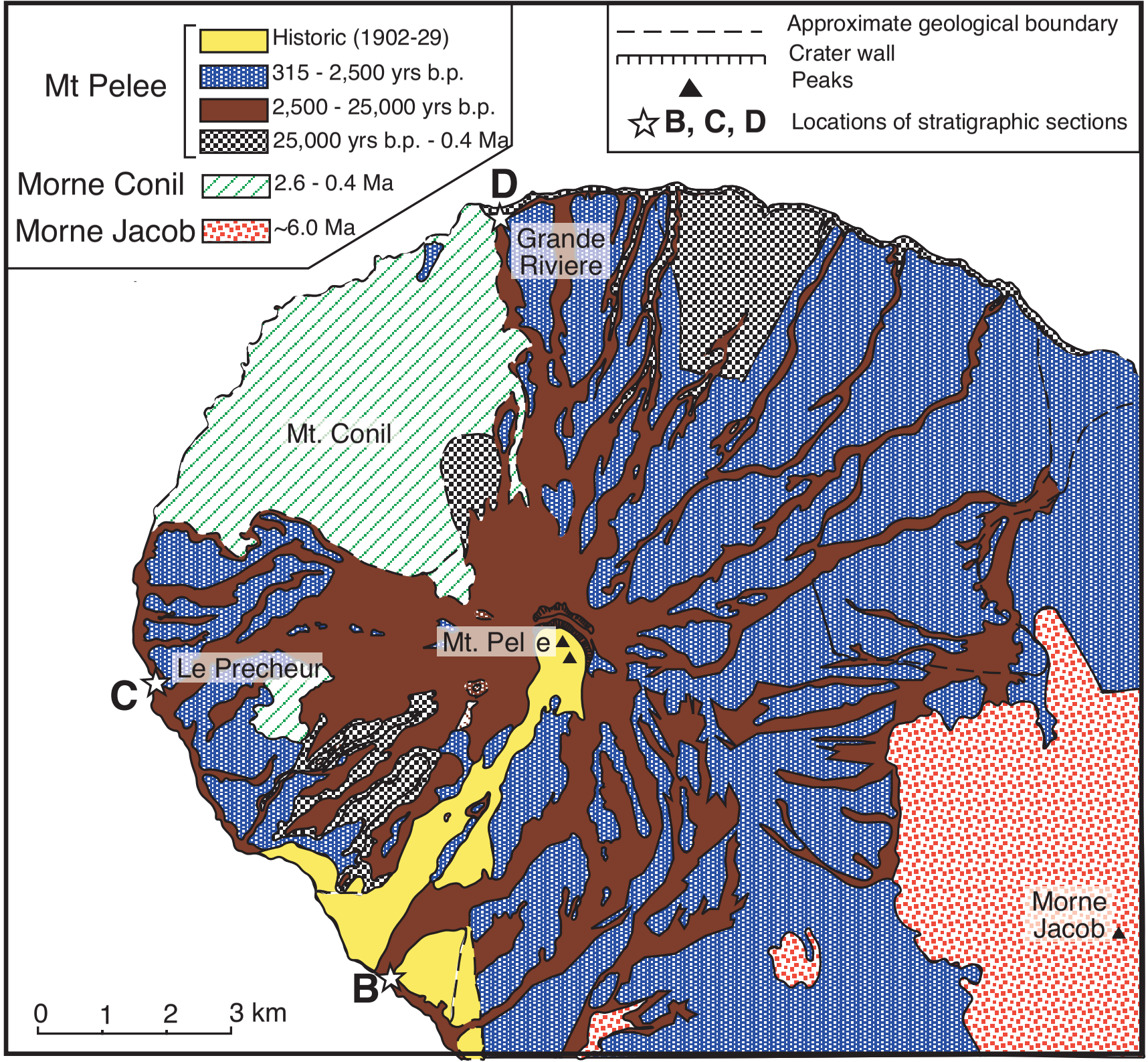
Mt Pelee
Historic (1902-29)
315 - 2,500 yrs b.p.
2,500 - 25,000 yrs b.p.
25,000 yrs b.p. - 0.4 Ma
Morne Conil
2.6 - 0.4 Ma
Morne Jacob
~6.0 Ma
Approximate geological boundary
Crater wall
Peaks
B, C, D
Locations of stratigraphic sections
D
Grande Riviere
Mt. Conil
Mt. Pel e
Le Precheur
C
B
Morne Jacob
0 1 2 3 km

Figure 3a

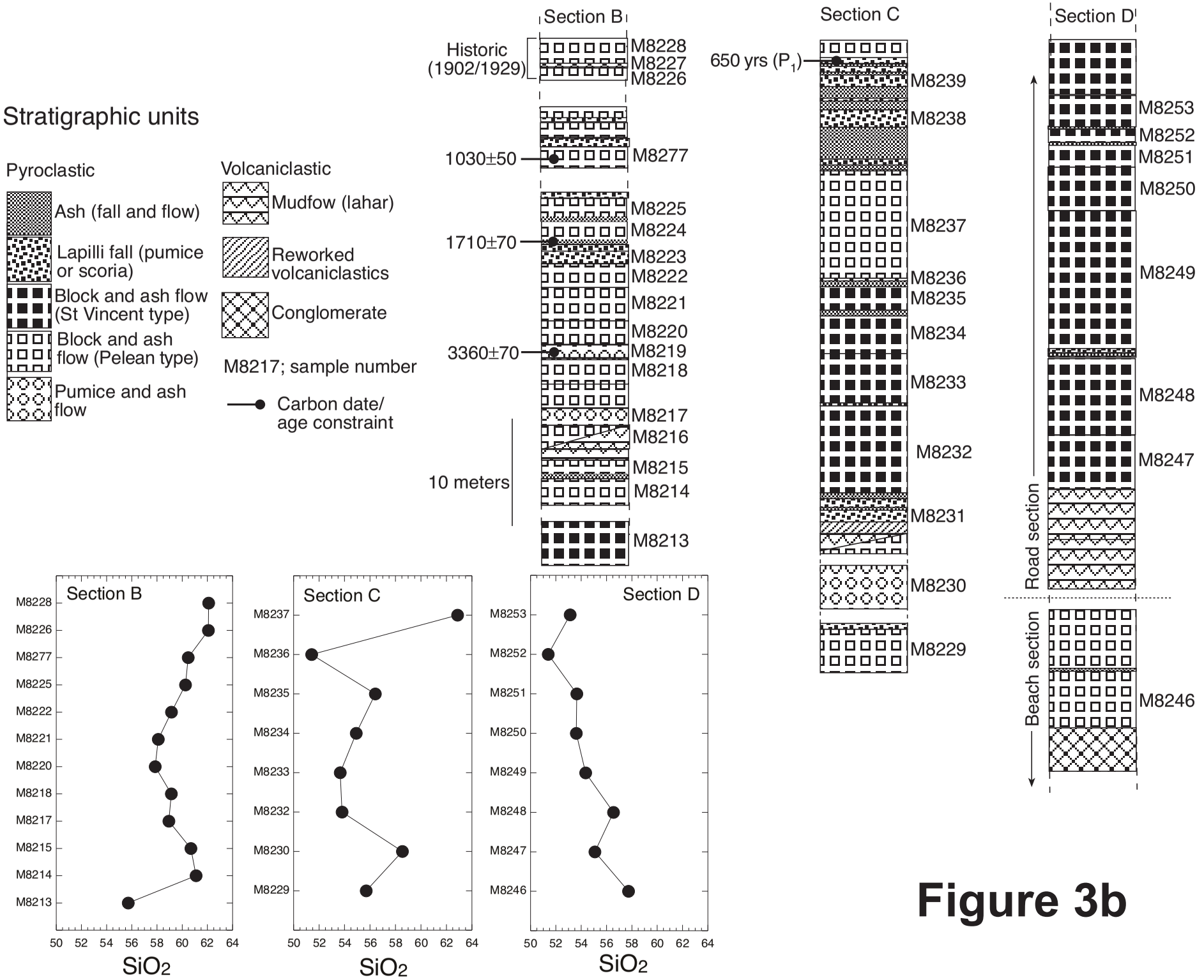
Stratigraphic units
Pyroclastic
Ash (fall and flow)
Lapilli fall (pumice or scoria)
Block and ash flow (St Vincent type)
Block and ash flow (Pelean type)
Pumice and ash flow
Volcaniclastic
Mudfow (lahar)
Reworked volcaniclastics
Conglomerate
M8217; sample number
Carbon date/ age constraint
Section B
Historic (1902/1929)
M8228
M8227
M8226
1030±50
M8277
M8225
M8224
1710±70
M8223
M8222
M8221
M8220
3360±70
M8219
M8218
M8217
M8216
M8215
10 meters
M8214
M8213
Section C
650 yrs (P1)
M8239
M8238
M8237
M8236
M8235
M8234
M8233
M8232
M8231
M8230
M8229
Section D
M8253
M8252
M8251
M8250
M8249
M8248
M8247
Road section
Beach section
M8246
Section B
M8228
M8226
M8277
M8225
M8222
M8221
M8220
M8218
M8217
M8215
M8214
M8213
50 52 54 56 58 60 62 64
SiO2
Section C
M8237
M8236
M8235
M8234
M8233
M8232
M8230
M8229
50 52 54 56 58 60 62 64
SiO2
Section D
M8253
M8252
M8251
M8250
M8249
M8248
M8247
M8246
50 52 54 56 58 60 62 64
SiO2

Figure 3b

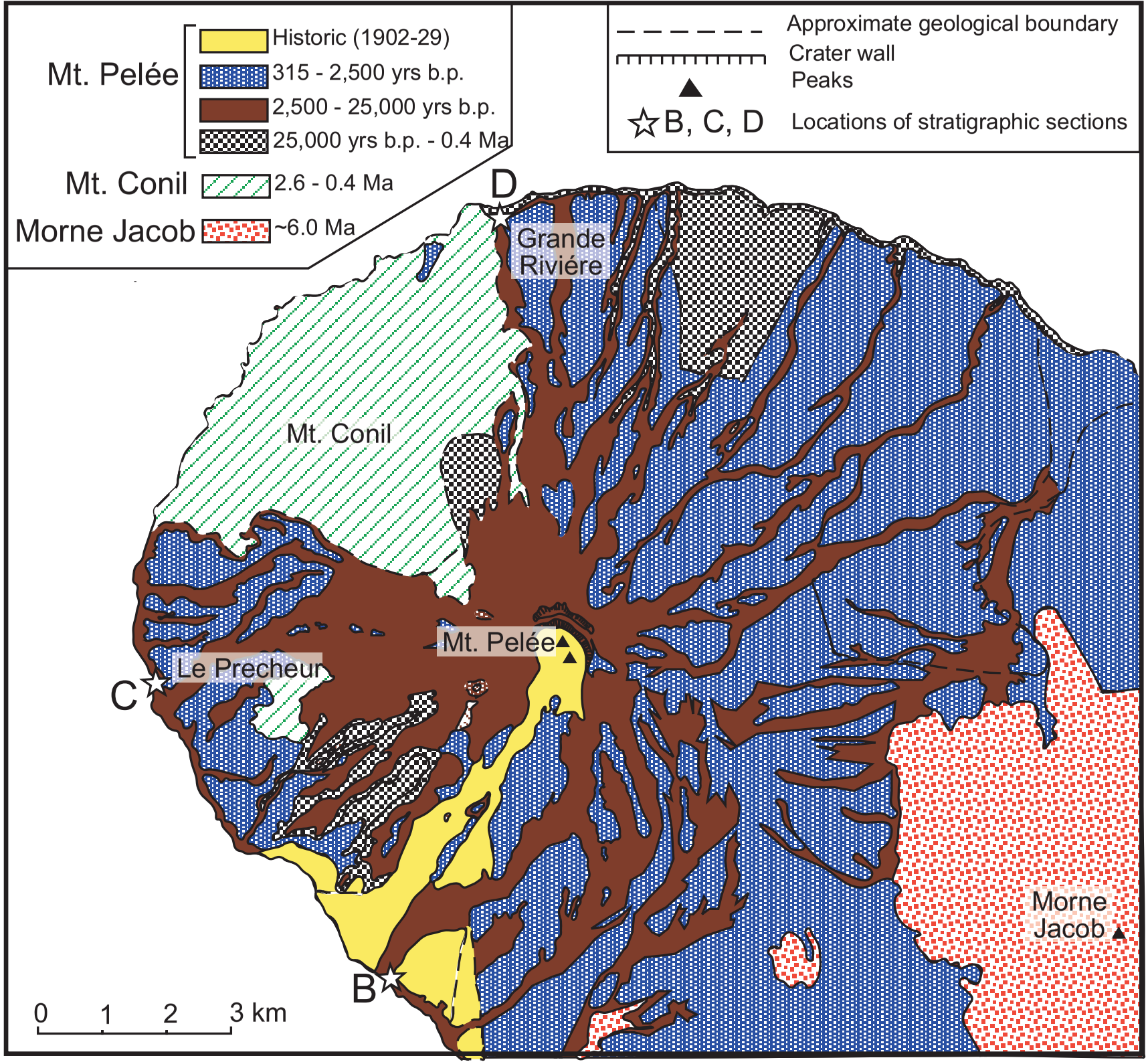
Mt. Pelée
Historic (1902-29)
315 - 2,500 yrs b.p.
2,500 - 25,000 yrs b.p.
25,000 yrs b.p. - 0.4 Ma
Mt. Conil
2.6 - 0.4 Ma
Morne Jacob
~6.0 Ma
Approximate geological boundary
Crater wall
Peaks
B, C, D
Locations of stratigraphic sections
D
Grande Riviére
Mt. Conil
Mt. Pelée
Le Precheur
C
B
Morne Jacob
0 1 2 3 km

Figure 4a

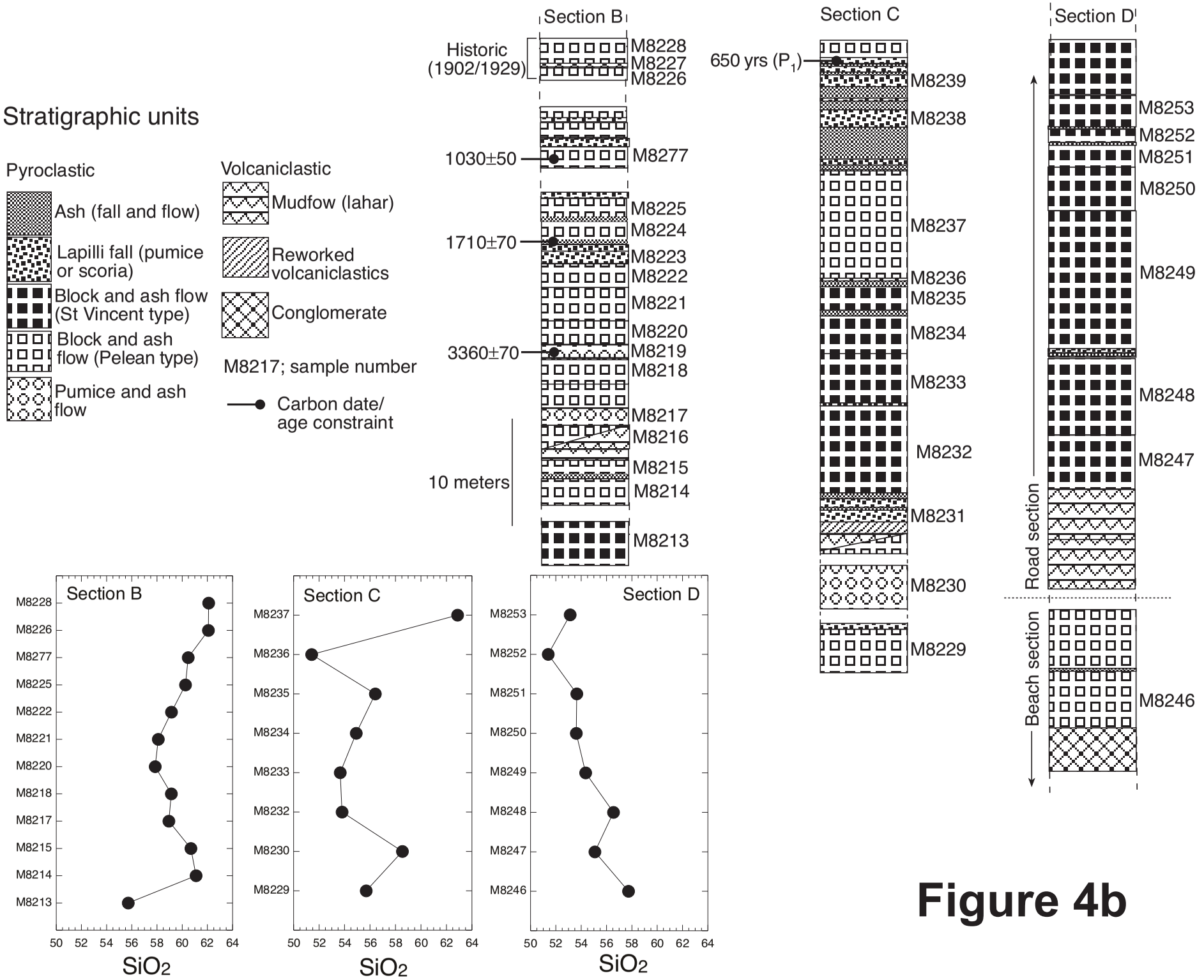
Stratigraphic units
Pyroclastic
Ash (fall and flow)
Lapilli fall (pumice or scoria)
Block and ash flow (St Vincent type)
Block and ash flow (Pelean type)
Pumice and ash flow
Volcaniclastic
Mudfow (lahar)
Reworked volcaniclastics
Conglomerate
M8217; sample number
Carbon date/ age constraint
Section B
Historic (1902/1929)
M8228
M8227
M8226
1030±50
M8277
M8225
M8224
1710±70
M8223
M8222
M8221
M8220
3360±70
M8219
M8218
M8217
M8216
M8215
M8214
10 meters
M8213
Section C
650 yrs (P1)
M8239
M8238
M8237
M8236
M8235
M8234
M8233
M8232
M8231
M8230
M8229
Section D
M8253
M8252
M8251
M8250
M8249
M8248
M8247
Road section
Beach section
M8246
Section B
M8228
M8226
M8277
M8225
M8222
M8221
M8220
M8218
M8217
M8215
M8214
M8213
50 52 54 56 58 60 62 64
SiO2
Section C
M8237
M8236
M8235
M8234
M8233
M8232
M8230
M8229
50 52 54 56 58 60 62 64
SiO2
Section D
M8253
M8252
M8251
M8250
M8249
M8248
M8247
M8246
50 52 54 56 58 60 62 64
SiO2

Figure 4b

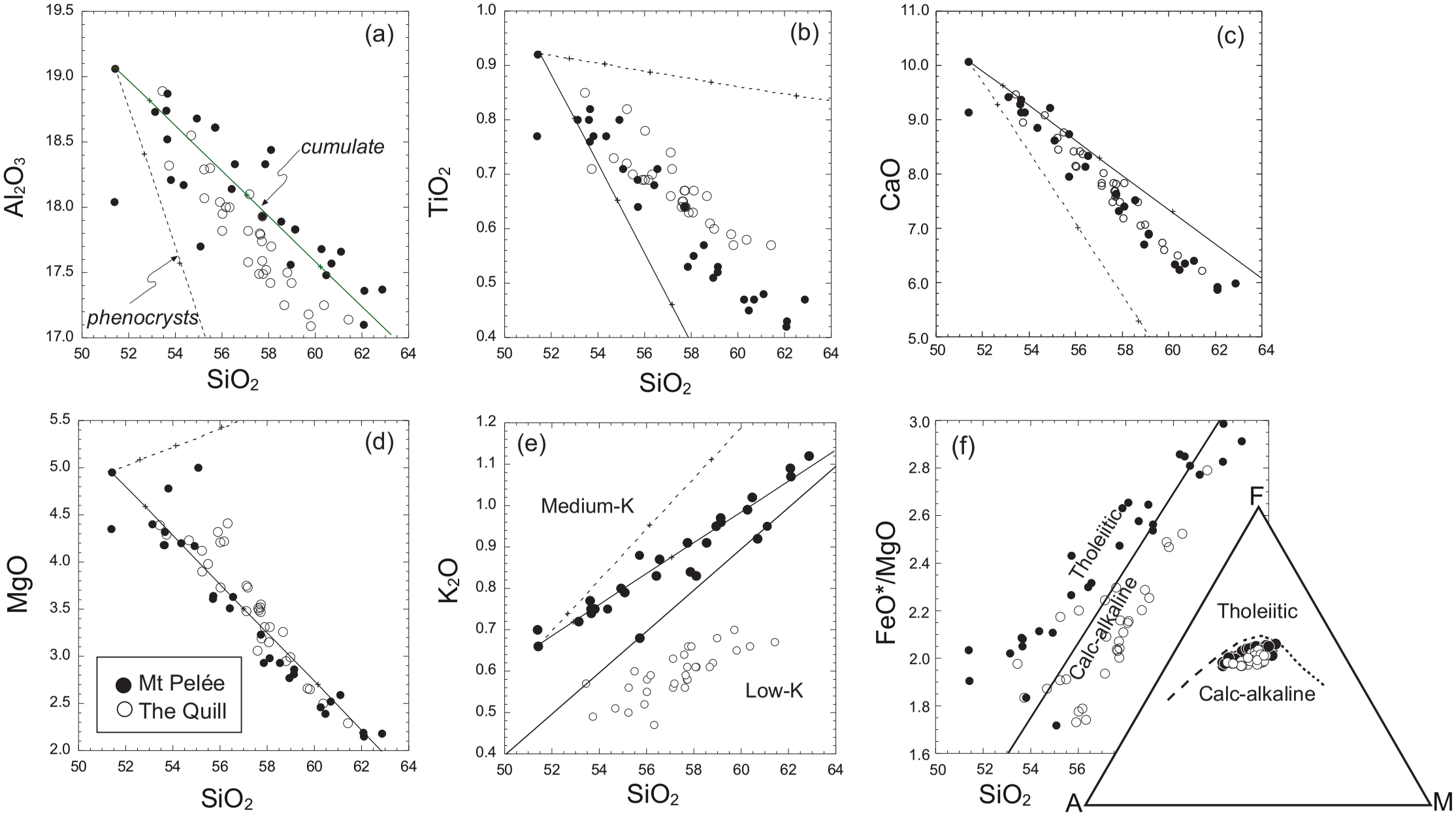
(a)
Al_2O_3
SiO_2
cumulate
phenocrysts
(b)
TiO_2
SiO_2
(c)
CaO
(d)
MgO
Mt Pelée
The Quill
(e)
K_2O
Medium-K
Low-K
(f)
FeO*/MgO
Tholeiitic
Calc-alkaline
F
A
M

Figure 5

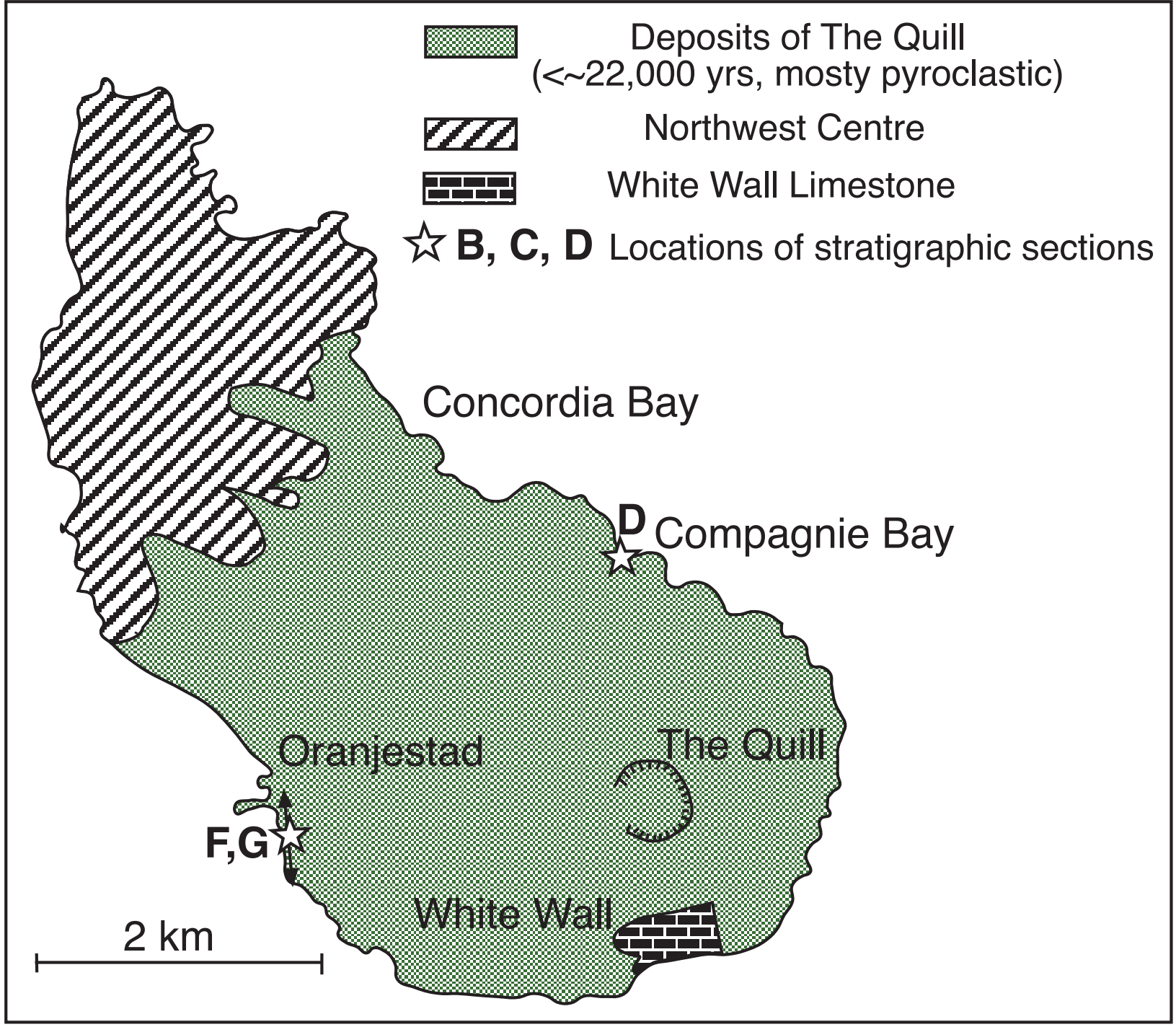
Deposits of The Quill
(<~22,000 yrs, mosty pyroclastic)
Northwest Centre
White Wall Limestone
B, C, D Locations of stratigraphic sections
Concordia Bay
D
Compagnie Bay
Oranjestad
The Quill
F,G
White Wall
2 km

Figure 5a

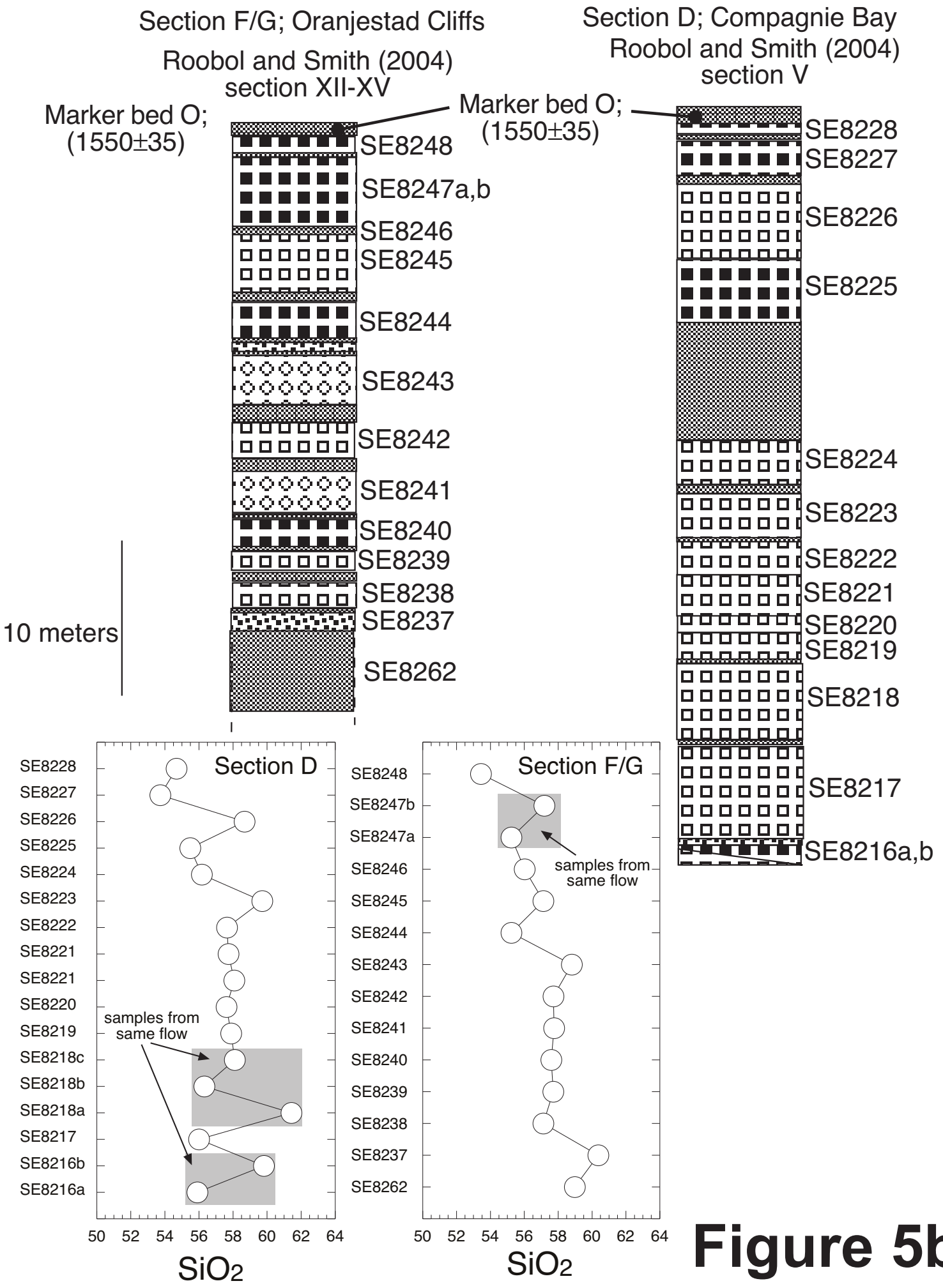
Section F/G; Oranjestad Cliffs
Roobol and Smith (2004)
section XII-XV
Marker bed O;
(1550±35)
SE8248
SE8247a,b
SE8246
SE8245
SE8244
SE8243
SE8242
SE8241
SE8240
SE8239
SE8238
SE8237
SE8262
10 meters
Section D; Compagnie Bay
Roobol and Smith (2004)
section V
Marker bed O;
(1550±35)
SE8228
SE8227
SE8226
SE8225
SE8224
SE8223
SE8222
SE8221
SE8220
SE8219
SE8218
SE8217
SE8216a,b
Section D
SE8228
SE8227
SE8226
SE8225
SE8224
SE8223
SE8222
SE8221
SE8221
SE8220
SE8219
SE8218c
SE8218b
SE8218a
SE8217
SE8216b
SE8216a
samples from
same flow
50 52 54 56 58 60 62 64
SiO2
Section F/G
SE8248
SE8247b
SE8247a
SE8246
SE8245
SE8244
SE8243
SE8242
SE8241
SE8240
SE8239
SE8238
SE8237
SE8262
samples from
same flow
50 52 54 56 58 60 62 64
SiO2

Figure 5b

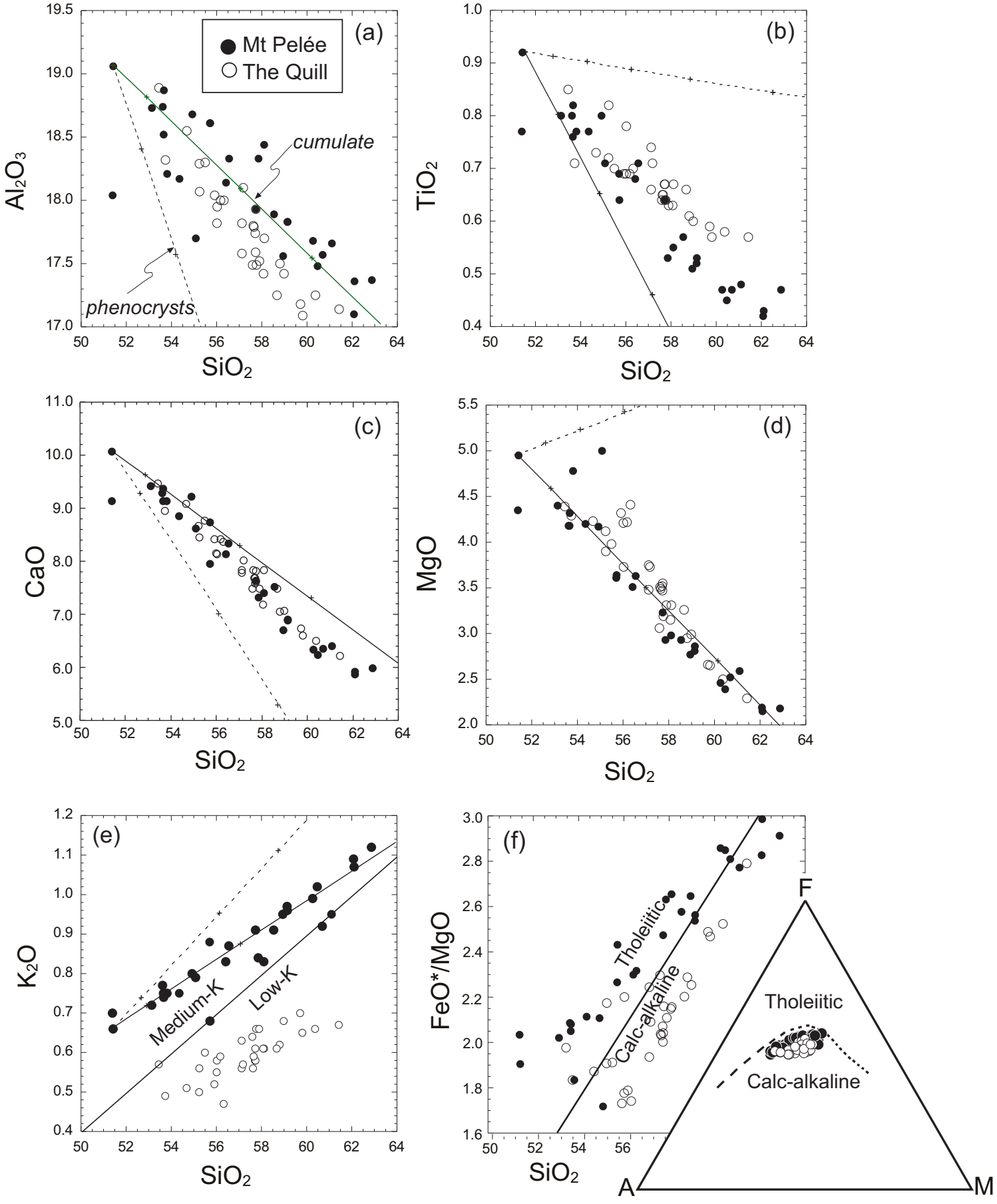
(a)
Mt Pelée
The Quill
cumulate
phenocrysts
Al2O3
SiO2
(b)
TiO2
SiO2
(c)
CaO
SiO2
(d)
MgO
SiO2
(e)
K2O
Medium-K
Low-K
SiO2
(f)
FeO*/MgO
Tholeiitic
Calc-alkaline
SiO2
F
A
M
Tholeiitic
Calc-alkaline

Figure 6

Figure 7

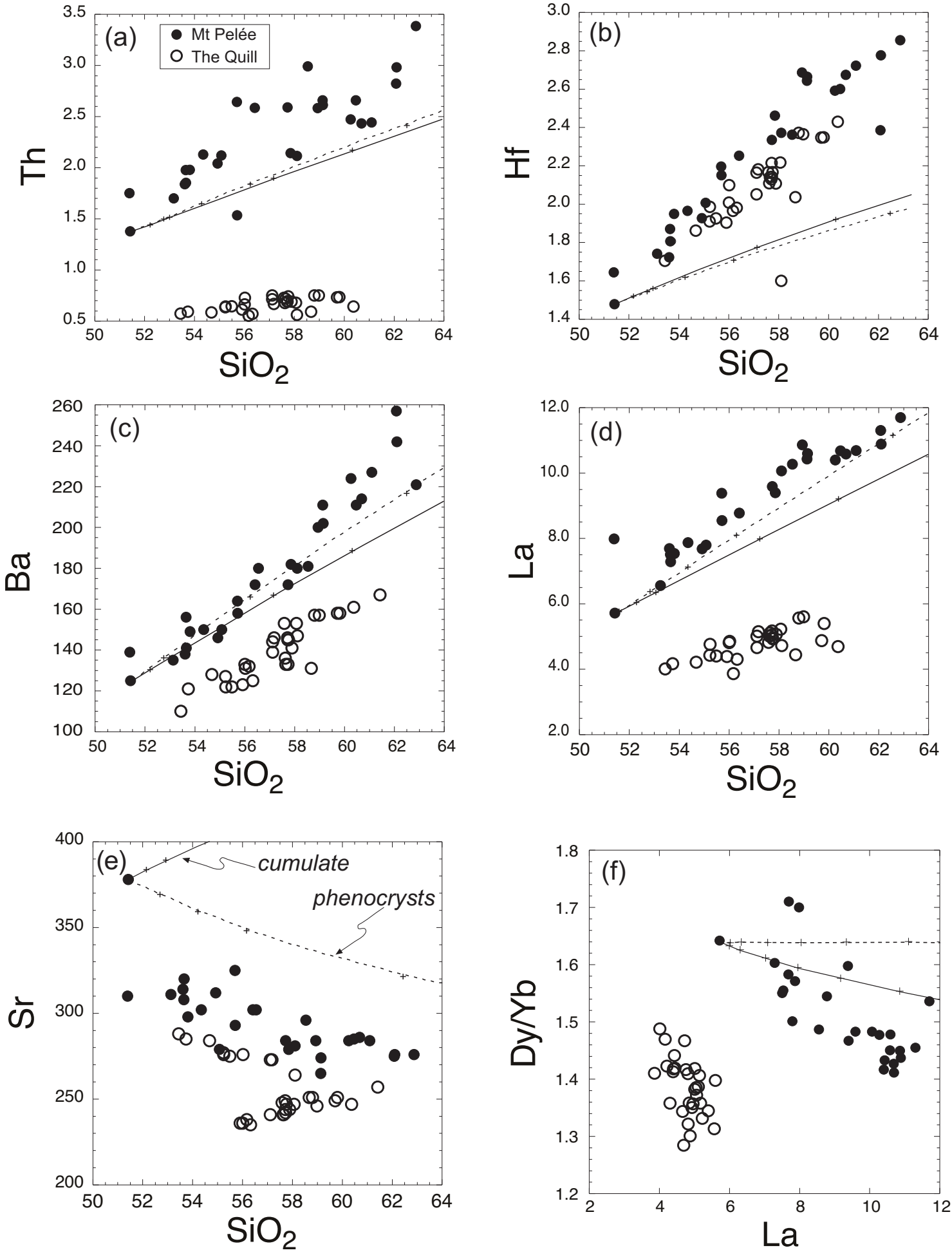
(a)
Mt Pelée
The Quill
Th
SiO2
(b)
Hf
SiO2
(c)
Ba
SiO2
(d)
La
SiO2
(e)
cumulate
phenocrysts
Sr
SiO2
(f)
Dy/Yb
La

Figure 8

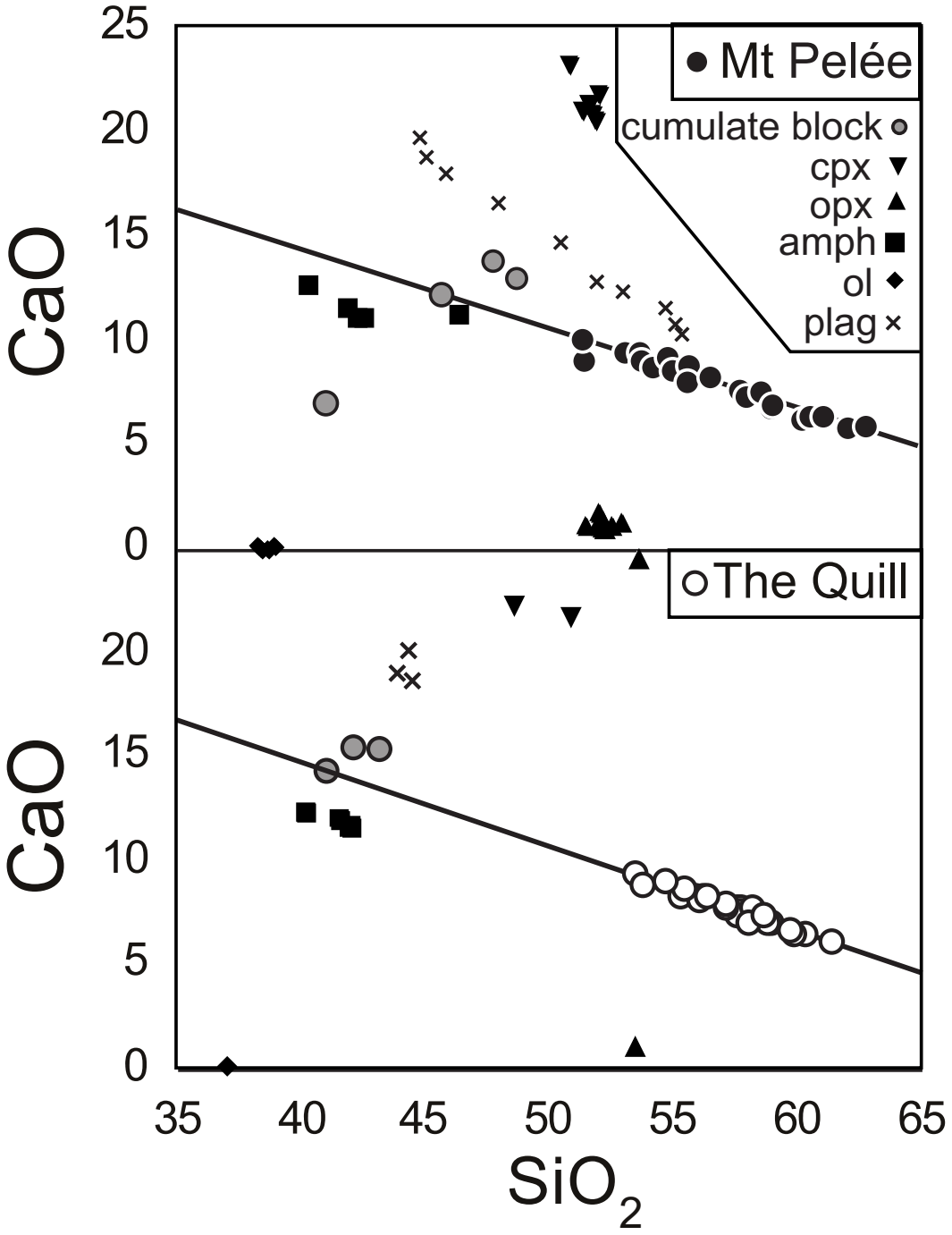
Mt Pelée
cumulate block
cpx
opx
amph
ol
plag
The Quill
CaO
CaO
SiO2
25
20
15
10
5
0
20
15
10
5
0
35
40
45
50
55
60
65

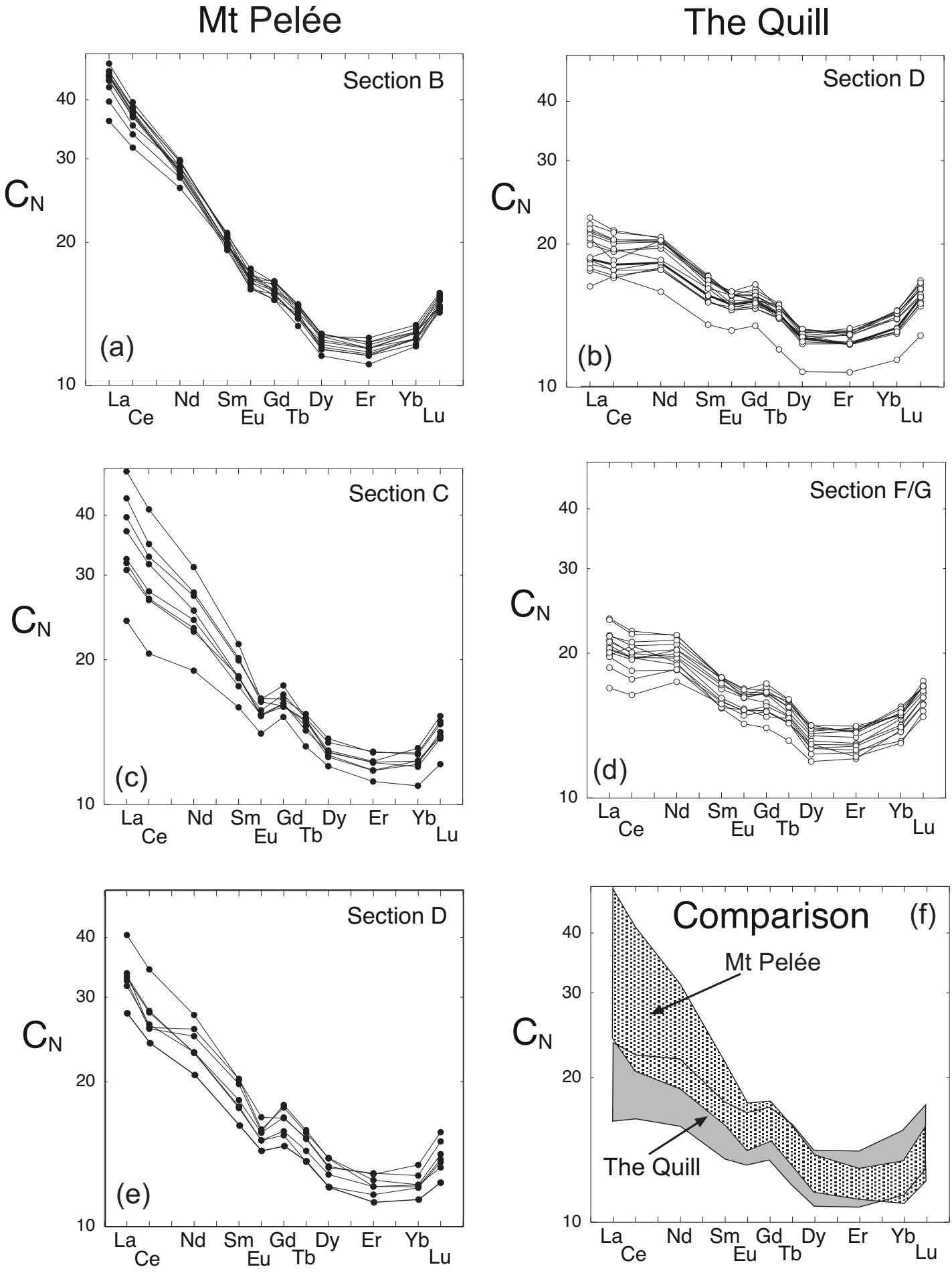
Mt Pelée
The Quill
Section B
Section D
Section C
Section F/G
Section D
Comparison
(f)
Mt Pelée
The Quill
(a)
(b)
(c)
(d)
(e)
C_N
40
30
20
10
La
Ce
Nd
Sm
Eu
Gd
Tb
Dy
Er
Yb
Lu

Figure 9

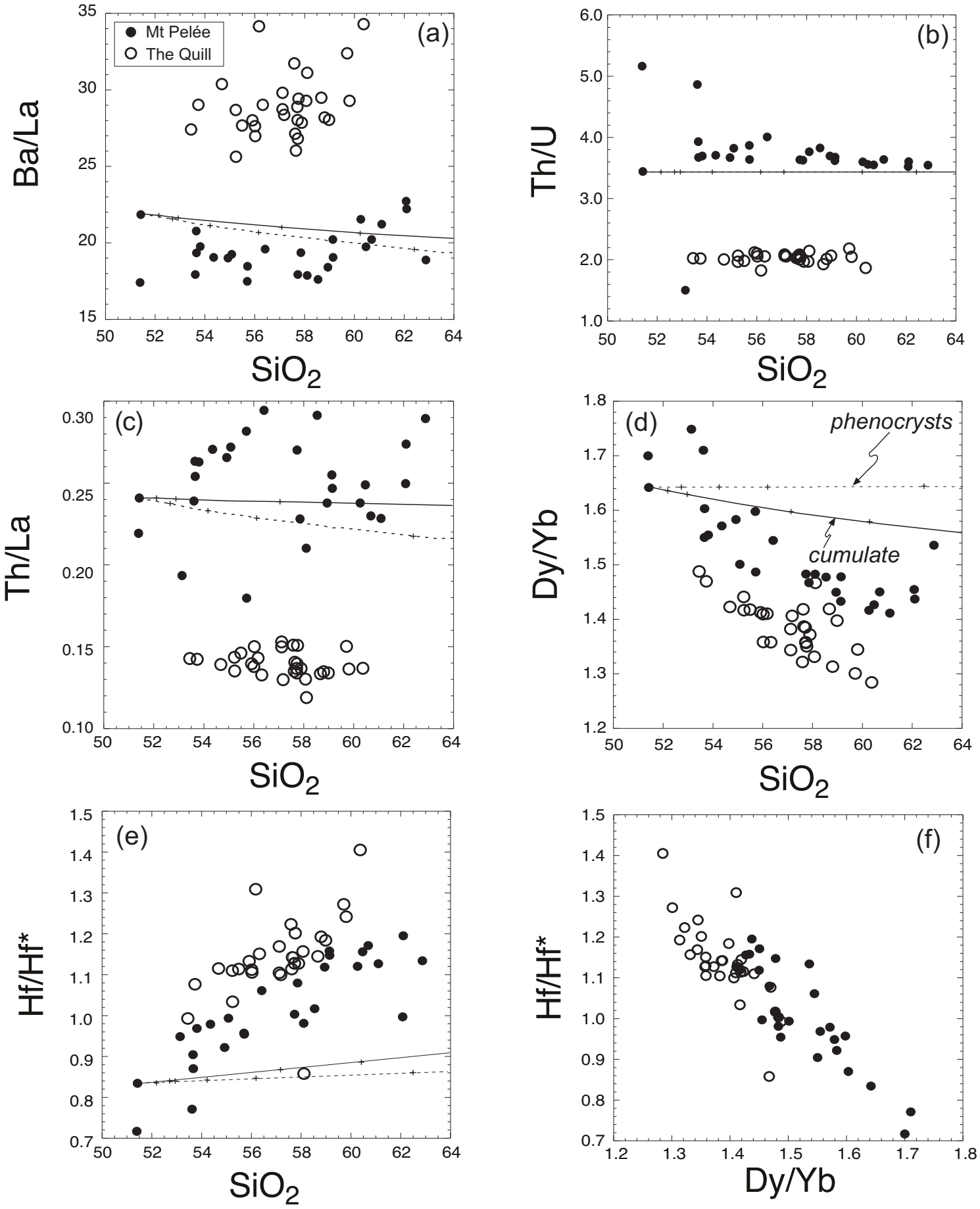
(a)
Mt Pelée
The Quill
Ba/La
SiO2
(b)
Th/U
SiO2
(c)
Th/La
SiO2
(d)
phenocrysts
cumulate
Dy/Yb
SiO2
(e)
Hf/Hf*
SiO2
(f)
Hf/Hf*
Dy/Yb

Figure 10

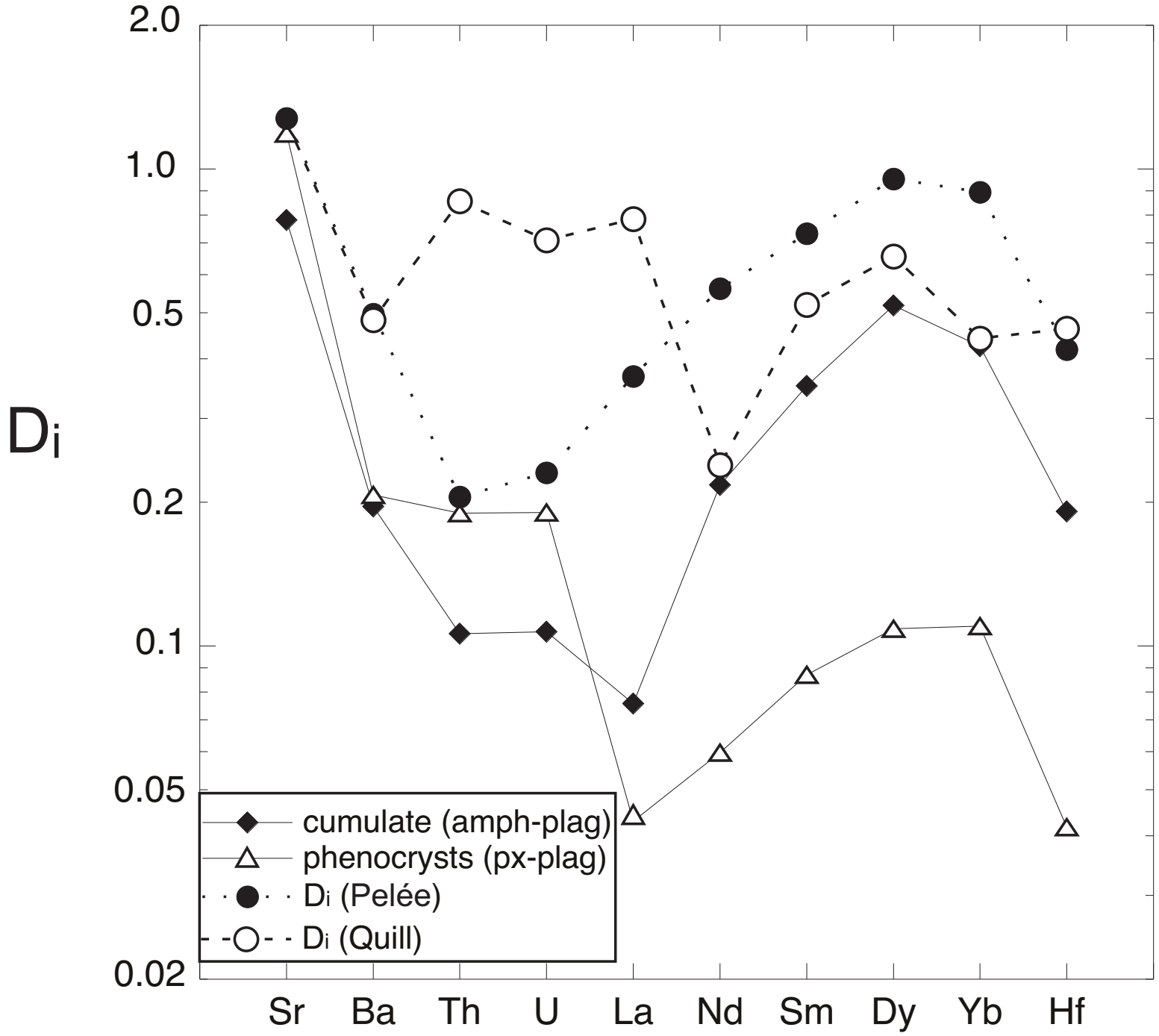
2.0
1.0
0.5
0.2
0.1
0.05
0.02
Di
Sr
Ba
Th
U
La
Nd
Sm
Dy
Yb
Hf
cumulate (amph-plag)
phenocrysts (px-plag)
Di (Pelée)
Di (Quill)

Figure 11

Figure 12

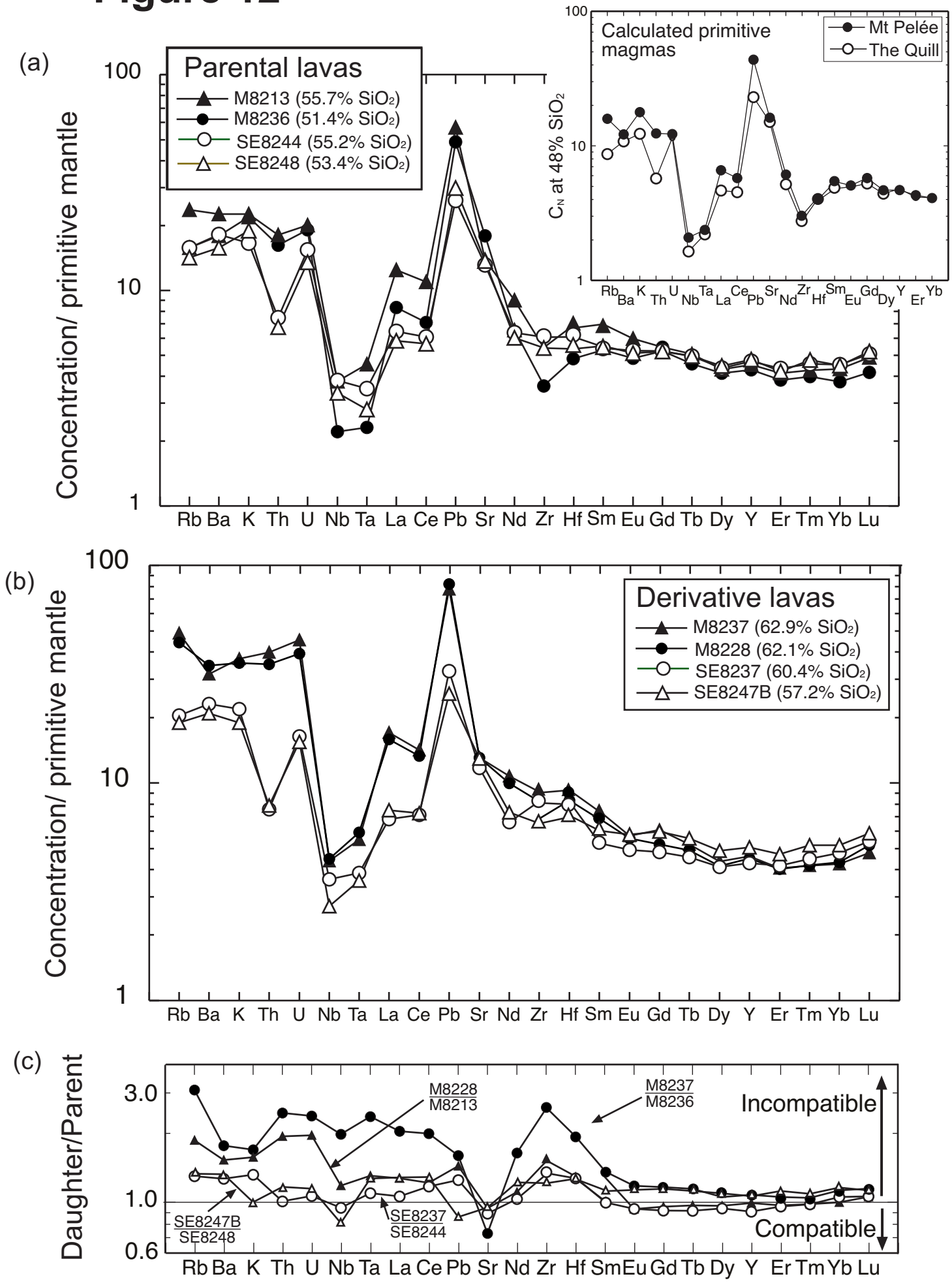
(a)
Parental lavas
M8213 (55.7% SiO2)
M8236 (51.4% SiO2)
SE8244 (55.2% SiO2)
SE8248 (53.4% SiO2)
Concentration/ primitive mantle
100
10
1
Rb Ba K Th U Nb Ta La Ce Pb Sr Nd Zr Hf Sm Eu Gd Tb Dy Y Er Tm Yb Lu
Calculated primitive magmas
Mt Pelée
The Quill
CN at 48% SiO2
Rb Ba K Th U Nb Ta La Ce Pb Sr Nd Zr Hf Sm Eu Gd Dy Y Er Yb
(b)
Derivative lavas
M8237 (62.9% SiO2)
M8228 (62.1% SiO2)
SE8237 (60.4% SiO2)
SE8247B (57.2% SiO2)
Concentration/ primitive mantle
100
10
1
Rb Ba K Th U Nb Ta La Ce Pb Sr Nd Zr Hf Sm Eu Gd Tb Dy Y Er Tm Yb Lu
(c)
Daughter/Parent
3.0
1.0
0.6
M8228/M8213
M8237/M8236
SE8247B/SE8248
SE8237/SE8244
Incompatible
Compatible
Rb Ba K Th U Nb Ta La Ce Pb Sr Nd Zr Hf Sm Eu Gd Tb Dy Y Er Tm Yb Lu

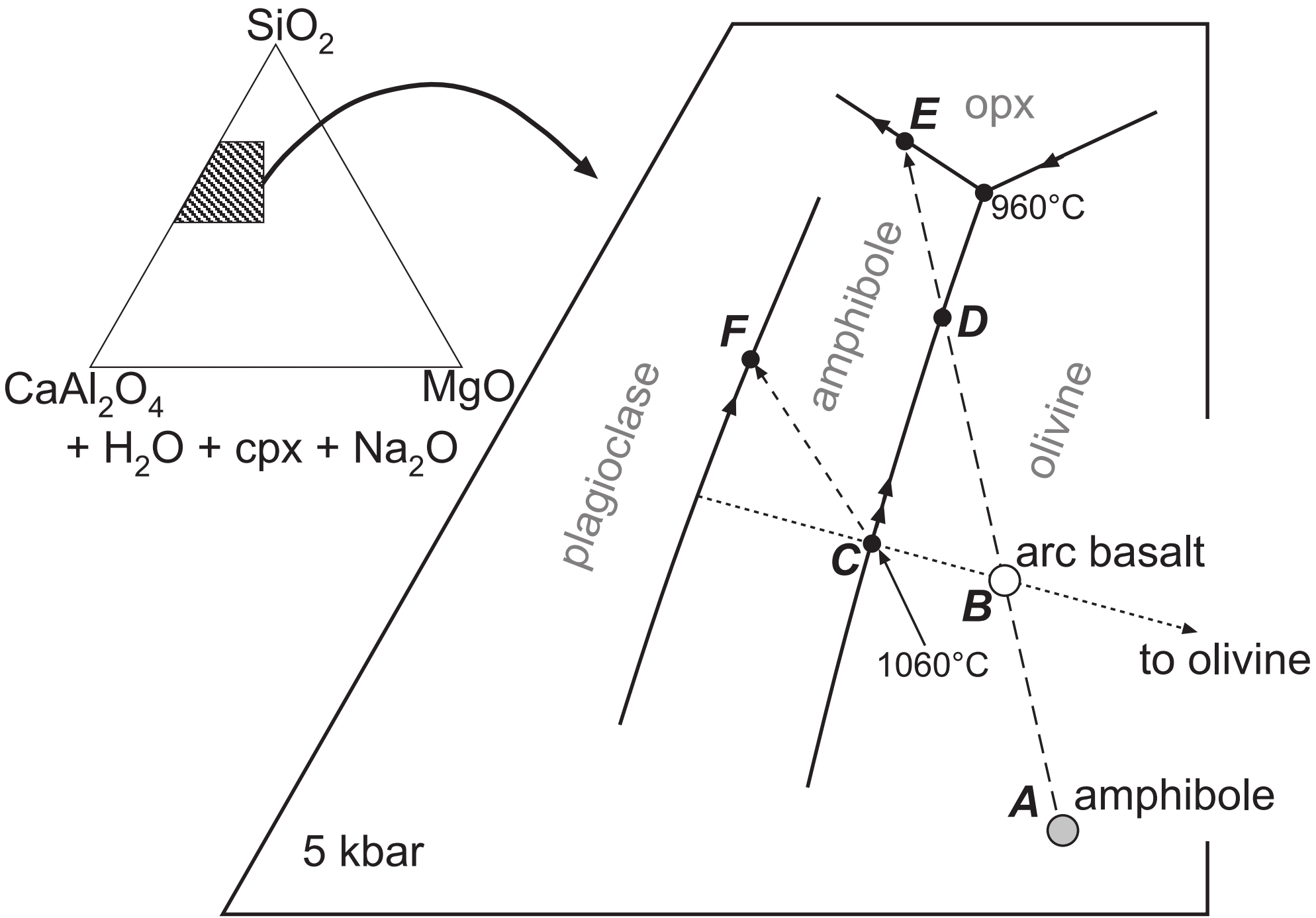
SiO2
CaAl2O4
+ H2O + cpx + Na2O
MgO
E
opx
960°C
F
amphibole
D
plagioclase
olivine
C
arc basalt
B
1060°C
to olivine
A
amphibole
5 kbar

Figure 13

Figure 14

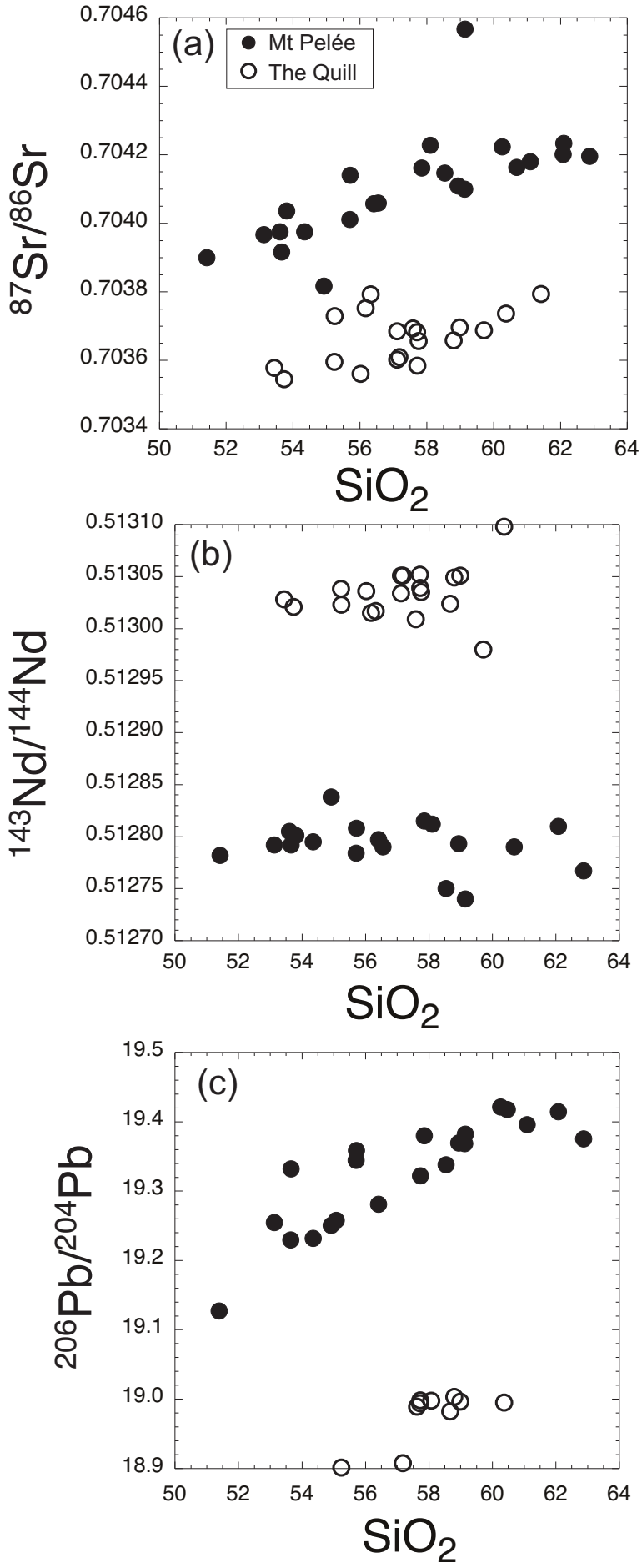
(a)
Mt Pelée
The Quill
$^{87}Sr/^{86}Sr$
0.7046
0.7044
0.7042
0.7040
0.7038
0.7036
0.7034
50
52
54
56
58
60
62
64
SiO_2
(b)
$^{143}Nd/^{144}Nd$
0.51310
0.51305
0.51300
0.51295
0.51290
0.51285
0.51280
0.51275
0.51270
SiO_2
(c)
$^{206}Pb/^{204}Pb$
19.5
19.4
19.3
19.2
19.1
19.0
18.9
SiO_2

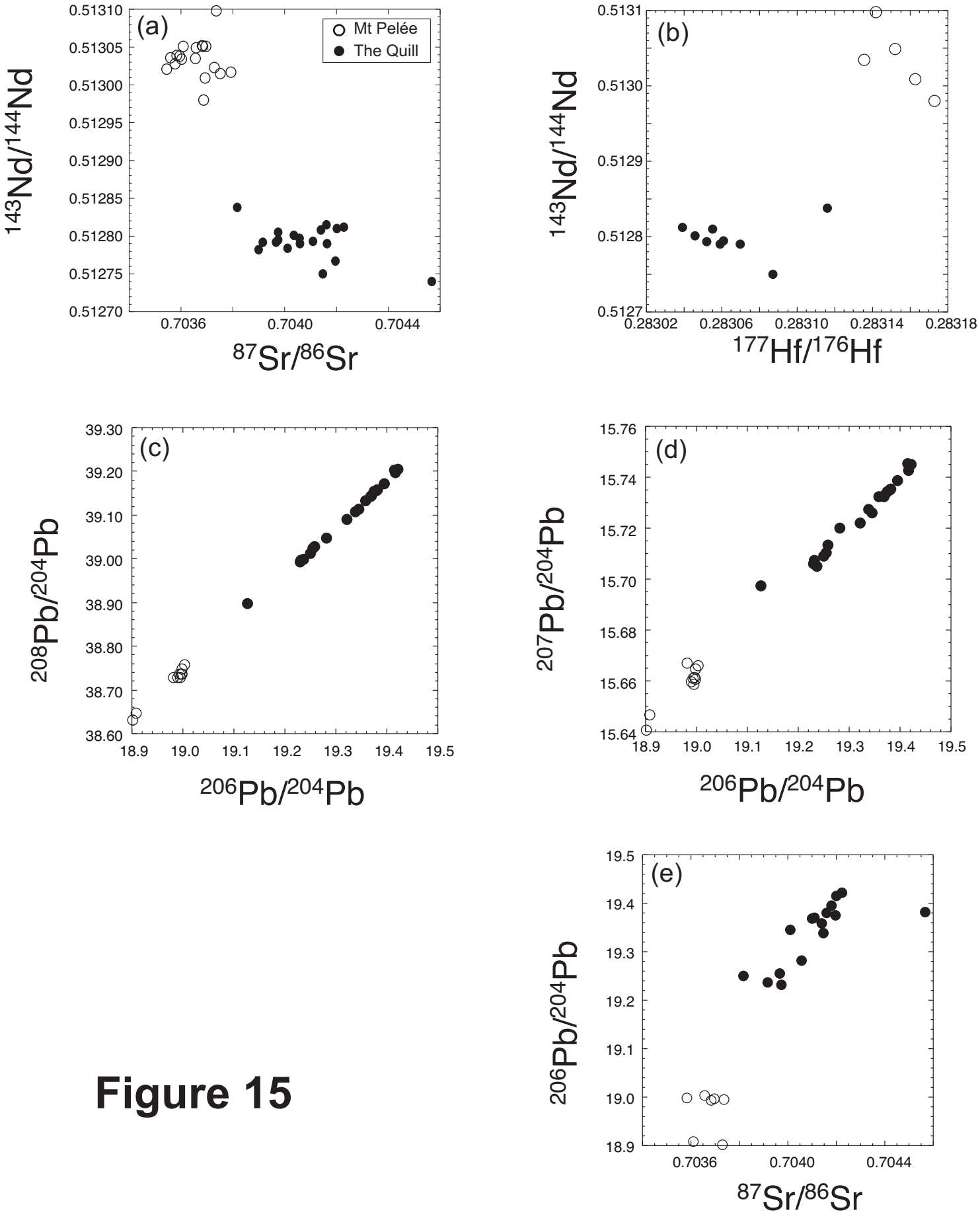
(a)
Mt Pelée
The Quill
$^{143}Nd/^{144}Nd$
$^{87}Sr/^{86}Sr$
0.51310
0.51305
0.51300
0.51295
0.51290
0.51285
0.51280
0.51275
0.51270
0.7036
0.7040
0.7044
(b)
$^{143}Nd/^{144}Nd$
$^{177}Hf/^{176}Hf$
0.5131
0.5130
0.5129
0.5128
0.5127
0.28302
0.28306
0.28310
0.28314
0.28318
(c)
$^{208}Pb/^{204}Pb$
$^{206}Pb/^{204}Pb$
39.30
39.20
39.10
39.00
38.90
38.80
38.70
38.60
18.9
19.0
19.1
19.2
19.3
19.4
19.5
(d)
$^{207}Pb/^{204}Pb$
$^{206}Pb/^{204}Pb$
15.76
15.74
15.72
15.70
15.68
15.66
15.64
(e)
$^{206}Pb/^{204}Pb$
$^{87}Sr/^{86}Sr$
19.5
19.4
19.3
19.2
19.1
19.0
18.9

Figure 15

Figure 16

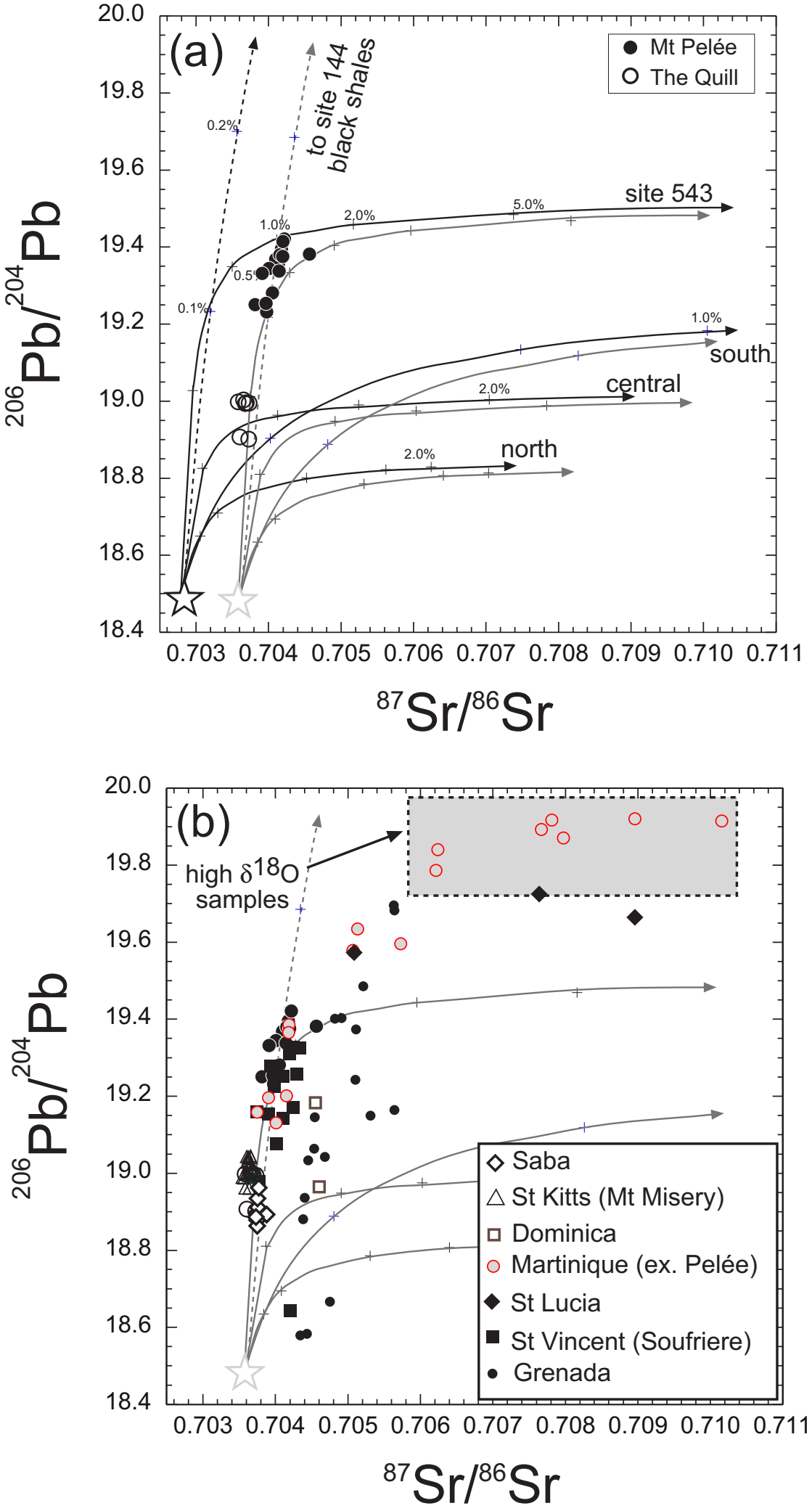
(a)
Mt Pelée
The Quill
to site 144 black shales
site 543
south
central
north
0.2%
0.1%
0.5%
1.0%
2.0%
5.0%
$^{206}Pb/^{204}Pb$
$^{87}Sr/^{86}Sr$
20.0
19.8
19.6
19.4
19.2
19.0
18.8
18.6
18.4
0.703 0.704 0.705 0.706 0.707 0.708 0.709 0.710 0.711
(b)
high $\delta^{18}O$ samples
Saba
St Kitts (Mt Misery)
Dominica
Martinique (ex. Pelée)
St Lucia
St Vincent (Soufriere)
Grenada

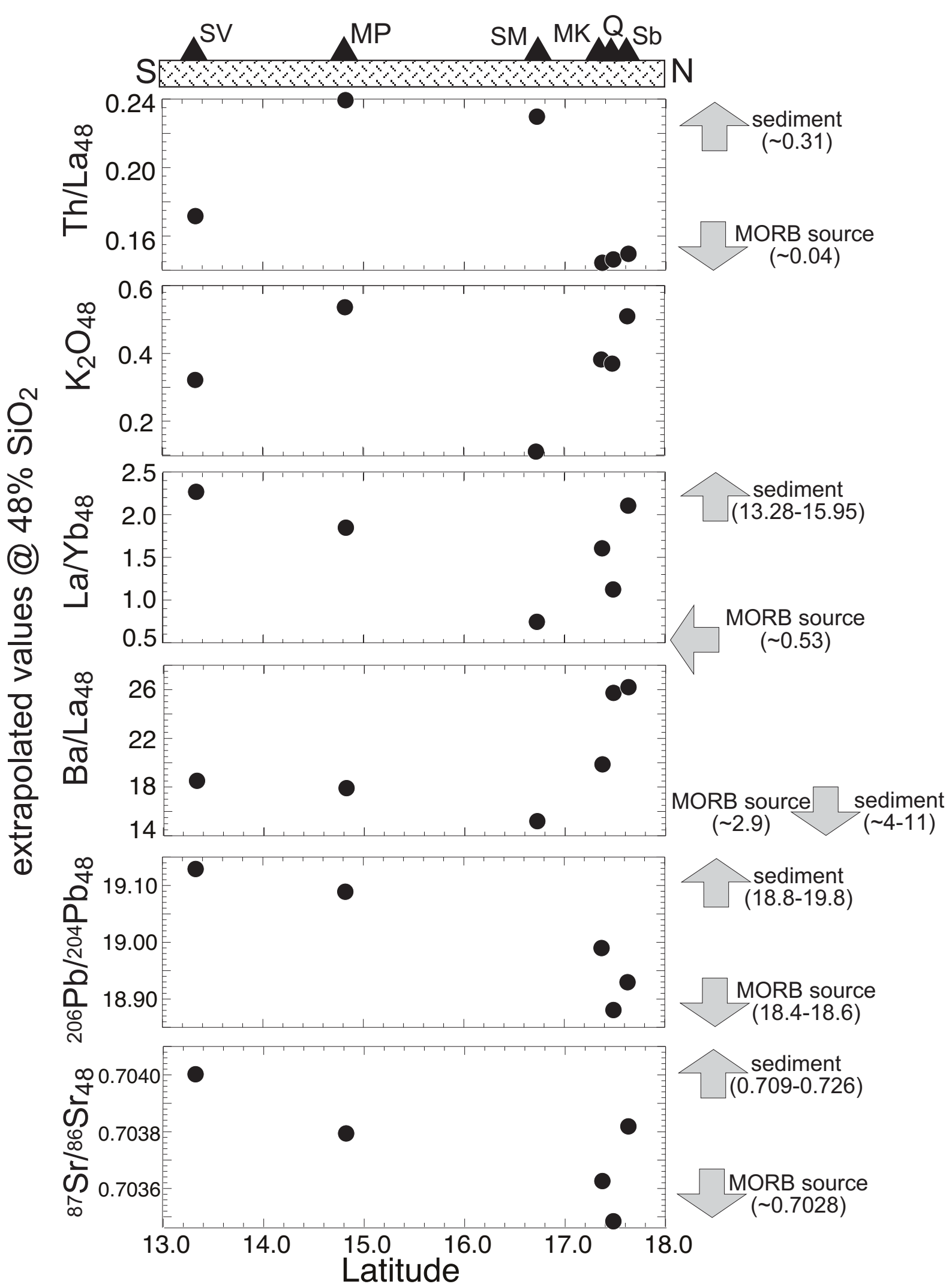
SV
MP
SM
MK
Q
Sb
S
N
Th/La48
0.24
0.20
0.16
sediment
(~0.31)
MORB source
(~0.04)
K2O48
0.6
0.4
0.2
La/Yb48
2.5
2.0
1.5
1.0
0.5
sediment
(13.28-15.95)
MORB source
(~0.53)
Ba/La48
26
22
18
14
MORB source
(~2.9)
sediment
(~4-11)
206Pb/204Pb48
19.10
19.00
18.90
sediment
(18.8-19.8)
MORB source
(18.4-18.6)
87Sr/86Sr48
0.7040
0.7038
0.7036
sediment
(0.709-0.726)
MORB source
(~0.7028)
13.0
14.0
15.0
16.0
17.0
18.0
Latitude
extrapolated values @ 48% SiO2

Figure 17

Figure 18

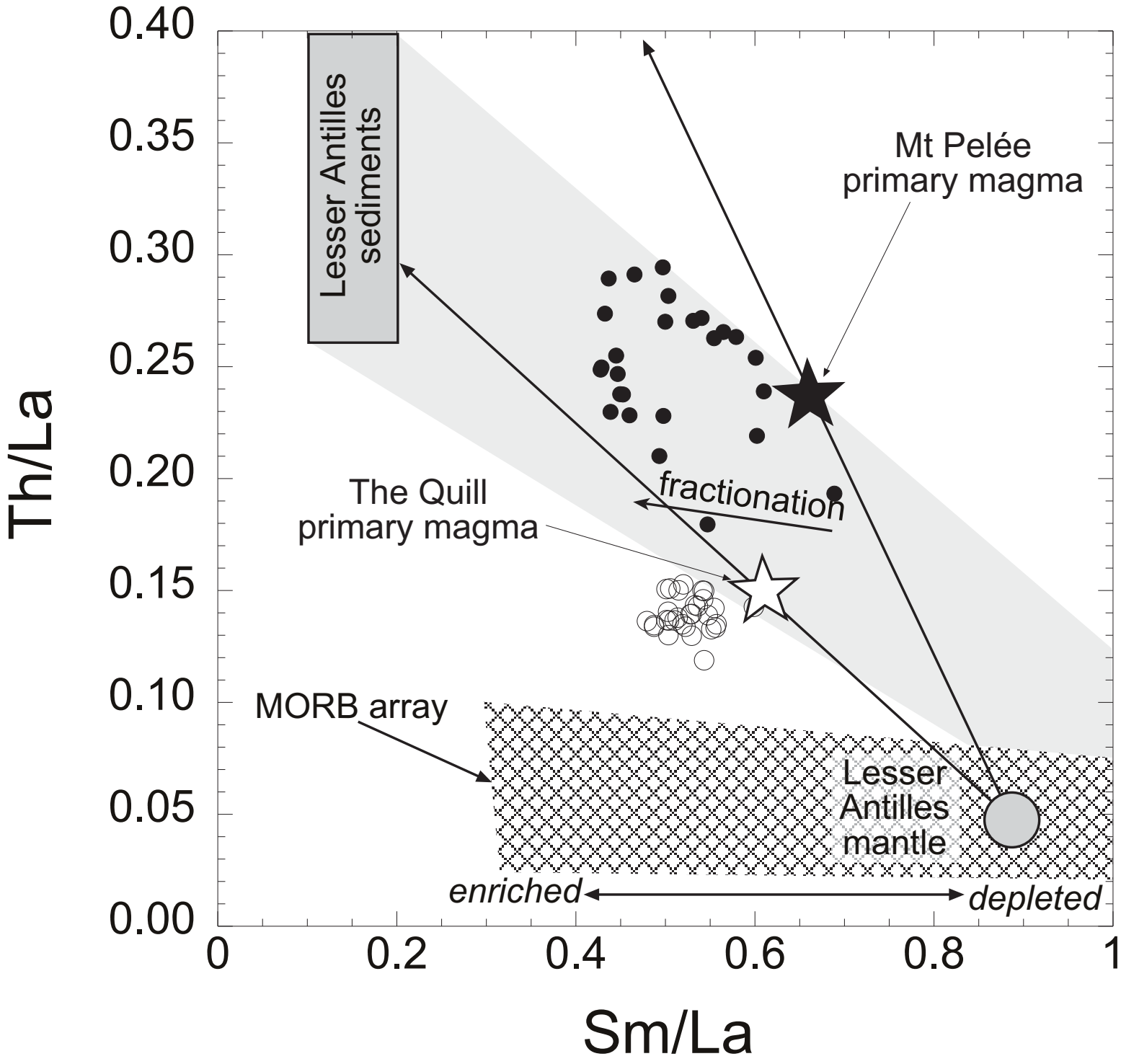
0.40
0.35
0.30
0.25
0.20
0.15
0.10
0.05
0.00
Th/La
0
0.2
0.4
0.6
0.8
1
Sm/La
Lesser Antilles sediments
Mt Pelée primary magma
fractionation
The Quill primary magma
MORB array
Lesser Antilles mantle
enriched
depleted

Figure 19

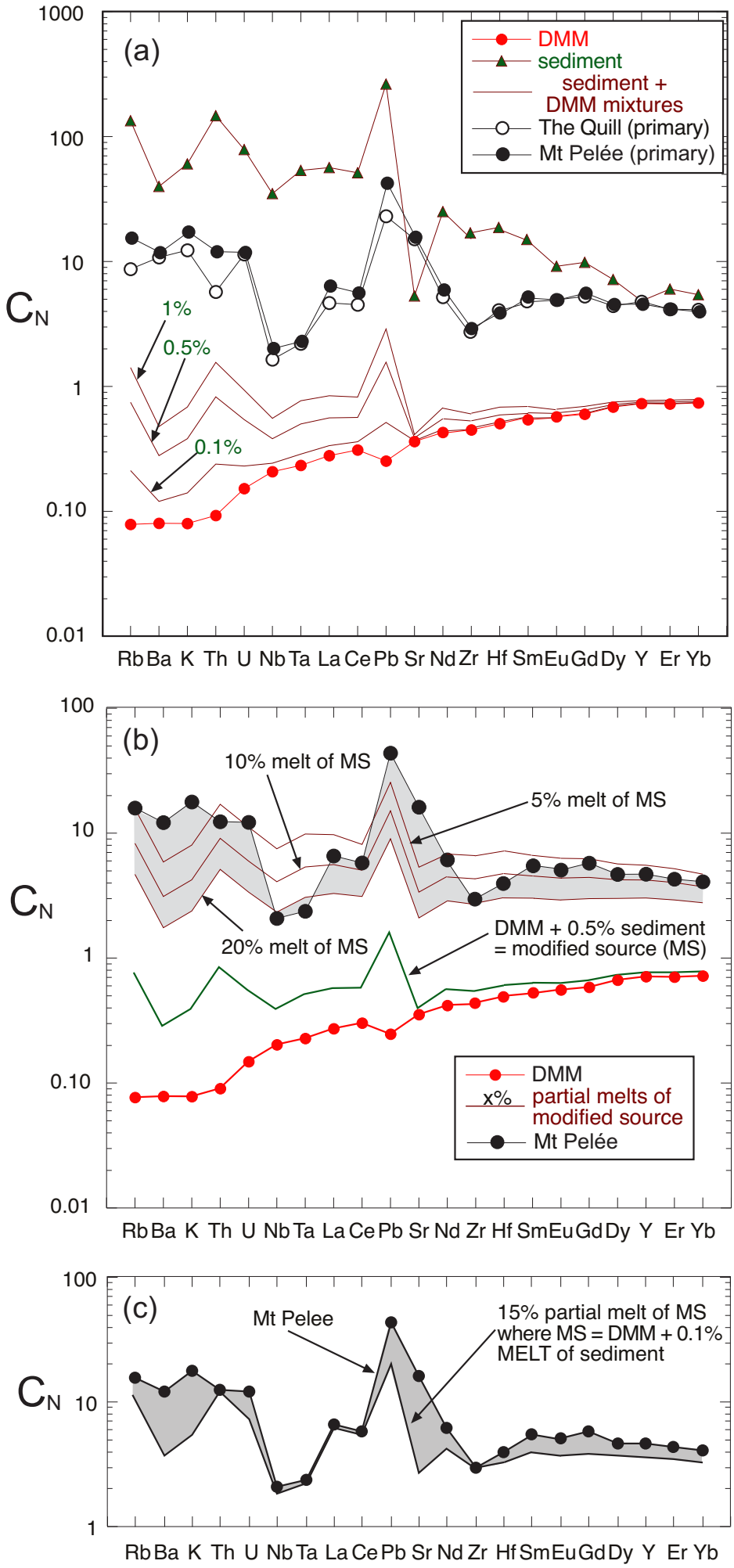
(a)
DMM
sediment
sediment + DMM mixtures
The Quill (primary)
Mt Pelée (primary)
1%
0.5%
0.1%
C_N
1000
100
10
1
0.10
0.01
Rb Ba K Th U Nb Ta La Ce Pb Sr Nd Zr Hf Sm Eu Gd Dy Y Er Yb
(b)
10% melt of MS
5% melt of MS
20% melt of MS
DMM + 0.5% sediment = modified source (MS)
DMM
x% partial melts of modified source
Mt Pelée
100
10
1
0.10
0.01
C_N
Rb Ba K Th U Nb Ta La Ce Pb Sr Nd Zr Hf Sm Eu Gd Dy Y Er Yb
(c)
Mt Pelee
15% partial melt of MS where MS = DMM + 0.1% MELT of sediment
100
10
1
C_N
Rb Ba K Th U Nb Ta La Ce Pb Sr Nd Zr Hf Sm Eu Gd Dy Y Er Yb